UNIVERSITY OF SOUTHAMPTON

DEGRADATION PROCESSES OF VOIDS IN SOLID DIELECTRICS UNDER AC APPLIED FIELDS

By

TIANYU BAI

A thesis submitted for

the degree of Master of Philosophy

Electronics and Computer Science

Faculty of Physical Sciences and Engineering

University of Southampton

United Kingdom

October 2013

UNIVERSITY OF SOUTHAMPTON

ABSTRACT

FACULTY OF PHYSICAL SCIENCES AND ENGINEERING

ELECTRONICS AND COMPUTER SCIENCE

Master of Philosophy

DEGRADATION PROCESSES OF VOIDS IN SOLID DIELECTRICS UNDER AC APPLIED FIELDS

by Tianyu Bai

This Thesis is concerned with an experimental study into the degradation processes that occur when voids in solid dielectric materials experience high applied electric fields. A method has been developed for manufacturing 2mm thick samples of silicone rubber that contain a single gas void of around 1mm diameter. Samples are simultaneously electrically stressed under an applied ac sinusoidal voltage of 11-12kV for 6 hours that is then increased to 12-17kV. During the stressing period, partial discharge (PD) data is regularly acquired. The samples are then inspected for signs of degradation. Degraded samples that have not suffered catastrophic failure and contain pits or evidence of damage were then cut open using an RMC MT-7 ultra-microtome equipped with a CR-21 cryo-system set at -110° C in order to provide a surface containing open segments that can be assessed using spectroscopic techniques.

The experiment is repeatable and the obtained degraded samples and the degradation areas of microtomed samples have been analysed using Raman spectroscopy to identify the chemical content of the degraded areas and obtained improved images using a scanning electron microscope (SEM) at the void /silicone rubber interface. In addition, the obtained PD patterns have been used to make a comparison between measurement and simulation results obtained using a physical model implemented in Matlab.

Contents

List of Figures

List of Tables

List of Appendixes

Academic Thesis: Declaration Of Authorship

I, Tianyu Bai declare that this thesis entitled

"Degradation Processes of Voids in Solid Dielectrics under AC Applied Fields"

and the work presented in it are my own and has been generated by me as the result of my own original research.

I confirm that:

1. This work was done wholly or mainly while in candidature for a research degree at this University;
2. Where any part of this thesis has previously been submitted for a degree or any other qualification at this University or any other institution, this has been clearly stated;
3. Where I have consulted the published work of others, this is always clearly attributed;
4. Where I have quoted from the work of others, the source is always given. With the exception of such quotations, this thesis is entirely my own work;
5. I have acknowledged all main sources of help;
6. Where the thesis is based on work done by myself jointly with others, I have made clear exactly what was done by others and what I have contributed myself;
7. Either none of this work has been published before submission, or parts of this work have been published as:

1. Chang, C, Bai, T, Lewin, P L, Morshuis, P F, Pilgrim, J A, Cavallini, A, Vaughan, A S, Montanari, G C and Serra, S "Developing an Experimental Method for a Cavity PD

based Life Model". IEEE 2013 International Conference on Solid Dielectrics, Bologna, IT, 30 Jun - 04 Jul 2013. 4pp, 780-783.

2. Bai, T and Lewin, P L " Degradation Processes of Voids in Silicone Rubber under Applied AC Fields". The Fifth UHVnet Colloquium, University of Leicester, Leicester, UK, 18 - 19 Jan 2012. , 34.

3. Bai, T. and Lewin, P.L. " Degradation behaviour of voids in silicone rubber under applied AC electric fields". 2012 IEEE Conference on Electrical Insulation and Dielectric Phenomena, Montreal, Canada, 14 Oct 2012. 4pp, 589-592.

4. Bai, Tianyu, Swaffield, D J and Lewin, P L "Modelling of Partial Discharge Activity in a Cavity within a Dielectric Insulation Material". UHVnet 2011, Winchester, UK, 18 - 19 Jan 2011. , 69.

Signed:……

Date:……

Acknowledgements

I would like to present my sincere appreciation to my supervisor, Prof. Paul L. Lewin. Paul gives me patient guidance and essential suggestions on the simulation and experiment work on PD degradation processes in solids. He also provides valuable comments and solutions to the oncoming experimental problems during the research. I must thank him gratefully for his quality supervision.

Thanks are also given to Dr. Nicky Freebody, Dr. Celia Yeung, Dr. Ian L Hosier, and Dr. Kwan Yiew Lau, who gave me training on the experimental techniques, especially on how to use Raman spectroscopy and RMC microtome machine. Thanks to Dr. Alex F Holt who gave me a lot of help on optical microscope and SEM. Thanks to Dr. Richard Chippendale who help me to solve the problem of simulations. Thanks are given to Mr. Cheng Chang who gives me help on understanding theory to the degradation behavior of the voids in solids. And I give my thanks to the Lab technicians for their support on experimental work in the Tony Davies High Voltage Laboratory.

Finally thank all my friends for their companies in Southampton and special thanks to my family for their keen support from China.

Definitions and Abbreviations

Symbols

α	a primary ionization coefficient ($mm\,kV^{-1}$)
n	the number of free electrons
n_0	the number of original electrons
γ	Townsend 's secondary ionization coefficient ($mm\,kV^{-1}$)
E_{lp}	The applied electric field ($kV\,mm^{-1}$)
B	Boltzmann constant
U^+	The inception voltage (V)
U^-	The extinction voltage (V)
U_c	The voltage in the cavity without the influence of space charge (V)
U_s	The voltage in the void due to charges on the void surface (V)
C_c	the capacitance corresponds to the cavity (F)
C_b	corresponds to the capacitance which is in series with C_c (F)
C_a	the capacitance of the rest of the dielectric (F)
E_{th}	threshold value for partial discharge occurring in channel ($kV\,mm^{-1}$)
E_a	The apparent electric field in the channel ($kV \cdot mm^{-1}$)
b	a material dependent constant

τ	time elapsed from initiation of the growth generating avalanches (s)
L	The length of channel (mm)
e	Electric charge of the electron (C)
f	Frequency of the applied voltage (Hz)
f_c	Field enhancement factor in the cavity
h_{mat}	Thickness of the material (mm)
k_{cav}	Thermal conductivity of the cavity ($WK^{-1}m^{-1}$)
K_{mat}	Thermal conductivity of the material ($WK^{-1}m^{-1}$)
m_e	Electron mass (kg)
n_e	Number of electrons in the streamer channel
p_0	Initial pressure in the cavity (kPa)
r	Cavity radius (mm)
q_{max}	Maximum charge magnitude (pC)
q_{min}	Minimum charge magnitude (pC)
q_{PD}	PD charge magnitude (pC)
$q_{PDtotal}$	Total PD charge magnitude (pC)
t	Time (s)
t_{PD}	Time of PD occurrence (s)
C_{cav}	Specific heat capacity of the cavity ($Jkg^{-1}K^{-1}$)
C_{mat}	Specific heat capacity of the cavity ($Jkg^{-1}K^{-1}$)
D_f	Electric displacement field (Cm^{-2})
E_{cav}	Field in the cavity centre ($kV\ mm^{-1}$)
E_{cav0}	Field in the cavity centre in the absence of surface charge ($kV\ mm^{-1}$)
E_{ext}	Cavity extinction field ($kV{\cdot}mm^{-1}$)
E_{ext0}	Initial cavity extinction field ($kV{\cdot}mm^{-1}$)
E_{inc}	Cavity inception field ($kV{\cdot}mm^{-1}$)
E_{inc0}	Initial cavity inception field ($kV{\cdot}mm^{-1}$)

E_{ons}	Field on the cavity surface ($kV\ mm^{-1}$)
E_s	Field due surface charge ($kV\ mm^{-1}$)
$E_{sfreePD}$	Field due to free surface charge immediately after a PD event ($kV\ mm^{-1}$)
$E_{strapPD}$	Field due to trapped charge immediately after a PD event ($kV\ mm^{-1}$)
E_{sPD}	Field due to surface charge immediately after a PD event ($kV\ mm^{-1}$)
E_{PD1}	Cavity field of the previous PD occurrence ($kV{\cdot}mm^{-1}$)
E_{PD2}	Cavity field of the current PD occurrence ($kV{\cdot}mm^{-1}$)
E_0	Applied field ($kV{\cdot}mm^{-1}$)
I_{cav}	Current through the cavity (A)
J_{cav}	Current density in the cavity (Am^{-2})
J_f	Free current density (Am^{-2})
L	Likelihood of a PD occurrence
N_e	Electron density (Cm^{-3})
N_{es}	Electron generation rate due to surface emission (s^{-1})
N_{es0}	Initial electron generation rate due to surface emission (s^{-1})
N_{es0H}	Higher initial electron generation rate due to surface emission (s^{-1})
N_{es0L}	Lower initial electron generation rate due to surface emission (s^{-1})
N_{et}	Total electron generation rate (s^{-1})
N_{ev}	Electron generation rate due to volume ionization (s^{-1})
N_{PD}	Number of free electron generated due to previous PD per unit time (s^{-1})
Q_{cav}	Heat source density in the cavity (Wm^{-3})
Q_{mat}	Heat source density in the material (Wm^{-3})
R	Random number

T_{amb}	Ambient temperature (K)
T_{cav}	Temperature in the cavity (K)
T_{mat}	Temperature of the material (K)
T_{ons}	Temperature on the cavity surface (K)
T_0	Initial temperature in the cavity (K)
U_{app}	Applied voltage amplitude (V)
U_{ext}	Cavity extinction voltage (V)
U_{inc}	Cavity inception voltage (V)
U_{incapp}	Measured cavity inception voltage (V)
V	Potential (V)
V_c	Voltage across the cavity capacitance (V)
V_0	Potential at time zero (V)
α_e	Coeffcient related to electron energy distribution and mean free path ($mm\,kV^{-1}$)
β	Thermal coeffcient for the cavity surface conductivity (K)
ε_{rcav}	Permittivity of the cavity
ε_{rs0}	Permittivity of the cavity surface on no degradation areas
ε_{rs1}	Permittivity of the cavity surface on degradation areas
ε_{rmat}	Permittivity of the material
κ	Constant for inception field equation ($kV{\cdot}mm^{-1}$)
λ_e	Electron mean free path (m)
ρ_{cav}	Density of the cavity (kgm^{-3})
ρ_f	Free charge density (Cm^{-3})
ρ_{mat}	Density of the material (kgm^{-3})
σ_{cav}	Cavity conductivity (Sm^{-1})
σ_{cavmax}	Maximum cavity conductivity (Sm^{-1})
σ_{cav0}	Initial cavity conductivity (Sm^{-1})
σ_e	Electron conductivity in the plasma (Sm^{-1})
σ_{mat}	Material conductivity (Sm^{-1})

σ_s	Cavity surface conductivity (Sm^{-1})
σ_{smax0}	Maximum cavity surface conductivity on no degradation areas (Sm^{-1})
σ_{smax1}	Maximum cavity surface conductivity on degradation areas (Sm^{-1})
σ_{s0}	Initial cavity surface conductivity on no degradation areas (Sm^{-1})
σ_{s1}	Initial cavity surface conductivity on degradation areas (Sm^{-1})
τ_s	Cavity surface time constant (s)
τ_{mat}	Material time constant (s)
τ_{dec}	Effective charge decay time constant (s)
τ_{stat}	Statistical time lag (s)
$\tau_{T decay}$	Temperature decay time constant (s)
χ	Constant for inception field equation ($kV \cdot mm^{-1}K^{-1}$)
Δt_0	Time step during no PD event (s)
Δt_1	Time step during PD event (s)
Ω	Cavity volume (m^3)

Abbreviations

AC	Alternating current
DC	Direct current
EGR	Electron generation rate
FEA	Finite Element Analysis
FDM	Finite Difference Method
GUI	Graphical user interface

MSE	Mean square error
PC	Personal computer
PD	Partial discharge
PDE	Partial differential equation
PRPDA	Phase resolved partial discharge analysis
DSO	Digital signal oscilloscope
SEM	Scanning electron microscope
RMS	Root mean square
CCD	Charge coupled device
EAA	Ethylene Acrylic Acid

Chapter 1 Introduction

1.1 Background

Micro-defects such as micro-cavities, protrusions and contaminants will occur in insulation materials due to defects introduced during manufacture [1]. These defects might not be detectable during factory testing of equipment, but their effect might become obvious when they are operating under service stress [2]. One possible defect is the inclusion of voids within a solid dielectric. The lower permittivity in the voids leads to a higher electric field within the void than in the surrounding electrical insulator [3], which may result in partial discharge (PD) activity. The two conditions that lead to PD occurring in the void are that the applied field is above the inception field and there are also free electrons available [2]. During the PD event, free charges with high energy will bombard the surface of the void [4]. Due to chemical modification and thermal degradation to the surface of void, it is hypothesized that pits will initially occur at the interface between voids and the insulation dielectric due to a further intensification and localization of the PD process [5]. In the next stage, it is proposed that initiation of bow-tie electrical trees will generate from micro-cavities under sustained high electric fields due to further concentration of PD behaviour at the tip of pits [1,3,4]. If this is the case then ultimately, the insulation material will breakdown due to the propagation of electrical trees generated from voids [1,3,4]. Therefore, according to the development of degradation processes from voids described above, it will have a detrimental impact on the insulation integrity of power equipment.

1.2 Research aims and objectives

According to previous research [3,5], the degradation processes of voids have been focused in polyethylene. The PD patterns, PD current and PD magnitude have been detected and analysed following with aging time [6,7,8]. Moreover, Morshuis [9] has found that degradation processes in polymers such as polyethylene can create three categories of by-products: gases, liquids and solids. A number of images on degraded voids in polyethylene have been taken by microscope [5,10,11]. However, the degradation processes of voids silicone rubber have not yet been reported. From the experiments conducted within the Tony Davies High Voltage Laboratory into the investigation of electrical trees in silicone rubber, it has been shown that it is easier to degrade silicone rubber than other commonly used insulator materials. Therefore, this project concentrates on studying the development of bow-tie electrical trees from voids in silicone rubber. In addition, revised physical models based on time-step analysis of local electric fields using Finite Element Analysis (FEA) [2] have been developed to simulate the observed PD behavior. These models have been adapted to include the degradation processes observed in experiments, this offers some understanding into the changes in electrical property as samples degrade. Raman spectroscopy is used to analyse the chemical content (carbon) of degraded samples and identify chemical changes that the samples experience due to degradation processes under high electric fields. This analysis also aids identification of the root cause for breakdown during degradation processes.

1.3 Contributions of the Thesis

This thesis contributes to the understanding of the degradation processes due to partial discharge in voids in silicone rubber under ac electrical fields. In this project, the following contributions have been made:

1) Development of an experiment to study degradation behaviour of voids in silicone rubber.

2) Proposed modifications to an existing physical model simulating PD patterns and pulses which were obtained from measurement in voids in order to account for degradation processes according to changing different parameters (EGR, effective charge decay time constant, maximum surface conductivity on degradation areas).

3) Through the use of spectroscopy, establishment of links between chemical changes of the surface of the void with changes in electrical properties during degradation.

1.4 Outline of the Thesis

From a review of the published literature, PD behaviour in the voids and tree initiation and tree propagation from voids are introduced in detail in Chapter 2 and Chapter 3. Sample preparation, the experimental setup, as well as experimental methodology is presented in Chapter 4. In Chapter 5, the results including PD patterns of degradation processes, images of degraded samples. Raman microprobe analysis and SEM microscopy on microtomed samples and unmicrotomed samples are described and discussed in Chapter 6. In addition, Raman microprobe analysis on breakdown of epoxy resin containing voids is also presented in Chapter 6. The comparison between experimental results and simulation results for silicone rubber samples is discussed in Chapter 7. Finally, Chapter 8 contains conclusions and suggested future work for this project.

Chapter 2 PD in Voids in Solid Dielectrics

It is assumed that during the process of forming an electrical tree-like growth, PD can be detected occurring in the void at first. This chapter describes that main processes by which PDs occur in a void. Specifically, avalanche processes, streamer processes, voltage variation in the voids and other factors which have an impact on PD behaviour in the void are discussed.

2.1 Avalanche Processes

The mechanism of an avalanche breakdown process is well understood [3, 12]. When the applied field within the void is larger than an inception field and there are free electrons available, PD will take place in the void. At first, the avalanche process will occur within the void, which is a non self-sustaining process. An original electron close to the cathode causes an avalanche. This single avalanche will lead to a discharge which was not self-sustaining. The discharge plasma will stop very quickly. The primary avalanche probably indirectly creates other ' secondary ' electrons from or close to the cathode which probably leads to secondary avalanches for different reasons discussed below. Therefore, this process probably becomes self-sustaining. After the ions and electrons created by the first avalanche have make a movement through the gap, a current will go on flowing. The inception voltage for Townsend discharges is related to the size of void and the configuration of the void and the category of gas. Also, the density of gas molecules is another important factor.

An electron injected from the cathode obtains kinetic energy from the electric

field in Townsend theory. If the mean free path related to collisions in a specific field is very high, then the energy probably is sufficient to lead to ionization when the collision with the molecule, which can generate a free electron. Therefore, these two electrons will then collide with other molecules and an avalanche probably is created. An initial ionization coefficient, α, is defined by Townsend as the number of electrons generated via an electron when moving via unit distance of gas in the field. In a distance dx, the increase of the number of free electrons, dn, is defined as $n\alpha dx$. n is the number of free electrons at a distance x from the cathode; ie

$$\frac{dn}{dx} = \alpha n \tag{2.1}$$

Integrating $dn = \alpha n dx$ and readjusting gives the number of electrons at x as :

$$n(x) = n_0 \exp\{\alpha x\} \tag{2.2}$$

n_0 can be defined as the number of initial electrons at x equals zero, the cathode. Due to the electron avalanche, the current thus increases when the anode is close to it. As the anode is collided by the electrons, the immediate establishment of current due to electrons is also almost exponential with the maximum current taking place

The theory of a single avalanche has been described above. This is not self-sustaining unless there are a number of cathode electrons available and that is not normally in agreement with it. Typically, times for the finish of such an avalanche are of the order of nanoseconds. Thus, this cannot clearly indicate the terminated discharge which is of the order of microseconds in typical. In the description from [3], Townsend suggested that the avalanche will lead to further '

secondary ' electrons which are produced from cathode, thus if at least another one secondary electron is generated from the cathode for each avalanche, the process will carry on indefinitely. The three most important factors of secondary electron emission are, excited and metastable atom impact emission, photoelectric emission and positive ion impact emission.

It is also reasonable other ionization and electrode processes (e.g. photo-ionization of gas molecules) appear. The behavior lead to streamer processes and are discussed in the next section. The probability that a secondary electron is created at the cathode as an indirect creation of a initial collision process in the gap is defined as Townsend 's secondary ionization coefficient, γ. The critical value of γ for which a self-sustained avalanche takes place means that one secondary electron is created for all the initial collision processes taking place in one avalanche. For every avalanche, it will create a secondary electron in indirectly way at the cathode which will cause the following avalanche ad infinitum. As the number of primary ionization collisions is normally high, a small value of γ can still lead to a self-sustaining discharge.

For each electron emitting from the cathode, there will be,

$$e^{\alpha d} - 1 \tag{2.3}$$

ionization collisions before the electrons reach on the anode, a distance x is equal to d, from the cathode. The number of secondary electrons created will therefore be,

$$\gamma(e^{\alpha d} - 1) \tag{2.4}$$

If this is at least unity, another avalanche will be created and the process is self-sustained. Therefore, the Townsend criterion for a self-sustained discharge is :

$$\gamma(e^{\alpha d} - 1) \geq 1 \tag{2.5}$$

Or

$$\gamma e^{\alpha d} \geq 1 \tag{2.6}$$

because $e^{\alpha d}$ is usually much greater than 1.

2.2 The Streamer Processes

The theory behind the streamer process has been widely reported in [3,12]. It is found that if an overvoltage is increased adequately and the void is not so small, the discharge current, though beginning like a Townsend discharge, immediately increases by at least an order of magnitude as streamer discharge. This occurs at approximately the process of the discharge which will be related to the decreases in electric current in a Townsend discharge. When it has reached a maximum level, the current quickly decays in order that the total discharge time is in comparison with the Townsend discharge. It will show that the size of consecutive avalanches immediately begins to increase quickly due to the distortion of field created by the occurrence of positive space charge across the void. When the avalanching develops, higher energy photons probably lead to ionizations in the gas which accelerate avalanches from within the gap and also

those from the cathode. Due to an interaction between physical degradation and penetration of hot electrons, the surface of the anode will be more conductive in fields of especially intensive behavior. This which follows with the positive space charge will further intensify the local field. Avalanches which from the cathode and created from within the gas, will enhance these localities and then the discharge will separate into filaments. The positive space charge will make a movement towards the cathode resulting in intensification of further field. This can be defined as the return stroke of the streamer and then when reaching the cathode, a plasma of electrons and positive ions occurs in filaments across the void. After a streamer has appeared, the effective resistivity of the void with gas becomes low. Charges are quickly established on the dielectric surface, which increases the voltage across the solid dielectric and thus decreases the voltage across the void. This decreases void resistance and reduces void field and the increases in surface conductivity quickly terminates the discharge.

2.3 Influence of Applied Field and Space charge

Ionization of the air can cause free positive charges and electrons within the voids during the process of gas discharge, the free charges will make a movement towards their charged electrode which polarity is opposite to them because of the presented electric field, which will have an important impact on the variation of voltage in the voids.

The inception electric field of the void can be defined as [12-15]

$$E^{+} = E_{lp}\, p[1+\frac{B}{(2pr)^{n}}] \tag{2.7}$$

The parameters of ionization processes characterization in the gas include E_{lp}, B and n, the pressure in the cavity can be defined as p and the radius of the cavity can be defined as r. E_{lp} is $24.2 VPa^{-1}m^{-1}$, n is ½ and B is $8.6Pa^{-1/2}$ [3,15] for air. The inception voltage of cavity U^{+} can be produced by a FEA model [3]. U^{+} is the

voltage throughout the cavity while the inception electric field is achieved. While the voltage U_c throughout the cavity is larger than the inception voltage U^+, a discharge will occur in the cavity which will provide a free electron in the cavity to make an avalanche begin to take place. When the voltage U_c through the cavity decreases to the value is smaller than extinction voltage U^-, PD will stop in the void.

Figure 2.1 describes a figure of a dielectric where the thickness of a disc-shaped cavity is d and the thickness of a disc is t. Also, an analogue circuit is shown in the figure 2.1. In the figure 2.1, C_c means the capacitance of cavity, C_b means the capacitance in series with C_c, and C_a means the capacitance of the other dielectrics.

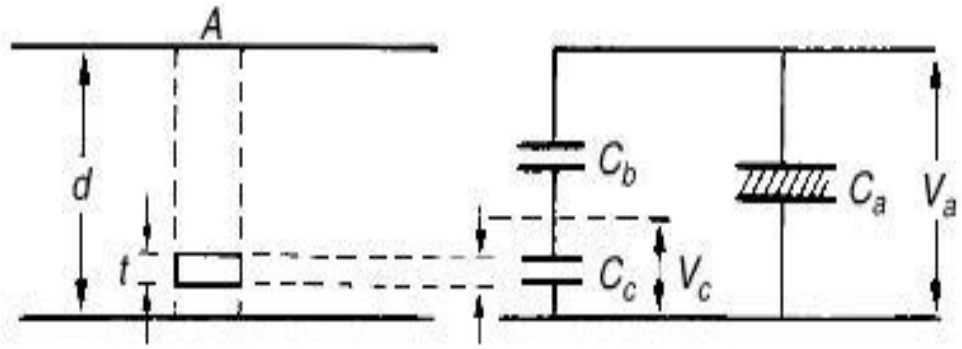

Figure 2.1 A discharge in void and the equivalent circuit of the discharge in the cavity [12]

When voltage across the cavity V_c is larger than inception voltage U^+ of the gap under an applied voltage V_a, PD will take place in voids. Figure 2.2 indicates that as V_c reaches U^+, a discharge will happen, the voltage V_c decreases and the discharge stops. Then, the voltage through the cavity is rising until it achieves U^+ when another discharge takes place. The discharge will occur when V_c is equal to U^+ in every time. The dotted curve describes the voltage will appear in the cavity

if it cannot breakdown [5]. V_c reduces rapidly after the first PD has occurred because of charge deposition on the surface of cavity U_s, which polarity is opposite to V_c [16].

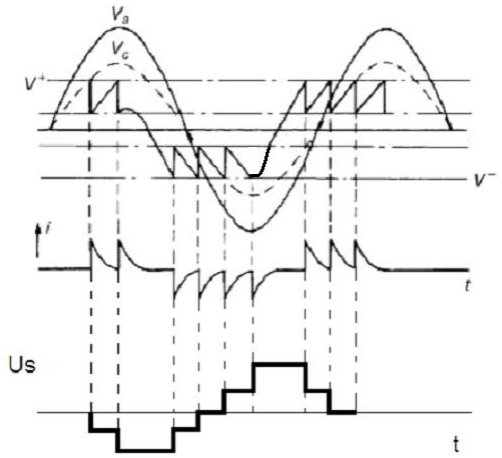

Figure 2.2 Voltage U^+ across the cavity, the opposite voltage U_s in the void due to charges on the void surface and sequence of discharge i under applied voltage [12,16]

2.4 Factors that Influence PD in Voids

Some factors have an important impact on PD behaviour in the void. The occurrence of PD in the void is related to the decay of void surface charge, statistical time lag and the frequency and magnitude of the applied voltage.

2.4 .1 Cavity Surface Charge Decay

There are two conditions that cause cavity surface charge decay during the PD process. The first is recombination behavior between negative charges and positive charges. The second is electron diffusion behavior that the electrons move from shallow traps onto deep traps near to the surface of void in the solid

dielectric.

The accumulated charges decay rate because of PD on the surface of cavity via conduction along the surface of cavity is determined by the applied frequency and the surface conductivity [17-19]. The changes of conductivity on cavity surface is determined by the degradation level [20,21]. Figure 2.3 describes the conductivity on the surface of the cavity depending on the direction of U_0 and the magnitude of U_s.

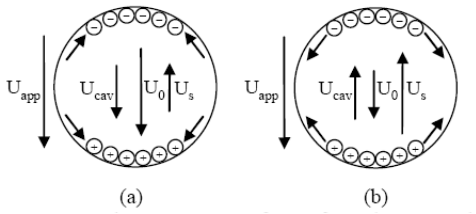

Figure 2.3 The changes of movement of PD free charges and electric field conditions (a) when U_{cav} has the opposite polarity in comparison with U_S and (b) when U_{cav} has the same polarity in comparison with U_S respectively [22].

Figure 2.3(a-b) presents the PD free charges move along the cavity surface, which is related to the polarity of voltage of the cavity. When voltage because of the applied field in the cavity, U_s and voltage because of surface charge from previous PD, U_s have opposite polarity, however, when the magnitude of U_0 is larger than U_s, voltage throughout the cavity, the polarity of U_{cav} then is opposite to U_s. This leads to free charges because of previous PD which are deposited on the surface of cavity to make a movement towards the center of the lower and upper surface of cavity where they are accumulated by PD because of the impact of the electric field in the cavity, as shown in Figure 2.3(a).

When the voltage because of the applied field in the cavity, U_0 and voltage because of the surface charge from previous PD, polarity of U_s is opposite.

However, when the magnitude of U_s is larger than U_0, or the polarity of U_{cav} is similar with U_s when both of them have similar polarity. This results in free charges because of previous PD that are deposited on the surface of cavity making a movement towards the opposite way to where they are remained through the previous PD because of the impact of the electric field in the cavity, as shown in Figure 2.3(b)

2.4.2 Statistical Time Lag during PD Activity

Statistical time lag is an important factor in PD activity. Generally, the time interval between the initial generation rate and inception voltage is defined as the statistical time lag [23].

Due to the change of the electron generation rate under electric field, the statistical time lag will be determined by the frequency and amplitude of the applied voltage [24]. The statistical time lag may vary between consecutive discharges [24]. The free electrons availability and the rate of charge decay determine the delay between two consecutive discharges [24].

As described in [3], electrons emitted from the cathode must obtain sufficient energy to overcome the work function barrier. This is impossible to take place as the spontaneous thermionic emission at temperatures below the melting point of most polymers and the void gas has a relatively low. It is impossible that the field would significantly improve the probability of electron emission due to the Fowler-Nordheim or Schottky effects [25]. The production of such electrons will therefore be from cosmic radiation, background radioactivity, and UV phonon incidents on the cathode surface. This will be a random process. Typical statistical lags are of the order of milliseconds and so cannot be ignored in the

analysis of the discharge process. Therefore, these are lags generally greater than the formation time of the avalanche.

2.4.3 Magnitude of applied voltage, Frequency and Size of void

According to some measurements [26,27], the magnitude and frequency of the applied voltage will have a crucial impact on PD behaviour. Many authors have described that ‘turtle’ like patterns are obtained and the 'rabbit-ear' like curves disappear using phase resolved PD (PRPD) analysis [27]. While the applied frequency is reduced, there are more PDs associated with a higher magnitude of charge than lower magnitude when the applied frequency is decreased. This probably is because of the reason that surface charge decay influences within the cavity between continuous discharges are more important while the duration of the applied voltage rises. This leads to a reduction of the electron generation rate, which results in a rise of the statistical time lag and then discharges appears at voltage which is higher than the inception voltage. Also, the maximum PD magnitude on the ‘rabbit-ear’ like increases while the applied voltage is rising. The number of PDs taking place with lower magnitude also rises. This is because the original electrons are easier to be obtained from surface of voids while the electric field is raised. Thus, this leads to in the increase of electron generation rate, which leads to the reduction of the statistical time lag.

Additionally, it has been found that the number of PDs per cycle is higher in a smaller cavity than that in a larger cavity [28]. A larger cavity has a lower extinction voltage, which increases the duration for the voltage through the cavity to reach to the inception voltage for the following PD event, which results in that PD repetition rate is lower. Moreover, mean charge amplitude, the total charge per cycle and the maximum and minimum PD amplitude are lower for the smaller cavity than for the larger cavity. The diameter of cavity assures the maximum distance of propagation of the avalanche which occurs at the direction parallel to

the applied field and also the size of head of avalanche at the direction is perpendicular to the applied electric field. Therefore, for larger cavity, the size of avalanche can be larger, which will lead to individual PD charge with larger magnitudes.

2.4.4 Paschen's law and the influence of gas in the void

Gas generally has a lower permittivity (ε_g) than polymeric insulators (ε') [29] and so, when there is a gas filled void within a polymer under an impact of electrical field (E), the lower permittivity in the void results in electric field in the void (E_v) is higher than in the polymer insulation material [3], which will ensure that PD occurs in the void first. The conditions such as the type of insulation, the category of gas of the void, the size of the void and the configuration of the void, the gas pressure and the temperature of the system [29] all affect PD behaviour. For a disk-like void:

$$E_v = \frac{E\varepsilon'}{\varepsilon_g} \quad [29] \tag{2.8}$$

If the voltage across the voids is raised to be larger than the breakdown voltage, then breakdown in the void can occur through the process of an accumulative Townsend electron avalanche ionization [18,30] and a PD will occur in the void. If ε_g is equal to 1, then the breakdown voltage is given by [30],

$$V_b = E_g d'[1+(d/d'-1)/\varepsilon'] \tag{2.9}$$

E_g can be defined as the dielectric electric strength of the enclosed gas, and d, d' are the thickness of the specimen and the cavity, respectively. The discharge in the void is in line with Paschen's law which indicates that the breakdown voltage (V_b) across a uniformly stressed gap is determined by the product between the

distance of the gap (d) and the density of the gas (ρ) as shown by [3]:

$$V_b = f(\rho d) \tag{2.10}$$

Figure 2.4 [31] shows a typical Paschen's curve for air and from this it can be concluded that there is a minimum breakdown voltage regardless of the size of gap or density of gas (for air this is 327V at a standard atmospheric pressure and a gap of 7.5 um [18]). Also, this law shows that, for a constant gap spacing, the voltage required to break down the gas increases rapidly with a decrease in pressure below the point where the minimum voltage occurs due to a decrease of molecules within the gas and therefore an increase of the mean free path associated with the hot electrons [31].

Paschen's law can be applied to PD behaviour in voids and allows identification of factors which influence behaviour and degradation of the polymer. The initial PD activity leads to an increase in temperature and in pressure within the void. Therefore, it will result in the breakdown voltage increasing until the gas cools or dissipates through the bulk of the polymer. Also, the PD causes polymer degradation to create gaseous products and increase the gas pressure.

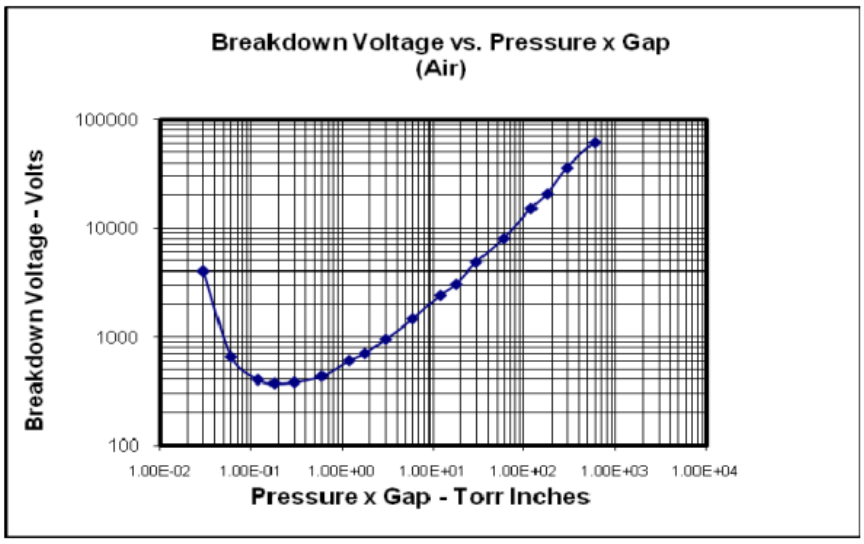

Figure 2.4 Typical Paschen curve for air across a gap [31]

2.5 . PD patterns in voids

Typical PRPD patterns in voids are called either rabbit-like pattern or turtle-like pattern [32]. The typical PRPD patterns on rabbit-like pattern or turtle-like pattern are shown in Figure 2.5. The PRPD patterns for the turtle-like pattern is described in Fig.2.5(a). There is a number of electronegative gas in the void such as water and oxygen [33] at this stage. Fig.2.5(b) shows the PRPD patterns for the rabbit-like pattem. The appearance of this pattern can be shown as below. There is not a lot of electronegative gas at this stage. However, its electron attached ability is strong. Thus, a much larger discharge occurs before a large time lag is obtained. The gas capable of further electron attachment is consumed after the first discharge in the same half cycle. This causes a decrease of the discharge statistical time lag and leads to a series of discharges with small magnitude.

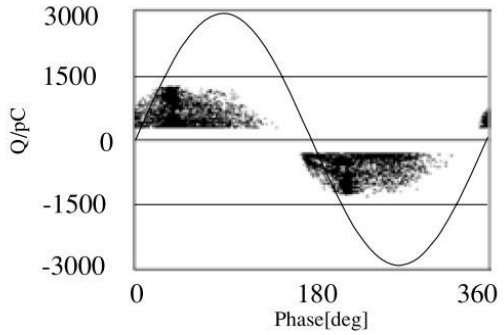

a)

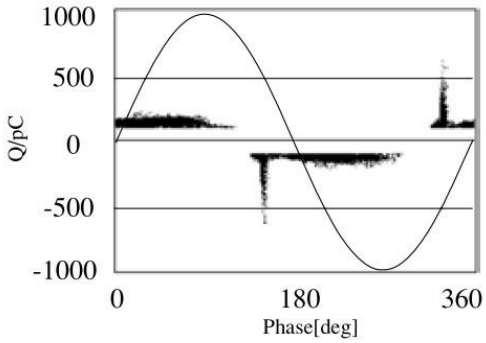

b)

Figure 2.5 PRPD patterns from a void a) turtle-like b) rabbit-like [32]

2.6 Summary

The PD process can be divided into avalanche processes and streamer processes. Ionization of the gas will cause electrons and free positive ions within the void during the process of the formation of a discharge. The free charges will make a movement towards the charged electrode which polarity is opposite to them under the local electric field, which will make a collision on the surface of the void with extremely high speed. This behavior can lead to degradation, specifically, localized increase of temperature or initiate chemical by-products (such as O_3 and NO_2), therefore, degradation area, pits and channels may be formed, which are introduced in detail in the following chapters.

Chapter 3 Electrical Trees in Solid Dielectrics

This chapter describes the mechanism of degradation behaviour for a void in a solid dielectric. The theoretical process that creates a tree from a void can be separated in to two parts: degradation processes to the solid dielectric material, formation of pits and ultimately generation of bow-tie electrical trees. Currently, the theory of bow-tie electrical trees has yet to be validated by experiment, so electrical trees produced using needle electrodes will be discussed in this chapter. Additionally, PD patterns of electrical trees generated from needles are included as they may be applicable to identification of trees growing from voids that do not have a needle present.

3.1 Degradation behaviour in voids

From a point with the enhanced field (such as the boundary at the interface between electrode and dielectric) or from a void with gas, an electrical tree probably begin to grow [34]. Because a tree is generated from a void with gas, the PD behavior occurs in the void is required to be focused on a specific area. The growth of crystal on the surface of a more oblate, flat cavity [35] indicates the PD behaviour and a serious degradation behavior of the insulation. This can be shown in Figure 3.1.

The reason for the degradation behaviour can also be explained by [5]. Internal discharges in polyethylene initially cause surface erosion followed by the formation of a transparent resin which fluoresces in ultra-violet light.

a)

b)

Figure 3.1 Serious damage of the polyethylene surface of a void. In the boundary of crystals, a crater is formed. The a) and b) were concentrated on the surface of cavity and on the surface of crater respectively [10].

Approximately 10pC (6×10^7 electrons) degraded some 10^{-15} cm^3 of polyethylene (4×10^7 -CH_2 groups) for each discharge, and this has been related [10] to thermal degradation as there will be a local immediate temperature rise of several hundred degrees centigrade if all the energy of discharge were changed into thermal energy at the dielectric surfaces. The approximate equation relationship between the number of -CH_2 groups and the number of electrons generated from each discharge influenced proposes, as another description, that the collision breaks -CH_2 groups from the chains of polymer. Walder [29] has shown cracks in polyethylene caused by the impact of ultra-violet light, which enhances an oxidation process, which leads to chain scission and produce a cross-linked polymer of lower molecular weight. This degradation product is similar to the results caused by internal discharges in polyethylene in order that ultra-violet light produced when the discharge probably also is related to the degradation. The rate of degradation increases quickly with increase of voltage which is larger than the inception voltage and the discharges focus on forming one or more deep ‘pits’.

The energy created via each discharge increases with the length of the pit in order that the degradation propagates with increase of speed. In addition, the material which is obtained is further degraded to a dark brown non-transparent material and eventually to carbon.

The discharge by-products that have been observed have been separated into three types: liquids, solids and gases. Except for crystallization, the other by-products have been found and reported in [5,9,10]. Wolter et al. [36,37] described the by-products of gases of polyethylene with low density, which caused by the corona discharges. The damage by-products can be regarded as carbon monoxide, carbon dioxide, methane and hydrogen. The relationship between the radiative energy of the PD and polymer results in forming hydrogen. Oxidation from fragments of polymer chains was confirmed to cause the existence of carbon oxides.

Liquid by-products can be regarded as the form of droplets [38,39] at the insulator surface for different kinds of materials, for example, epoxy, polypropylene and polyethylene, which is shown in Figure 3.2. Gamez-Garcia et al. [40] described that the droplets occurred in an atmosphere which has carbon monoxide and water. Morshuis [41] described that no droplets can be found if one of the chemical contents hydrogen, carbon or oxygen was not obtained. The process below is indicated [10,39] to result in the formation processes of the droplets: oxidation of polymer chains and scission leads to the formation of chain fragments (oligomers). These fragments which dissolve in water lead to that clusters are shown on the dielectric surface. A combustion process or gas atmosphere occurring on the surface of dielectric can create water. Sigmond et al.[41] described that the surfaces of polypropylene and polyethylene which experience discharges that create a number of water if oxygen has been obtained. The experiments in Morshuis [10] indicated that droplets were shown in a dry air

(RH is less than 5%). The time for formation was longer and number of droplets was smaller, which agrees on the behaviour that water is created when PD occurs.

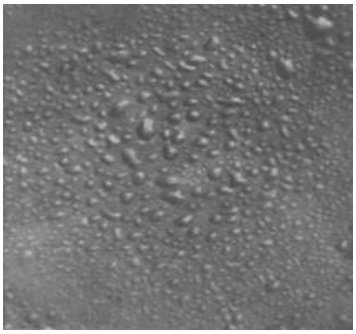

Figure 3.2 Liquid droplets on surface of artificial void in polyethylene specimen at 45X magnification [11]

The enhancement of field of crystal tips results in intensifying and localizing the PD behaviour and the formation of pit has been found [5], which is assumed to lead to the formation of an electrical tree and enhance the electric field of the insulation. By optical methods, it has been confirmed that tree growth probably starts from the boundary of crystals [35] for flat cavities. Through the way of micro charge probes, Garcia Colon [42] has indicated that injection of electrons occurs at the tips, which agrees on the behavior that the formation of tree probably begins from these pits. Also, [5] showed that as pits grow from the void because concentration of the field in the dielectric near the periphery of the void may lead to serious deterioration by localized discharges in this area, the boundary at erosion is more rapid than at the centre of the void [5]. A deep pit which is shown in Figure 3.4 was found at the edge of the cavity.

Additionally, following degradation processes to the surface of voids, pulseless PD or glow PD is normally thought to occur under a number of conditions in an enclosed void [43]. According to a number of reports [43,44,45], in the final stage of degradation process, PD current cannot be found. Then, a final breakdown will occur immediately. It is unable to assume the way to degradation of the insulation, when there is no PD detected. PD pulses obtained by optical or electrical

measurement method indicated that a number of very small PD pulses are detected, which cannot be obtained via traditional PD detection method with restricted ability of frequency.

Tiny pulses of 1pC or less have an order of microseconds on repetition rate. This behavior has been defined as swarming micro PD. The swarming micro PD is recognized to be relevant to the decrease of overvoltage because of the ready supply of original electrons. A result caused by a small PD charge is given by a small overvoltage as the inception and extinction voltage are closer with each other.

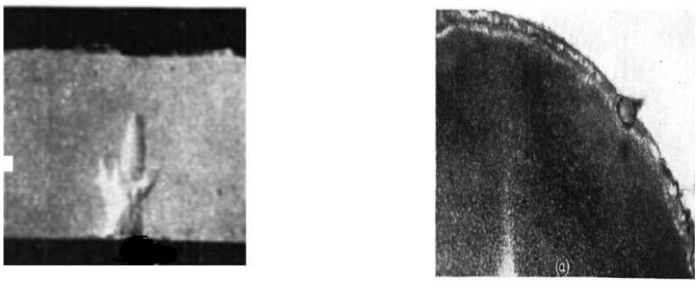

a) b)

Figure 3.3 Uncarbonized pits at the periphery of a void enclosed in polyethylene, after 10.8 kV (twice the inception voltage) had been applied for 12 hours [5].
(a)Void of diameter 0.3 cm and depth 0.008 cm in disc of 0.11 cm thickness
Surface erosion and pits at the periphery of void, magnified 50 times.
(b) Section across the deepest pit shown in (a), magnified 44 times.

Furthermore, authors in [5] have described the process of pits propagation. It can be seen from Fig 3.4 that a change in the processes of propagation of the pit appears to occur when the pit achieves a specific depth. When the primary pit occurred by degradation indicates a smooth circle configuration and the partial breakdown channel extends as an uncarbonized pit, the following degradation takes place when the diameter of a sharply narrow carbonized channel is much smaller than that of the degraded pit. In some instances shown in Fig 3.4(b), the

utmost end of the channel decreases in diameter with the restriction depending on resolution of the photograph which is probably about 4 microns. An explanation of this change of process is necessary because it is probably related with the process of breakdown in electric strength experiment for industry in which a material experiences a high electric stress due to surface discharges for a duration clearly which is too short for degradation to take place. However, breakdown takes place much below the intrinsic electric strength of the material. The next indication describe that the second process of breakdown probably create from concentration of electric field more than a length of some 10^{-4}cm at the end of the pit to a value close to the intrinsic electric strength. Propagation probably takes place by degradation of the material throughout this distance, which is accompanied by concentration of the electric stress at the end of the damaged and the conductive channel.

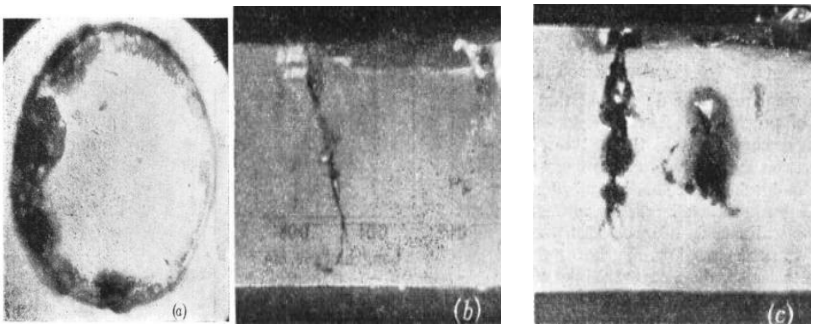

a) b) c)

Fig. 3.4. Carbonized pits at the edge of voids between polyethylene discs and brass electrodes [5].

(a) Surface erosion and pits produced after 9.5 kV (twice the inception voltage) had been applied for 5 hours, magnified 65 times. Void of 0.3cm diameter and 0.0095cm depth in disc of 0.079cm thickness.

(b) Section through the longest carbonized channel shown in (a), magnified 45 times.

(c) Section through carbonized pits in a second sample after 9.8 kV (twice the inception voltage) had been applied for 12.6 hours; magnified 55 times. Void of 0.1cm diameter and 0.0081cm depth in disc of 0.079cm thickness.

3.2 Electrical Tree inception

After observation of pits, tree inception may be found during the degradation processes. The basic description of tree inception is described in [3]. Pulses of electroluminescence that is the first visible behaviour [46] occurs which is before tree inception starts or at lower applied voltages in experiments [46]. An area of degradation (about 5um) at the needle electrode tip is created [47] during the behavior. The emission spectrum is almost not dependent on polymer morphology [48] and is different from void discharges [49] within the range of visibility [50]. Therefore, it has been led to the neutralization of injected space charge with the deeply trapped charges remained from the previous half cycle [51]. Thus, the onset field for luminescence depends on the barrier to charge injection which is decreased by the existence of electronegative gases [52]. The process can still take place in degassed samples [51], even if applied voltages are high.

In shallow traps a space charge is created within milliseconds [48] and then leads to the recombination centers occurs in the modified electric field due to space charge during injection. While the intensity of injection of space charge increases, the apparent onset field increases

The injection current obeys the Schottky emission law at the lowest field [53]. However, it changes to fowler-nordheim tunneling emission by the schottky-mott barrier at higher electric fields [53]. It has been mentioned [30] that electrons can obtain kinetic energy of 3-4eV which is adequate to cause bond scission. Typically, the luminescence onset fields are below the value of about 7×10^8Vm. It is probably that only some bonds are damaged during injection. The light created by recombination also has not enough energy to break bonds. However, the small UV component is an exception [51].

The centers of recombination are in the interface of amorphous crystalline in polyethylene [54] and modification of some structural probably occurs due to the electrostatic forces related to recombination and trapping. The degradation area [55] is probably consisted of tiny structural rearrangements on the amorphous-crystalline boundaries where the deep trapped charge is in degassed polyethylene [56].

Oxygen in the metal-polymer interface probably changes to an excited state [46] and cause bond scission [57] by oxidation [58]. When the excited molecules can make the diffusion at room temperature, the degradation can extend until the formation of strings of microvoid is close to the tip. The polymer movement is much limited and some chain scission occurs without the development of microvoids by contrast at 77K [50, 59]. Therefore, oxygen probably leads to tree enhancing damage especially at temperature around 20° C.

The real start of tree inception is the existence of current pulses generally. Pulses have been obtained in polyethylene before a tree channel extends. Current pulses normally occur on the positive half cycle with a small magnitude [60] (0.04-0.3pC) in the earliest time. The current pulses should be related with the emission of the electrons which are remained into deep traps at the half cycle. The charge density is 10^{-3}-10^{-2}pC. um^3 approximately.

Current pulses will be obtained during extraction occurs when the local field has achieved a magnitude adequate to form an avalanche due to heterocharge [60], which will start making the erosion to the polymer [61] in the method suggested by Ashcraft [62]. The electrons which obtain enough kinetic energy will make an ionization to the polymer (more than 10eV), create positive ions radicals (less than 10eV) and make the breaking on polymer bonds (about 3.5eV). Thermal

electrons will be captured by the positive ions radicals [63], which will lead to forming free radicals which probably results in chain scission [64]. The category of degradation processes should be determined by the polymer described previously [57].

Crazes [54] will extend by a microvoid coalescence is resulting from repetition of the avalanche occurrence in an AC electric field [65]. The tree will begin from this point if electroluminescent degradation in oxygen has taken place. The magnitude of current pulse will increase during this stage when the related charge is accumulated. Finally, space charge field and the degradation will have accumulated adequately for current pulses to occur [60]. In typical, a magnitude of PD pulses less than approximately 1pC will occur in polyethylene. The discharge pulse on the negative half cycle is likely produced by the avalanches which are caused via injected electrons, but the avalanches will only appear in the developed craze which has an amount of 'free volume'. Thus, the properties of the gas discharge associated with the local onset field should be determined by the category of gas and gas pressure. Then, burst-type acoustic emission can be obtained in polyethylene [66], which indicates the craze has been damaged into microcrack [67]. Where crazing is present before tree formation, the time to produce a tree is reduced accordingly [47].

3.3 Tree Propagation

The previous section details evidence that pits occur from voids as a precursor to bow-tie electrical trees. The propagation of pits may take place after experiencing high electrical field for a long period, which may lead to electrical trees growing from voids due to high stress concentration on the tip of pits. Tree propagation is the process of further degradation. The tree propagation from voids will lead to

final breakdown of material under high electric field. The section describes channel discharge, branch development and the PD patterns of electrical tree discharge, separately.

3.3.1 Channel Discharge Behaviour

The introduction to channel discharge process has been shown in [3]. A self-limiting growth behaviour appears in the first channel produced in AC treeing [30]. The behaviour may be caused by electro-fracture due to the level of how available is the strain energy and the spatial distribution of strain energy. However, it is impossible that this mechanism would give the visible discharge behaviour which indicates that current pulses have appeared on both half cycles while the development of channel after negative half-cycle pulses disappear and a decrease of that on the positive half-cycle to about 0.2pC when the channel growth is stopped [6,30,68,69]. These indications are in agreement with a process where electrical discharges that cause a degradation process to the channel are temporarily terminated. This is impossible to increase the discharge inception voltage of voids for this small size though some gaseous decomposition by-products have been created, which results in increasing the pressure of gas in the channel [70,71]. However, it is found that the breakdown value of the polymer is close to discharge inception voltages in the long cylindrical channels with diameters less than about 100 μm. In addition, special discharge behavior can be created in the gas avalanches because of the sidewalls of positive ions by absorption [72-75]. Tree channels belong to this type with a length to diameter ratio above 5. Moreover, it can be thought to behave according to the same method. Positively charged bands will be generated along the channel length because ions are caused by an avalanche in bands divided by an impact ionization path length [75]. These bands will make further discharges stopped in the channel due to their density of charge. Therefore, the local field is high enough to effectively neutralize the electrons [3]. According to [76], processes of this

category causes a change in the discharge-phase relationship between channels from needle and disc voids in which it is unlikely to make a discharge along the surface when the rise time of voltage supports the a number of discharges to take place while the voltage decreases. In conclusion, PRPDA can be used to follow the degradation processes from discharge in a void to channel propagation for trees generation caused by PD in epoxy resins [77,78] where a needle electrode is also present.

The extinction of forward-discharges in the first channel relies on the fields created by charge distribution on the sidewalls, but it could be presumed that the channel continues to grow when the local field is larger than a threshold value, E_{th}, for discharge formation [25,73]. However, through absorption the local field will depend on low mobility positive ions limited to the sidewalls. If the maximum number of positive ions absorbed per unit length is a constant, the ions can be assumed to decrease the apparent field E_a by an amount which is proportional to the length of channel. Therefore, describing the growth rate as proportional to the over-field, $E_a - E_{th}$, gives

$$\frac{dL}{d\tau} \propto E_a - E_{th} - bL \tag{2.11}$$

Where b is a material dependent constant, and τ is the time elapsed from initiation of the growth of generated avalanches.

3.3.2 The Development of Branches

According to the description in [3], development of the AC-treeing process will

firstly appear through the branches has been produced in the first channel. Figure 3.5 shows branch-like trees at 60Hz in Ethylene Acrylic Acid (EAA) under 12kV [79]. In some cases, both forward and backward discharges can take place within the trees in the support of combination and diffusion of the positive ions into the polymer [30]. When an adequate number of positive ions are concentrated on the sidewalls at the branch tips, even if discharges which occur in some existing channels probably temporarily stopped [80,81], back-avalanching of electrons which are deeply trapped in the polymer support the tree to extend through the formation of new branches.

This type of propagation gives rise to impulse-like acoustic emission and light pulses, connected with gas discharge which can also be regarded as PD pulses is more than 1pC [81-82].

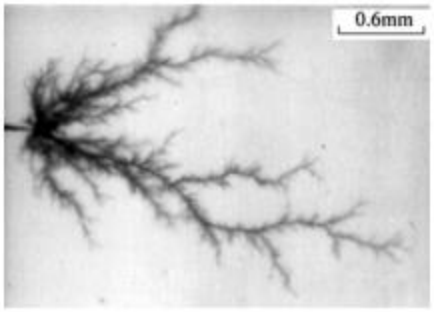

Figure 3.5 Branch-like tree shapes formed under 12 kV at 60 Hz. The material of the sample is EAA, the electrode distance is 3 mm and the needle tip radius is 3 μm [79].

0.002% of the discharge energy appears in the mechanical destruction wave. Mechanical destruction wave cannot lead to cracks in polyethylene though it may enhance previously damaged areas [83]. By contrast, the electron stream of discharges can achieve kinetic energies more than 10eV at the discharge tip which is adequate to propagate the channel by bond bombardment. However, degradation is caused by the positive ion streams which can lead to temperature increases of hundreds of Kelvin [84-85]. In air discharges, uniform degradation

(from oxygen) and pitting (from nitrogen) will extend the channels of trees in polyethylene and produce amount of gaseous decomposition products during acetylene has been confirmed by mass spectroscopy, and CO, CO_2 and H_2 through analysis of light emission spectra [78,86].

As the tree develops through the extension of existing channels and the development of new branches into channels, the first channel will extend into a crater and the branches into channels with diameters are above 10 μm [87]. The attendant discharges will quickly increase to about 100pC with a proportionally large acoustic emission [80, 81]. In addition, acoustic emission pulses have been detected in polyester resins in which it was indicated that the distribution of pulse was similar to that of the current pulses. Moreover, their magnitude is proportional to that of the discharge which is more than 300pC [81,88]. The acoustic pulses also have an impulse-shape, which is reasonable if they are caused by the channel discharges but not cracking in the polymer. The length of whole tree extends very slowly and development of tree is focused on the production of a sub-branch system which causes an increase in diameter of main branch to about 50 μm during this stage of propagation of branched tree [68].

3.4 PD Patterns in Channels

It has been found that PD pattern from a tree is typified by a wing-like pattern. Treeing aging can be basically identified and differentiated from PD patterns produced by voids etc [79].

From [79], The PD pattems obtained from an electrical tree has been found in polyethylene. The typical PD pulse sequence describing the tree from the needle-shaped void is shown in figure 3.6

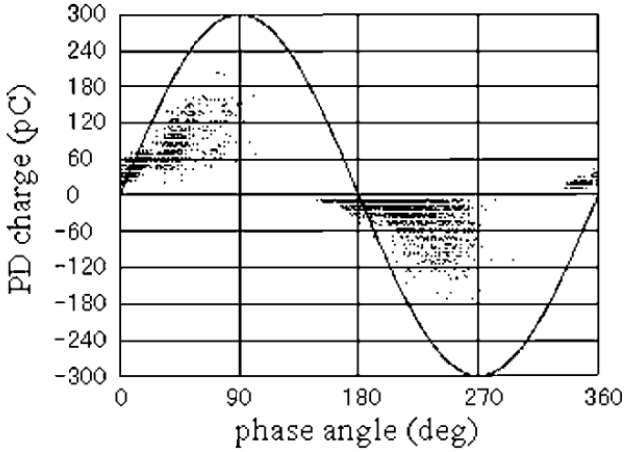

Figure 3.6 PRPD patterns from electrical trees [79]

3.5 Summary

The chapter describes the tree formation process due to the existence of a void in the dielectrics. The surface of the voids is aged due to the bombardment of the electrons and positive ions. Then, pits are created due to the degradation of the surface of the void. In the meantime, by-products will be created during degradation of wall of void and will cause further degradation. Bow-tie electrical trees may grow from the sharp pits because of this process due to the concentration and localization of PD processes which leads to bond-breaking. When the voltage in the channel is in excess of a critical voltage, PD will occur in the channel. Free electrons will be emitted from the wall of the channel. Any chemical degradation will cause the conductivity of the wall of the channel increase. On the tip of the channel, the electric field will be intensified, therefore, streamer processes will take place around the tip of channel. Electrons with high energy will collide with the wall of the channel, which will generate a number of additional channels. The creation of chemical by-products will widen the channel. Finally, the solid insulation will breakdown because of propagation of channels across the dielectric. Branch and bush-like tree propagation are two most important types of tree development. It should be noted that all experimental

results presented in this chapter are for voids that are formed at a needle electrode tip.

Chapter 4 Sample Preparation and Measurement Techniques

This chapter focuses on the preparation of the test samples that have been used for PD measurement in this work. The setup of the experiment, which is originally related to the technique of phase resolved partial discharge analysis (PRPDA) and the measurement method for degradation experiment are detailed. The results of the degradation experiment were then used for Raman microprobe analysis to identify the chemical content of the degraded areas at the void /silicone rubber interface.

4.1 Test Samples

4.1.1 Silicone rubber

According to [89,90], silicone rubber is a rubber-like material consists of silicone includes silicon with hydrogen, carbon and oxygen. The chemical formula for silicone rubber is shown in Figure 4.1. Silicone rubbers are commonly applied in factory. Silicone rubbers are generally supplied as one-part or two-part polymers. Also, it probably has fillers to enhance characteristics or decrease the cost of purchasing. In general, silicone rubber is stable, non-reactive, and is more resistant to environments which are extremely awful. Also, when experiencing temperatures from −55 °C to +300 °C, it still can maintain its most of properties. Because of these properties described above and the easier method to manufacture, silicone rubber can be used in most of products which include: automotive devices, baking, cooking and the products of food storage. Heat probably is need to be cured the silicone into the formation of rubber-like during the manufacture of products. During manufacture, this is basically carried out for

two stages into the required configuration. In the following processes, the products should be in a long process of post-cure.

The application of composite insulation material manufactured by silicone rubber has risen quickly for the recent fifteen years [91]. The application of composite insulation materials is described by experience of service [92] and laboratory measurement [93-95] in polluted environments.

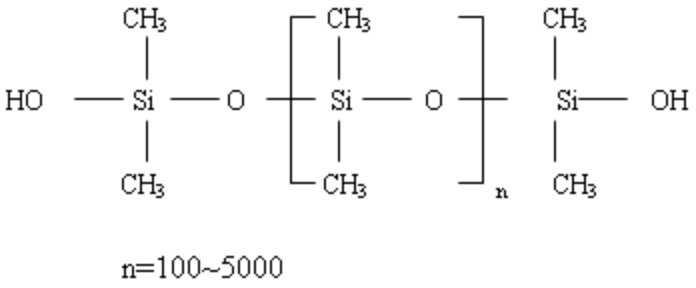

Figure 4.1 Formula of silicone resin

The voltage of flashover of porcelain or glass insulation materials is much lower than the new, polluted composite insulation materials [96]. Their quality is better than porcelain ones [92-95] though degradation decreases the voltage for flashover of the polluted composite insulation materials [97]. The most important reason for the better application of silicone rubber in comparison with glass and porcelain is hydrophobicity of surface. Rain water forms into drops rather than forming a film completely wetting the polymer surface. Therefore, this decreases the probability to the formation of the leakage current. In addition, it is useful to reduce the possibility of formation of dry band, which results in a higher inception voltage for flashover [96].

4.1.2 Preparation of test samples

The silicone rubber used in this work is Dow Corning Sylgard 184 Silicone Elastomer kit. There are two glass containers which contain silicone rubber and hardener separately. To prepare the samples, the mixture ratio between the

silicone rubber and its hardener is 10:1. It is a strong, powerful, high strength, long lasting adhesive, solvent free and heat, cold, water and oil resistant. It has a degassing time of 50 minutes after the mixture of silicone rubber and hardener in the vacuum oven at room temperature in order to prevent unwanted bubbles in the mixture. Before degassing, the mixture was stirred for at least two minutes to ensure all silicone rubber and hardener have completely mixed. The strength of the silicone rubber can be enhanced using a post curing process, depending on the post cure time duration and the temperature.

Generally, 11g of the mixture of resin and hardener should be used for sample preparation. The sample was prepared by using a plastic petri-dish. After degassing, the 11g mixture was poured into the petri-dish slowly. Before injecting a single void into the samples, a suitable pre-cure time duration of 10 minutes at 60° C in the fan oven was applied. Ten minutes later, a controlled volume of air was injected with a precise needle into the mixture to produce an artificial spherical cavity before the mixture post cures over the following half an hour at 60° C in the fan oven. The injected bubble does not move towards the top surface of the silicone rubber because the viscosity of the silicone rubber had increased as it was halfway through curing. There was no trace of tunnels or other cavities in the silicone rubber after the needle was pulled out. The volume of the void is 0.5uL. The volume of air injected in the silicone rubber determined the size of the spherical cavity. Thus, the diameter of the void is around 1mm. In order to obtain the possible bow-tie electrical trees, the smaller voids need to be injected centred at the middle of the samples. Therefore, the pre-cure time was raised to 14 mins and the volume of the void should be controlled around 0.4uL. After injecting a single void into sample, the sample was placed in the fan oven at 60° C for half an hour for post curing. Finally, the sample was cut into a suitable size for the degradation experiment. The thickness of samples can be measured by micrometer. The thickness of all samples used in the experiments was 2mm

±150μm.

After an air bubble has been injected into the silicone rubber and it has been cured, it cannot be assured that the void is a perfect spherical one. However, it is presumed that the void is approximately spherical void. This hypothesis is based on the cavity is observed under a microscope with light, where a circle has been observed from the largest circumference of the cavity. When the state of the sample with the void is checked by microtoming the sample into two pieces, a circle has been found after observed from the largest circumference of the void. Therefore, it is presumed that the shape of the void observed is similar with spherical void for all samples. Furthermore, this method is the basic method for obtaining a spherical void of diameter larger than 1 mm in a dielectric material and has been reported in the other work previously [21, 26, 98].

4.1.3 Other supplied test samples

Three additional samples containing some voids were supplied by ABB. The material used was epoxy resin. The samples had a large number of voids between two Aluminum electrodes. From figure 4.2, several voids can be observed very close to the top electrode.

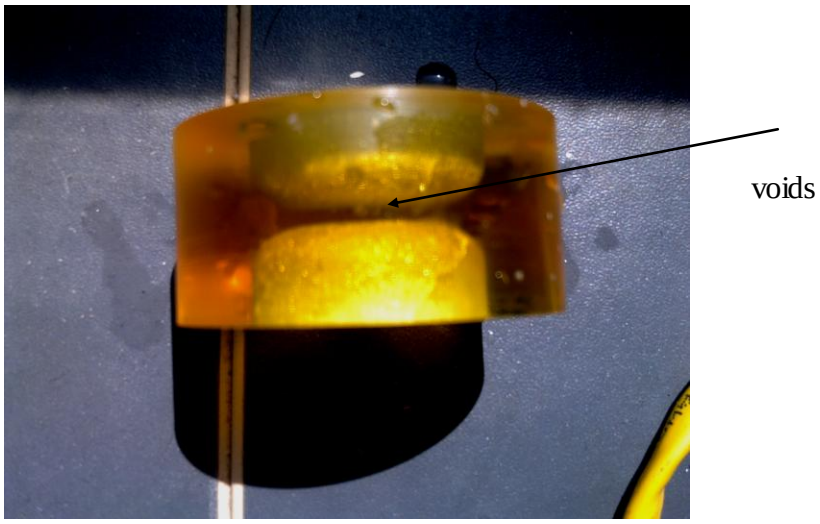

Figure 4.2 The sample of epoxy resin

The samples were stressed at 14kV for 7 hours. If one of the samples failed, then the others were carefully checked for any signs of degradation. The failed samples were cut open and Raman spectroscopy used in order to assess whether discharge activity had caused changes in the surface chemistry of the voids.

4.2 Setup for the test samples

Mushroom electrodes were used in the degradation experiment. Five pairs of electrodes were used. Figure 4.3 shows the schematic diagram of a test cell which consists of a silicone rubber sample containing a single spherical cavity. The whole test object was immersed in silicone oil to prevent surface discharges around the electrode and material boundary. An ac sinusoidal voltage was applied on the upper electrode while the lower electrode was always grounded.

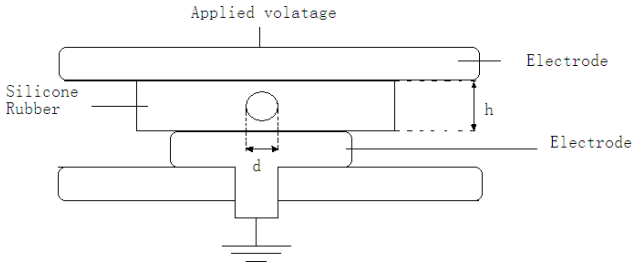

Figure 4.3 Schematic diagram of the test object

Table 4.1 is a summary of the samples prepared for experiments. All samples contain a spherical cavity of diameter d located in the silicone rubber. All cavities were around 1 mm diameter as this is known to be large enough to guarantee accumulation of charge on the cavity surface during the degradation processes. Table 4.2 details the experiment processes and the specific information of no degraded samples and failed samples. It should be noted that sample 1 to sample 5 were obtained by stressing with the other four samples simultaneously. However, the samples from sample 6 to sample 10 were obtained by stressing individually.

Figure 4.4 shows the test sample in the oil bath. The test arrangement consists of

a high voltage supply which is connected to a high voltage electrode through a copper pipe, the ground which is connected to ground electrode by a black thin wire and silicone rubber sample placed between the two electrodes. The electrodes and sample are placed between two sheets of paxolin, which are held by a plastic leg at each corner. The whole arrangement is immersed in an oil bath.

The experimental sequence	**Sample**	**Cavity diameter, d (mm)**	**Sample thickness, h (mm)**
1	1	1.4	2.2
2	2	1.0	2.1
1	3	1.0	2.2
3	4	1.1	2.1
4	5	1.0	2.0
5	6	1.8	2.2
6	7	1.5	2.1
7	8	0.9	2.1
8	9	0.5	2.1
9	10	1.4	2.2
Not used in electrical experiment	11	1.3	2.1

Table 4.1 Samples obtained from experiments used for thesis

The experimental sequence	**Sample number**					**Cavity diameter, d(mm)**					**Sample thickness, h(mm)**					**The state of voids**				
1	a	1	b	c	3	1.1	1.4	1.2	1.3	1.0	2.1	2.2	2.2	2.1	2.2	N	D	F	N	D
2	d	e	f	g	2	1.2	1.1	1.4	1.1	1.0	2.2	2.1	2.2	2.0	2.1	N	N	F	N	D
3	h	i	g	k	4	1.2	1.3	1.0	1.2	1.1	2.2	2.1	2.2	2.3	2.1	N	N	F	N	D
4	l	m	n	o	5	1.1	1.2	1.3	1.1	1.0	2.0	2.3	2.1	2.2	2.0	N	N	F	N	D

a) The specific information of all samples

The experimental sequence	The duration of experiment with only volts on	The periods of experiment with volts off
1	7 hours	27 hours
2	8 hours	28 hours
3	8.5 hours	28.5 hours
4	9.5 hours	29.5 hours
5	8 hours	28 hours
6	8 hours	28 hours
7	7.5 hours	27.5 hours
8	30 hours	74 hours
9	8.5 hours	28.5 hours

b) The different experiment durations for different conditions (volts on or volts off)

Table 4.2 The Details of experiment processes a) The specific information of all samples (a-o- The test samples include no degraded samples and failed samples; D-degraded samples, F-failed samples, N-No degraded samples) b) The different experiment durations for different conditions (volts on or volts off)

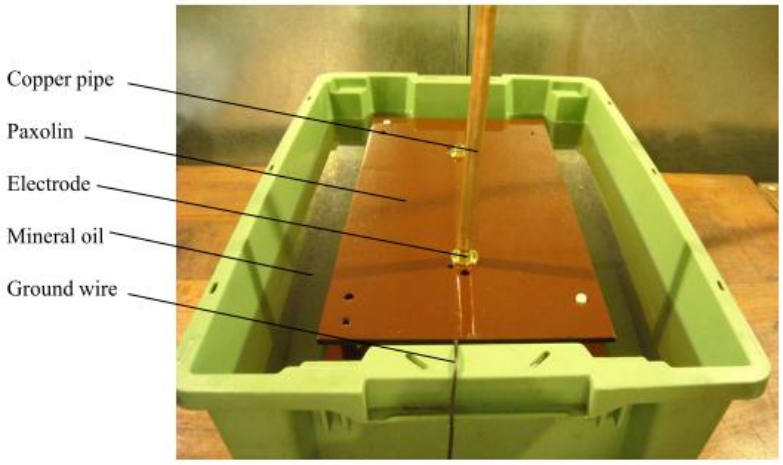

Figure 4.4 Test sample in an oil bath

4.3 The Experimental Setup

The equipment used to do measurement on PD degradation experiment is the Mtronix MPD 600 system, which is manufactured by OMICRON. The Mtronix MPD 600 system is a fully digital system which is suitable for laboratory and on-site measurement of PD measurement in high voltage equipment. This setup has more advantages than previous detection systems used for PD research. For the old method, a Robinson PD detector and an associated with a digital signal oscilloscope (DSO), where the PD detector detects PD pulses from the test object and the DSO was used to display, detect and save the PD pulses obtained from the PD detector.

Figure 4.5 shows the schematic diagram of the experiment that has been used to measure PD degradation processes. The experiment consists of a high voltage supply, a high voltage filter, a coupling capacitor C_k, a test object, a coupling device, a PD detector and a USB controller which is connected to a personal computer (PC) via fiber optic cables. The system captures any detected PD signal of center frequency in the range of 0 Hz to 32 MHz with bandwidth range of 9 kHz to 3 MHz. The system noise is less than 15 fC. The PD event time resolution is less than 2 ns, which makes the detected phase angle of a pulse very precise. In this experiment, the system noise level is around 500fC.

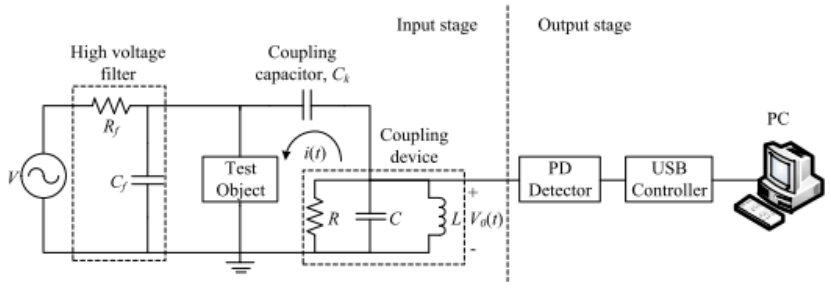

Figure 4.5 Schematic diagram of the experiment [27].

A high voltage source is provided from a low voltage generator signal, which has output frequency range of 0.1 mHz to10 MHz and output voltage range of 5 mV to 20 V AC peak-to-peak with a 1 mV resolution. The low-voltage signal can be amplified by a high voltage amplifier of 1V/2000V gain and a maximum output voltage of 20 kV. Its input voltage range is 0 to 20 V AC peak-to-peak and input impedance is 25 kΩ nominal. A high voltage filter is used to decrease high frequency noise from the input signal amplified through the high voltage amplifier into the setup and also to make high frequency surface discharge signals disappear between the tip of the amplifier output and the ground of its insulation.

The low pass filter are composed of three capacitors, C_f of 150 pF and voltage rating of 15 kV each which are connected in parallel and two resistors, R_f of 22 kΩ and voltage rating of 2.2 kV connected in series. C_f and R_f are connected between the test object and high voltage amplifier. The setup of this low pass filter is selected as it controls to remove unwanted high frequency signals from the measurement system. Although noise signals below 50 pC is impossible to be filtered, it in practice does not influence the PD experiment results as the detected minimum PD charge magnitude from the test object is larger than 50 pC. If higher resistance is used in the filter, the maximum effective RMS value of the high voltage output will be decreased when higher capacitance is used, the sine waveform from the high voltage supply will be different from normal sine waveform while the applied voltage amplitude is larger than 10 kV RMS.

The voltage rating of the capacitor is selected by the maximum applied voltage amplitude that is used in the measurement, which is 20 kV peak-to-peak when the voltage rating of the resistor is chosen lower than 20 kV. This is because the capacitor voltage rating has been adequate. However, if the test object breaks down during experiment, the resistors may be broken because of short circuit, however, this is impossible to occur as the breakdown strength of the test object

is higher than 20 kV applied voltage. The value of coupling capacitor, C_k used is 1 nF and has a blocking voltage of 50 kV. It is connected in series with the coupling device and in parallel with the test object. The important reason to this way of connection rather than connecting C_k in parallel with a serial connection of the coupling device and the test object is that the PD detector is preserved by C_k when the test object breaks down.

The theory of the PD detection system is based on detecting the current pulse across the test object. When a discharge occurs in the test object, charges are moving from the coupling capacitor, C_k to the test object to make compensation with the voltage decrease across the test object. Then, a current pulse, i(t) of short duration, which is within the nanosecond range forms in the circuit and a voltage pulse, $V_0(t)$ is created across the coupling device. The amount of charge movement is defined as the apparent charge. The magnitude of apparent charge is dependent on the induced number of dipole moments of the real charge from PD in the cavity that creates an immediate change of the test object capacitance and their relation with the electrodes of the system [12].

The coupling device or CPL 542 measuring impedance detects the short-duration voltage pulse, $V_0(t)$ when a PD occurs. The range of output frequency of this equipment is between 20 kHz and 6 MHz. A simplified parallel RLC circuit in the coupling device leads to formation of a wide-band PD measuring system. The value of each component in the coupling device is not offered by the supplier. According to Figure 4.7, the coupling device is the end of the input stage of the detection system.

The PD detector measures the magnitude of discharge pulse via its PD impulse input and the applied voltage amplitude via its voltage input. The PD impulse input frequency range of the device is 0 Hz - 20 MHz and the maximum PD

impulse input voltage is 60 V rms. The center frequency used for charge integration setting is 350 kHz and the bandwidth is 300 kHz. This setting is selected based on the IEC 60270 standard, which indicates frequency range is 30 kHz to 100 kHz for lower limit, 500 kHz for upper limit and 100 to 400 kHz for bandwidth [12].

The USB controller is integrated with the output signals from the PD detector by fibre optic cables and the data is obtained from the PC for user to display, analyse and store PD events. The USB controller supplies an interface between data obtained from the PD detector and the PC. The advantage of using fiber optic cables in comparison with conventional cables used in the previous PD measurement is that it ensures complete galvanic isolation between the PD detector and the USB controller. The elimination of ground loops decreases the system. The system has 500 channels for phase and 400 channels for discharge magnitude, where 200 channels are for positive and negative discharges separately.

After the Mtronix experiment is used every time, the system needs to be calibrated. The MPD 600 system needs charge calibration to be finished digitally. The test object is connected in parallel with a CAL 542 charge calibrator during calibration. The range of calibration charge is 1 to 100 pC. It should be noted that 1 pC is equivalent to 1 mV pulse. In this experiment, the calibration charge has been set to 20pC. The target value of the charge in 'Calibration Settings' is set as the target charge value of the calibrator and the 'Compute' button is pressed to complete the charge calibration. The calibrator is then taken away from the system. This method ensures that calibration can be obtained in a precise and simple way. The calibration of the previous system was conducted using a calibration pulse created in the PD detector and is in comparison with the pulse created by the calibrator. The pulse created in the PD detector is adjusted until its

magnitude is very close to the calibrator pulse magnitude. This method cannot give a precise calibration and is relied on the experience of the researchers.

When PD measurement is conducted using the Robinson PD detector and DSO, the normal difficulty found is setting the amplifier of the equipment. Because different conditions of the cavity and stress lead to different range of discharge magnitude, the amplifier gain needs to be adjusted manually based on the discharge magnitude range. If the amplifier gain is set too low, the detected PD pulse magnitude probably is lower than the noise level and this results in difficulty in identifying between PD pulses and noise. However, if the gain is set too high, PD pulse magnitude may be larger than the dynamic range of the amplifier and PD pulse cannot be detected. This problem is probably more difficult to overcome if the range of PD pulse magnitudes is very large. However, the amplifier gain of the MPD 600 system can be set to auto gain in the Mtronix GUI, where the gain responds automatically corresponding to the discharge magnitude. Therefore, this decreases the difficulties of resetting the amplifier every time measurements are conducted.

4.4 Measurement technique for PD experiment

It is vital to assure that the oil is bubble-free as the measurement results will be disturbed if some bubbles are in the oil. The use of sharp edges is in order to avoid that no corona discharge occurs during experiment.

Before the experiment proceeds, samples are inspected to ensure the single void is placed between the electrodes. In this experiment, when five new samples are tested, the voltage then needs to be raised slowly until it achieves the expected value. When the voltage is increasing, the magnitude of charge should be around 100pC~1nC in order to ensure one of the samples fails within one day because consistent PD patterns should be recorded every 10mins during the degradation

processes. Generally, a suitable voltage is 12kV~13kV which is applied to the samples. If there are no failures after 6~7 hours, the voltage is increased to 14~16kV to ensure one of the samples breaks down. When one of samples has failed, the other four samples are inspected to observe degradation changes to the single void/silicon rubber interface. The obtained degraded samples are analysed using Raman spectroscopy to identify the chemical content of the degraded areas at the void /silicone rubber interface.

Because the size of the voids of each sample is different to each other due to the manufacturing process, also, temperature and pressure cannot be completely same in the void during stressing period, which will have an influence on PD behaviour. Therefore, only one degraded or two degraded samples are usually found after one of the samples has failed. The other samples do not have observable degradation areas on the voids/silicone rubber interface.

Accordingly, PD measurements on a single sample have been undertaken to observe the transition of PD patterns from beginning to failure. The PD patterns were recorded over one hour. However, in order to obtain possible bow-tie electrical trees and decrease any thermal effect caused by PD to material, the PD magnitude was decreased by manufacturing smaller voids. However, to create PD in smaller voids is more difficult than in bigger voids because the inception voltage for smaller voids is higher and close to maximum applied voltage (20kV). The reason why the maximum applied voltage is 20kV is in order to prevent samples suffering surface flashover. The experiment has divided the magnitude level to three types: 5pC~20pC, 50pC~100pC, up to 100pC. When one of the samples failed, then the degree of degradation is checked for the other samples.

4.5 Phase distributions

The GUI of the Mtronix software has an 'Export Function' option for data acquisition, which the user can use to export PD data to MATLAB. The data is exported when the saved sequence of PD events is replayed in the Mtronix software. Therefore, the user can use and analyse data for other analysis, for example, it can assess the sequence of discharge events and achieving PD phase and charge magnitude distributions. It should be noted that the exported data from Mtronix cannot be read directly by MATLAB because it is saved as a binary file. Thus, MATLAB code has been obtained to read the data. The famous PD characteristics normally used to represent PD measurement results without explaining the PD patterns are total apparent charge per cycle, mean charge and maximum charge magnitude and the number of PDs per cycle. PRPD pattern and φ-q-n plot can be displayed by various PD phase distributions. The normally used PD phase distributions are:

$H_{qs}^{+}(\phi)$ and $H_{qs}^{-}(\phi)$ - Positive and negative total apparent charge magnitude per cycle against phase distribution respectively, where

$$H_{qs}^{\pm}(\phi_i) = \frac{1}{N}\sum_{j=1} q_j^{\pm} n(\phi_i, q_j^{\pm}) \tag{4.1}$$

$H_{qn}^{+}(\phi)$ and $H_{q_n}^{-}(\phi)$ - Positive and negative mean charge magnitude against phase distribution respectively, where

$$H_{qn}^{\pm}(\phi_i) = \frac{H_{qs}^{\pm}(\phi_i)}{H_{n}^{\pm}(\phi_i)} \tag{4.2}$$

$H_{qm}^{+}(\phi)$ and $H_{qm}^{-}(\phi)$ Positive and negative maximum charge magnitude against phase distribution respectively, where

$$H_{qm}^{\pm}(\phi_i) = \max\left|q_j^{\pm}(\phi_i)\right| \tag{4.3}$$

where Φ_i is i-th element of the phase, q_j is j-th element of the charge magnitude and N is the number of cycles.

Each phase distribution above indicates the behaviour of PD activity is related to phase of discharge occurrence. The $H_{qs}(\phi)$ distribution indicates the total apparent charge per cycle at each phase of the applied voltage. The $H_{qn}(\phi)$ distribution shows the average of frequency of discharge events at each phase. However, the $H_{qm}(\phi)$ distribution indicates the tendency of maximum charge magnitude associated with each phase of the applied voltage.

The least mean square error (MSE) of PD phase, $(MSE)_\phi$ and charge magnitude, $(MSE)_\phi$ distributions between measurement and simulation results are calculated using

$$(MSE)_\phi = \frac{1}{360}\sum_{i=1}^{360}\left[H_{qs}(\phi_i)_M - H_{qs}(\phi_i)_S\right]^2 \qquad (4.4)$$

where $H_{qs}(\phi)$ is charge magnitude per cycle against phase distributions while M and S are the measurement and simulation data respectively.

4.6 Summary

The material chosen for the experimental studies reported in this work is Dow Corning Sylgard 184 Silicone Elastomer kit. Samples with a spherical cavity within the silicone rubber have been prepared for degradation experiments under AC electric fields. The method to produce samples involves injecting single voids into a sample using a syringe. The most important factor for success of the method is the choice of pre-cure time and pre-cure temperature, which decide whether the voids remain in the samples or not. The setup of the experiment is

based around the Mtronix PD detector system. The degradation experiment creates degraded samples, which can then be used to analyse degradation processes and identify chemical content of degradation by-products. In addition, the PD data obtained from the degradation experiment can be analysed to understand the changes in PD signature that occur during the degradation process.

Chapter 5 Experimental Results Based on PD Degradation: Void Degradation and Partial Discharge

Following the degradation experiment, nine degraded samples were obtained. Images of the samples have been obtained using an optical microscope. During the PD degradation processes, PD data were recorded every ten minutes in order to analyse any changes in PD behaviour as the samples degrade.

5.1 Images of unmicrotomed degraded samples

The images of Figure 5.1-5.3 were obtained using a CCD camera and microscope. The images in Figure 5.3 show nine degraded voids with damage to the void walls parallel to the mushroom electrodes.

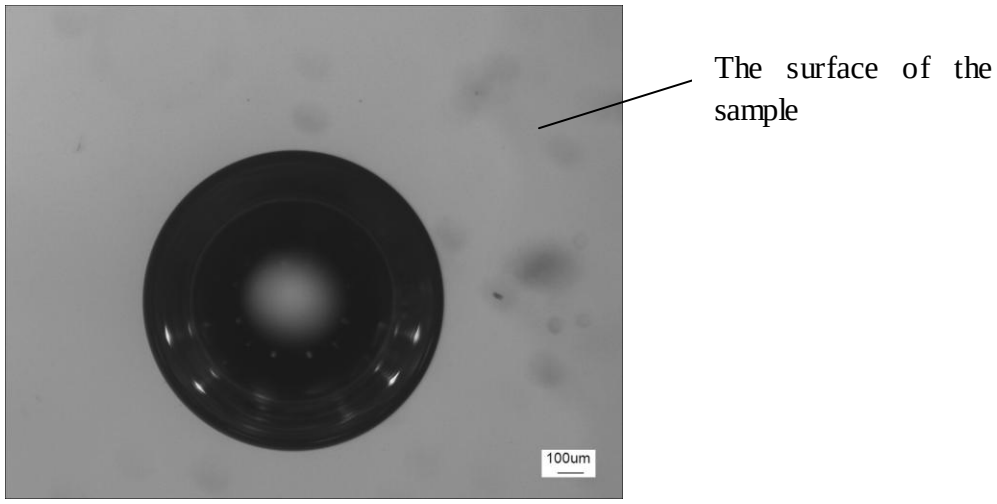

Figure 5.1 An image of the surface of a void for sample 2 before stressing experiment

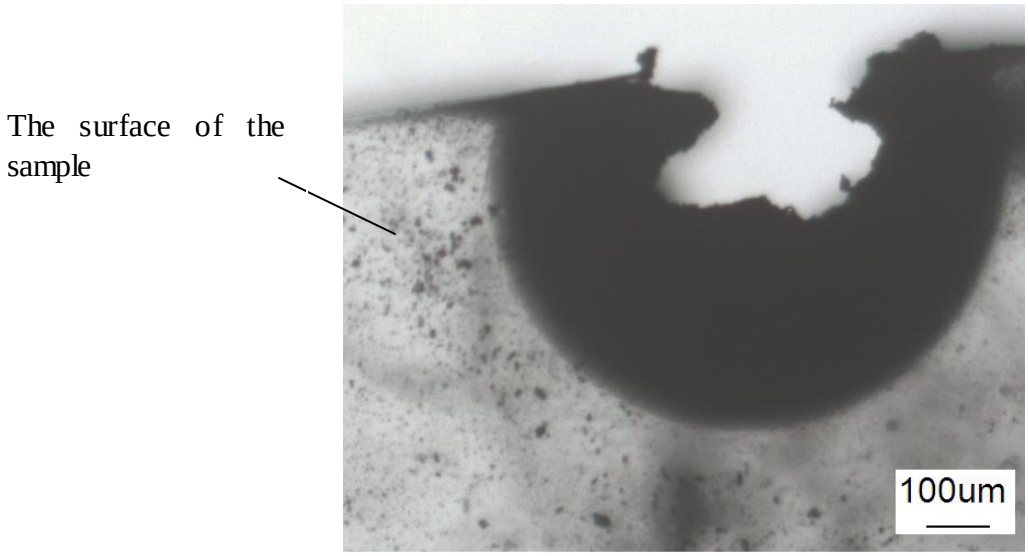

Figure 5.2 An indication of the surface of an electrode bounded cut sample 10

As can be seen from Figure 5.2, the surface of a damaged void of sample 10 is filled with black material (normally carbon). From Figures 5.3.1 to 5.3.4, the surface of voids have been degraded obviously compared with Figure 5.1. It can be seen from the images that the surface of degraded samples have experienced chemical and thermal modification, which has led to increased roughness of the surface. The degradation behaviour is caused by high magnitude PDs which have an apparent charge of 100pC to 200pC. However, crystallization and liquid by-products cannot be assessed from the visible changes on voids. From Figure 5.3.5 to 5.3.9, the four degraded samples experienced different PD magnitude levels (around 100pC for Figure 5.3.5; up to 500pC for Figure 5.3.6 and Figure 5.3.8; 50-100pC for 5.3.7; 5pC-20pC for Figure 5.3.9, respectively). Also, though images indicate voids have been degraded, it is not possible to identify pits or bow-tie electrical trees that have been generated. Therefore, the degraded samples need to be sectioned and then observed by microscope. In addition, from the images, some contaminants (the red area in figure 5.3.1) are on the surface of samples when under microscope. It has been identified that these contaminants are caused by the dust. The surface of samples has been shown in Figure 5.1-5.3.

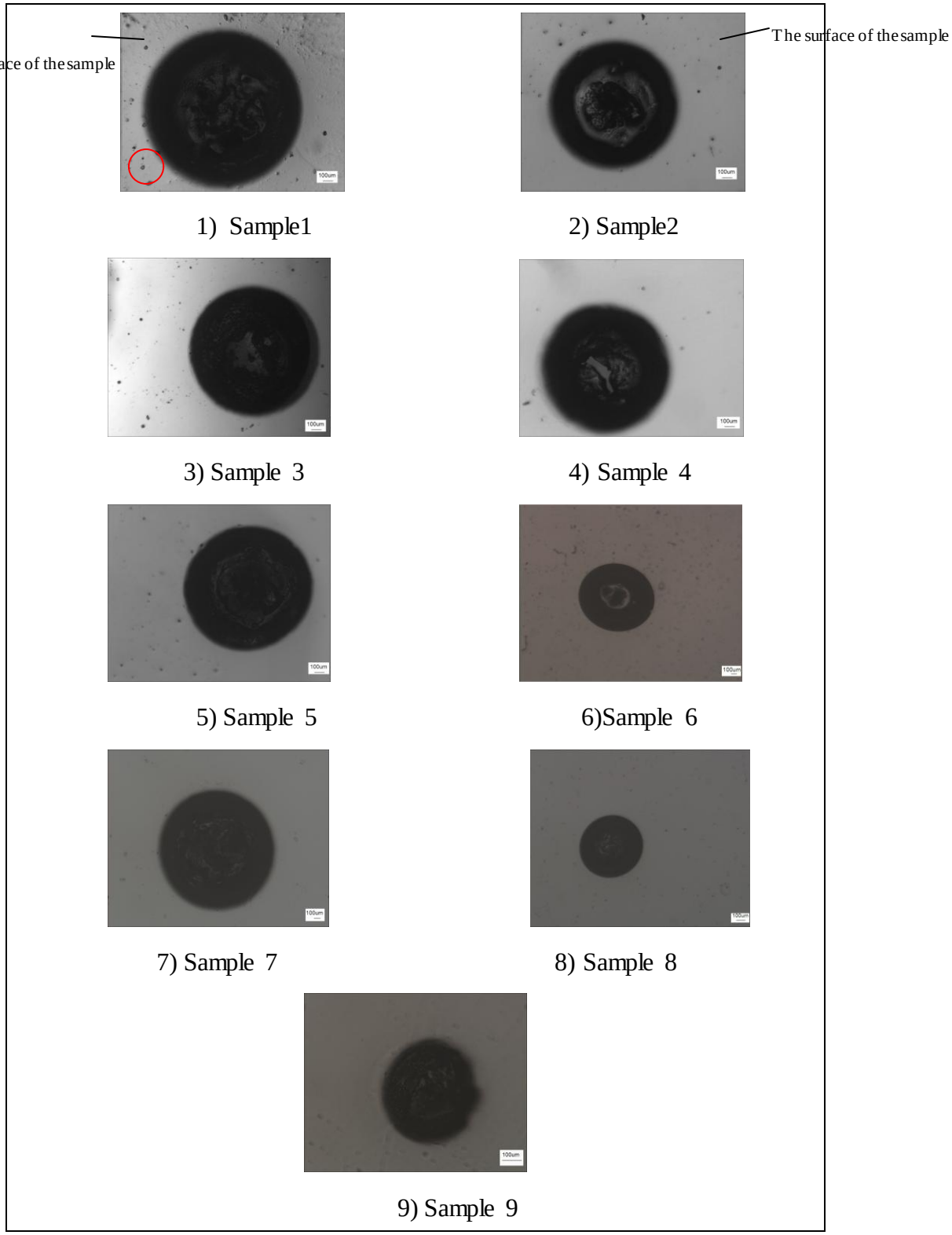

Figure 5.3 Indications of degradation to the surfaces of voids that are in line with the ac applied field

5.2 PD measurement results

In the stressing experiment, five samples are simultaneously electrically stressed under an applied ac sinusoidal voltage of 12kV for 6 hours that is then increased to 15kV until a sample fails. During the stressing period, PD data are regularly acquired. The remaining samples are then inspected for signs of degradation. The experimental setup and samples manufacture have been described in Section 4.2 and 4.3. The PD data obtained from the degradation experiment has been analysed to understand the changes in PD signature that occur during the degradation process.

5.2.1 Void discharge patterns

After 20 minutes, void discharge patterns are observed during the measurement. The typical void discharge patterns have been found in a number of publications [6,32]. The Figure 5.4 shows the PRPD patterns of void discharge behaviour of five degraded samples.

The similar PD patterns have been found by other researchers after around 20 minutes of voltage application. According to [24,32], these PD patterns of five degraded samples are similar with internal discharge. Also, it is found that partial discharge from a void is characterized by the so-called turtle-like or rabbit-like pattern. The patterns of internal discharge are obviously different from the patterns of electrical tree discharges which have a wing-like pattern. The results indicate that internal discharge takes place in the voids before degradation processes occur on the surface of the voids.

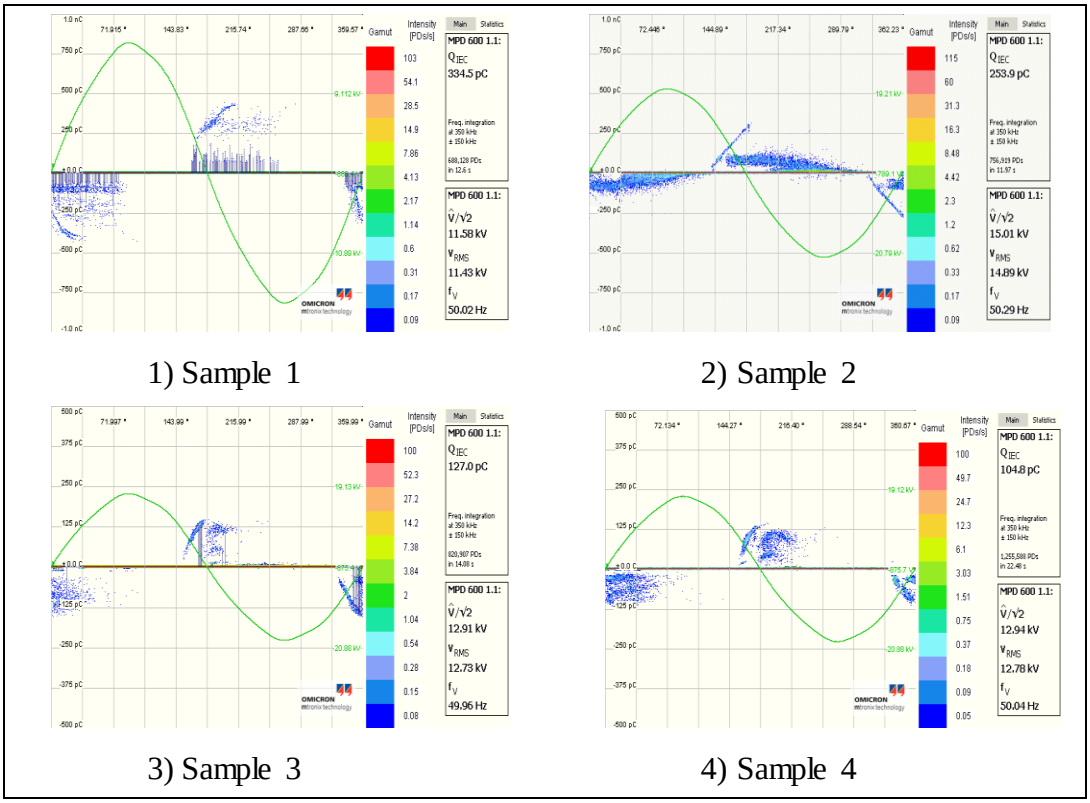

Figure 5.4 Indications of void discharge patterns after 20 mins during degradation processes

5.2.2 PD patterns before breakdown

After 6 hours, PD patterns just before breakdown are observed during PD measurement. The typical tree discharge patterns have been reported by [79]. However, some PRPD patterns shown in Figure 5.5 are very different from typical void discharge patterns or tree discharge patterns.

The similar PD patterns were found after electrically stressing under an applied ac sinusoidal voltage of 11-12kV for 6 hours that is then increased to 12-16kV until a sample fails. According to [79], it is found that partial discharge from an electrical tree is characterized by the so-called wing-like pattern. The patterns of electrical tree discharge are obviously different to patterns of void discharge which are called the turtle-like or rabbit-like patterns. According to observation on PD patterns above, these PD patterns on five degraded samples are different

from electrical tree discharge patterns.

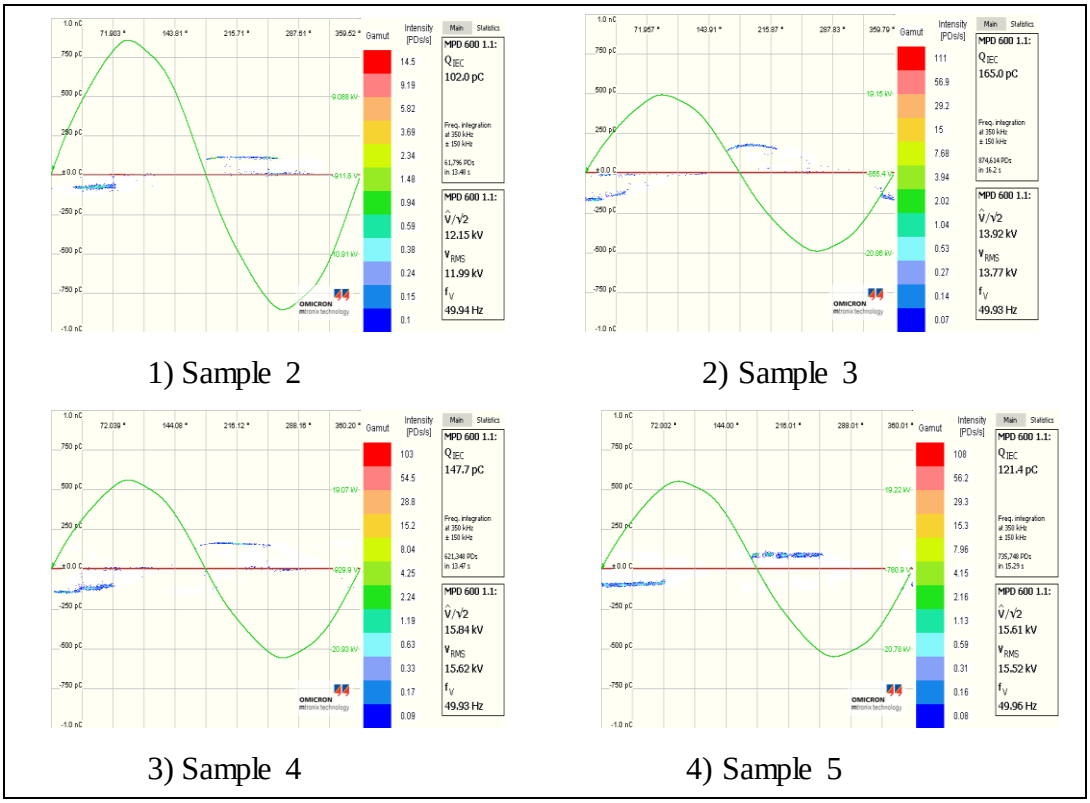

1) Sample 2 2) Sample 3

3) Sample 4 4) Sample 5

Figure 5.5 Indications of PD patterns after 6 hours degradation processes before breakdown

Also, they are different from typical void discharge patterns called turtle-like or rabbit-like pattern Therefore, the change of PD pattern is probably caused by the change of surface conductivity of the void wall due to chemical modification to surface of voids [10] or an increase of electronegative gases such as CO_2 obtained from degradation processes in the voids which may result in greatly increased electron attachment [8]. In addition, according to the images, the voids of five samples have been degraded. Therefore, it can be assumed that the changes of PD patterns may indicate that a degradation process has occurred. In order to identify the assumption further, results from PD measurement and the chemical content of the degraded samples were analysed using Raman spectroscopy.

5.2.3 The transition of PD patterns for single samples

During degradation processes, PD patterns should be acquired. The PD patterns shown from Figure 5.6 to Figure 5.8 have different PD magnitude scales.

As seen from Figure 5.6, there is very high magnitude PD (1nC) during the degradation processes. However, the degradation area includes the thermal damage channel caused by high magnitude PD, which has been shown in images. High magnitude PD may interrupt the formation of electrical trees. Figure 5.7 shows the progression of lower magnitude PD (above 50 pC) during the degradation processes. However, from the images of degraded samples, the degradation behaviour also seems like being caused by thermal damage. The transition of PD patterns for the two samples is similar, which were from turtle-like PD patterns to unidentified PD patterns. Therefore, it can be assumed that the PD transition and PD pattern before breakdown are the same as observed for samples which experience thermal degradation.

In addition, the transition of PD patterns is not consistent in the end of degradation processes in terms of low magnitude of PD. From Figure 5.7, the transition of PD patterns is from turtle like to unidentified PD patterns. However, the transition of PD patterns in Figure 5.8 is from unknown PD patterns to two different kinds of turtle-like patterns. The simulation in Chapter 7 has been used to study the reasons for transition of PD patterns observed as part of the measurement process.

It should be noted that the voltage was decreased from 13kV to 10kV in Figure 5.8 in order to decrease the kinetic energy of electrons and positive ions, which is reasonable to decrease the rate of thermal damage.

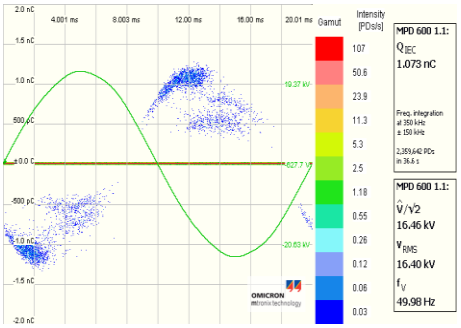

1) 1 hour

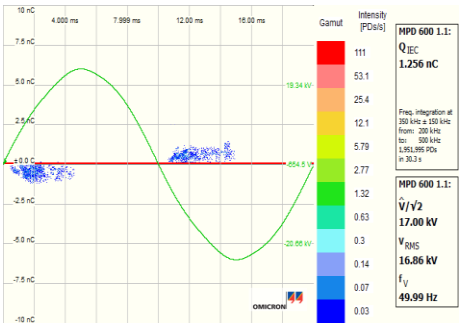

2) 3hours

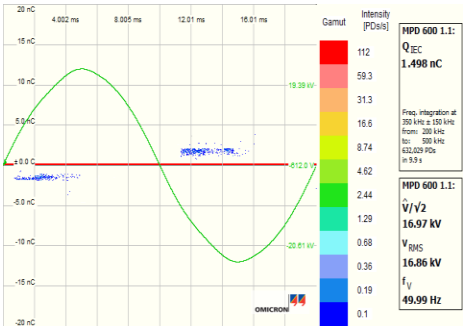

3) 7hours

Figure 5.6 The transition of PD patterns with around 1nC for Sample 6 under 16kV

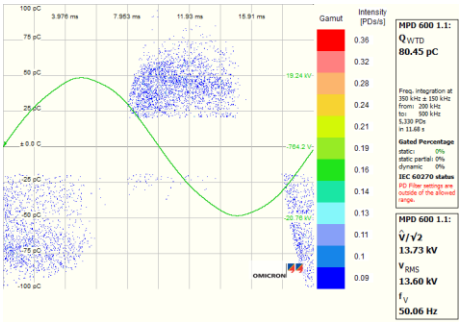

1) 1 hour

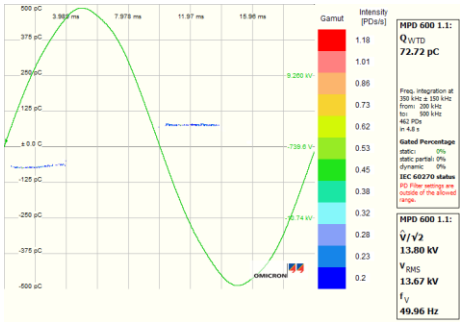

2) 3hours

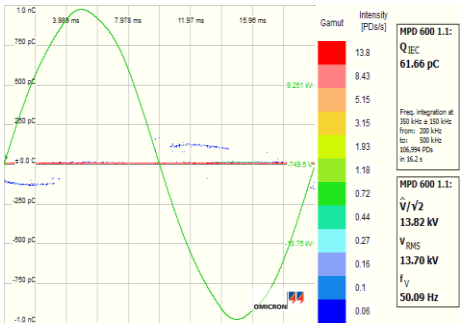

3) 7hours

Figure 5.7 The transition of PD patterns with above 50pC for Sample 8 under 14kV

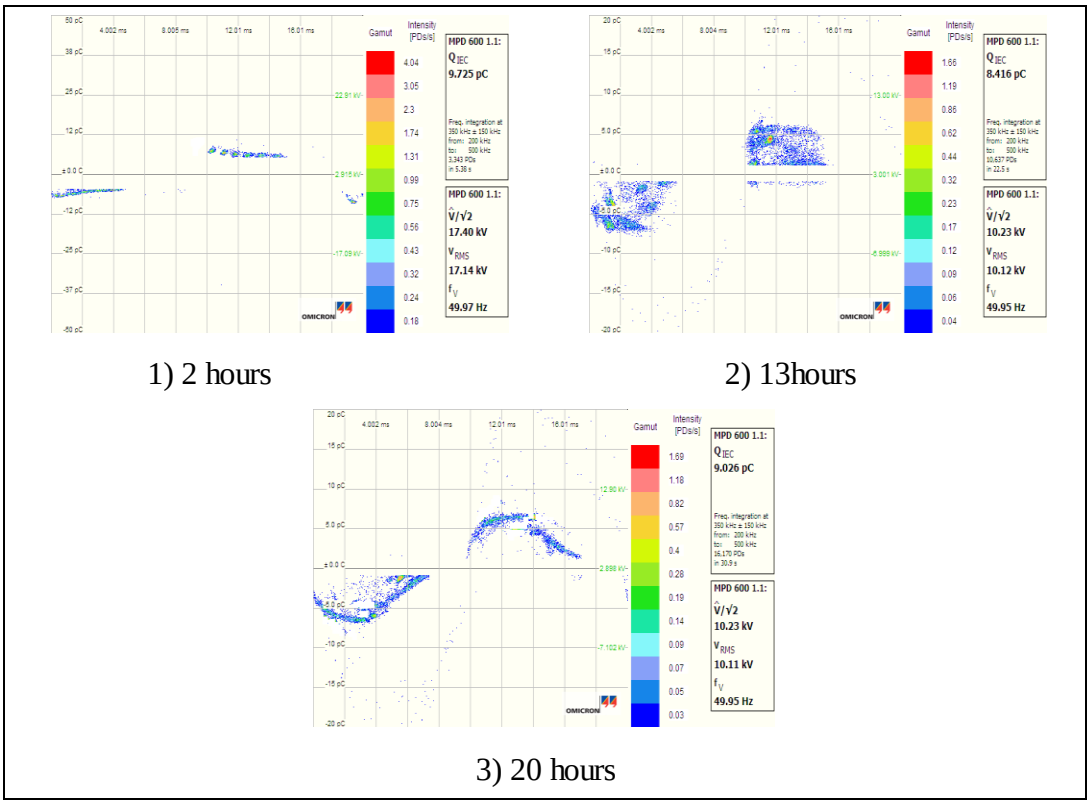

Figure 5.8 The transition of PD patterns with around 10 pC for Sample 9 under 10-13kV

5.3 Images of microtomed samples

Degradation processes were conducting in the silicone rubber samples by degradation experiment as Section 4.4 describes. Nine samples containing degradation areas were then cut open using an RMC MT-7 ultra-microtome equipped with a CR-21 cryo-system set at -110℃ in order to provide a surface containing open segments of degradation areas or pits.

Figure 5.9 consists of a microtomed untested sample, a microtomed breakdown sample and nine microtomed degraded samples. Figure 5.9.1 shows the untested sample 1 before PD experiment, Figure 5.9.2 shows the breakdown sample 10

and Figure 5.10 to Figure 5.12 show the different degraded samples.

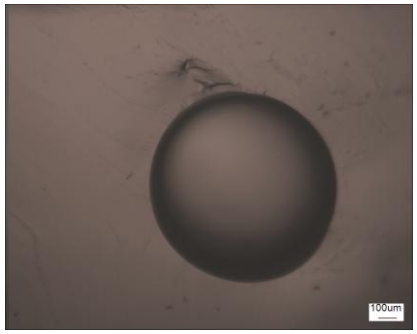

1) Sample 11 before stressing experiment

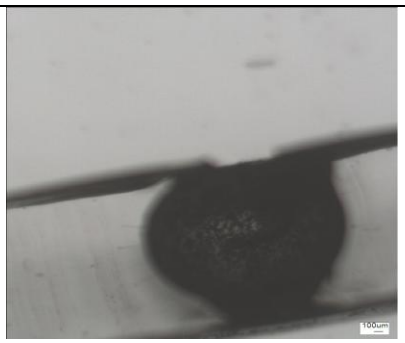

2) A breakdown sample 10

Figure 5.9 The untested sample and breakdown sample

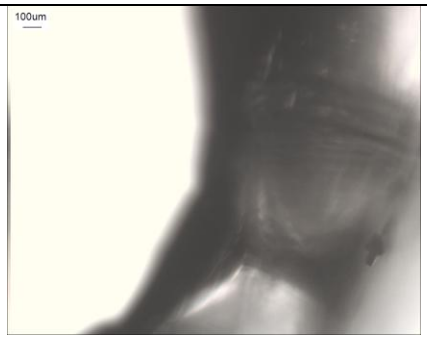

1) Around 1nC for Sample 6

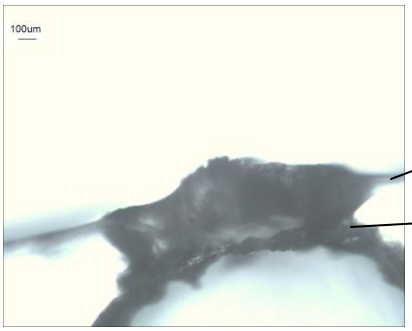

2) Around 300pC for Sample 7

3) Around 50pC for Sample 8

Figure 5.10 The relationship between degradation processes with PD levels

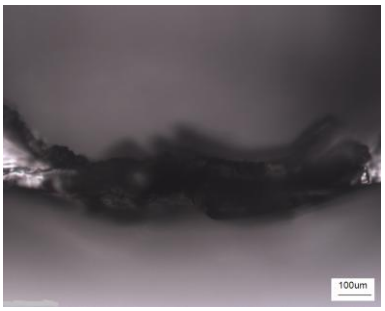

1) Sample 1

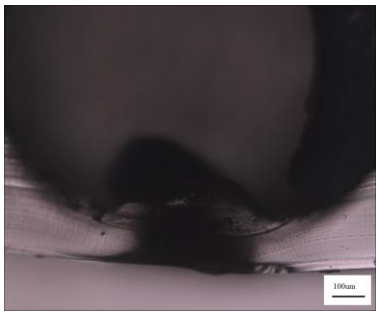

2) Sample 2

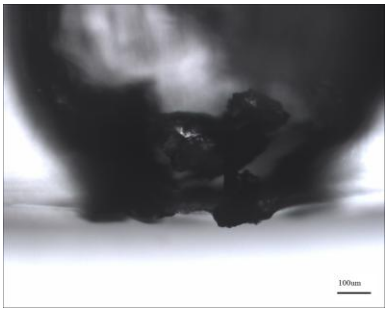

3) Sample 3

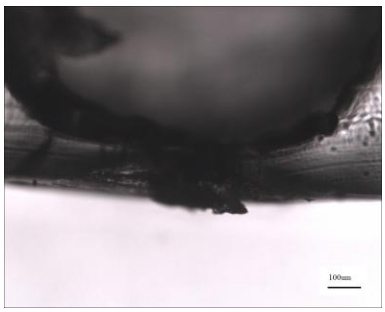

4) Sample 4

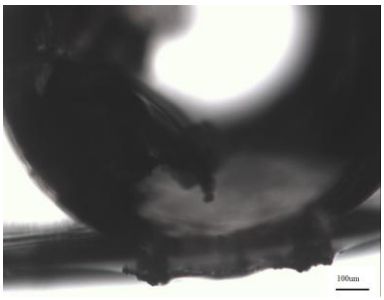

5) Samples 5

Figure 5.11 The evidence of degradation areas and pits

As can be seen from Figure 5.9.2, the inner surface of the failed void of sample 10 is filled with black material (normally carbon) and the interface between the void and sample surface has been carbonized due to high current during breakdown. Also, from Figure 5.10.1 to Figure 5.10.3, the three samples have experienced different PD levels (around 1nC for Figure 5.10.1; around 50pC for Figure 5.10.2; 5pC-20pC for Figure 5.10.3; respectively). As seen from the figures, all degraded areas were thermally damaged due to a large amount of heat.

Moreover, the surface of sample in Figure 5.10.2 has been distorted because of the high gas pressure caused by thermal degradation.

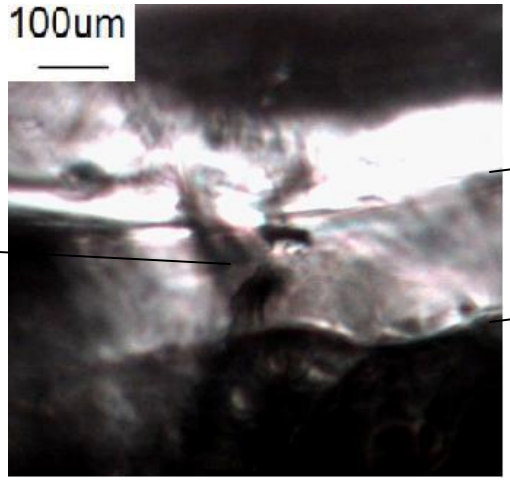

a)

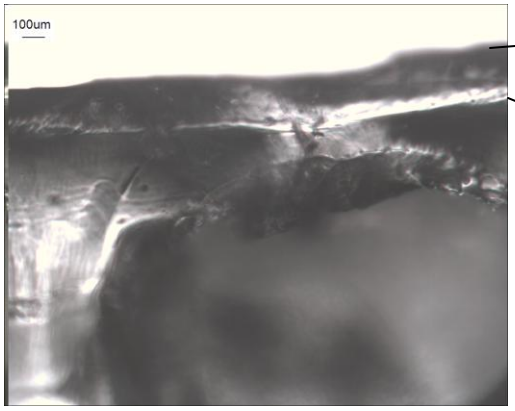

b)

12)

Figure 5.12 The effect of gas pressure during degradation process for Sample 9

From Figure 5.11.3 and 5.11.5, blunt pits have occurred at the voids/silicone rubber interface. Also, there are obvious degradation areas displayed in Figure 5.11.1, 5.11.2 and 5.11.4. However, authors in [4,5] describe that sharp pits may occur from surface of voids before bow-tie electrical trees grow from voids. Therefore, the pits shown in Figure 5.11.3 may be the start of thermal degradation processes. Further experiments were undertaken to identify chemical contents of these microtomed

samples. The method for identifying chemical contents is different from that used in previous section.

From Figure 5.12, the structure of the degradation area seems like channels. It should be noted that the upper surface (in Figure 5.12) of the sample was caused by which the bottom of the cut sample is not smooth, which therefore leads to the channel seems like growing outside upper surface of the sample. After 30 hours, the sample has experienced very low PD with around 10pC, which may be low enough to limit thermal damage but allow formation of electrical trees as electrical trees normally caused by the bond-breaking due to PD. It can be seen that channels have been displayed in the Figure 5.12. Moreover, some degradation areas are underneath the channels, which may be caused by the PD bombardment in the void. Electrical trees are believed to grow from a sharp pit at first. However, from the Figure 5.12, the sharp pits cannot be found. In addition, repeatable experiments to confirm that channels were caused by PD bombardment proved unsuccessful. Therefore, whether the channel was caused by the PD in the void cannot be assumed. Further experiment has identified the chemical content of degradation areas using Raman microscopy analysis and obtained improved images using a scanning electron microscope (SEM).

5.4 Images of breakdown in epoxy resin

The breakdown samples have been obtained by degradation experiment. The set up for degradation experiment and for samples containing voids is same as section 4.2 and 4.3. The degradation experiment processes are same as section 4.4. After a sample failed, no visible degraded samples have been found from the other samples. There are three failed samples displayed in Figure 5.13.

1) Epoxy Sample 1

2) Epoxy Sample 2

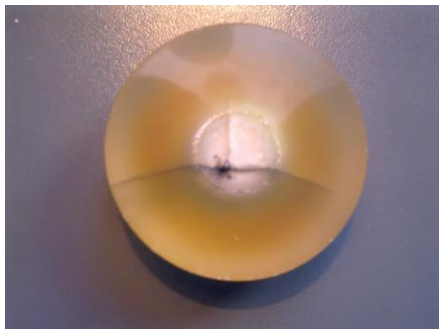

3) Epoxy Sample 3

Figure 5.13 Breakdown epoxy samples containing voids

From Figure 5.13, the three samples have been obviously failed because black areas and cracks can be found in the middle areas. The reason for this behaviour is the three samples have experienced a large number of electrons and positive ions impinging the surface of voids, which results in the gas pressure in the voids increasing and then leads to the severe mechanical damage to the epoxy resin. However, the chemical content of the failed samples cannot be identified. Therefore, Raman spectroscopy has been used to identify the chemical content of breakdown samples.

5.5 Summary

Images shown in this chapter show that voids have experienced degradation processes after images of unmicrotomed samples have been taken by microscope. Also, pits probably have occurred in the void/silicone rubber interface according to the images of microtomed samples. However, authors in [4, 5] describe that sharp pits may occur from surface of voids before bow-tie electrical trees grow from voids. Therefore, the pits shown in the Figure 5.11.3 may be the start of thermal degradation processes. Also, from Figure 5.10.1 to 5.10.3, the three samples have experienced different PD levels (1nC for Figure 5.10.1, 300pC for Figure 5.10.2, 50pC for Figure 5.10.3) respectively. As seen from the figures, all degraded areas were thermally damaged with a large amount of heat. From Figure 5.12, the structure of the degradation area seems to be like electrical channels. After 30 hours, the sample has experienced very low PD of around 10pC, which is reasonable to limit thermal damage but allow formation of electrical trees as the electrical trees normally are only caused by bond-breaking due to PD. Electrical trees normally grow from a sharp pit at first. However, from the Figure 5.12, the sharp pits cannot be seen. In addition, a repeatable experiment to confirm the electrical trees caused by PD bombardment proved to be impossible. Therefore, whether the electrical channels were caused by the PD in the void cannot be assumed. PD results indicate that at an early stage of the degradation processes, PD patterns can be identified as void discharge patterns. At the final stage of the degradation process before breakdown, PD patterns cannot be assured because different PD patterns have been found compared to void discharge patterns and electrical tree discharge patterns. Therefore, the change of PD pattern is probably caused by the change of surface conductivity of the void wall due to chemical modification to the surface of the voids [10] or increase of electronegative gases such as CO_2 obtained from

degradation processes in the voids which result in increased capability of electron attachment is strong [8]. From the experiment on a single sample, the transition of PD patterns is similar as the samples degrade. However, the PD transition for the sample which only experiences low magnitude PD is different from the others. Further investigation has been undertaken through comparing the PD patterns and pulses between experimental and simulated results and this is described in the Chapter 7.

Chapter 6 Experimental Results Based on PD Degradation: Raman and SEM microscopy

Following the degradation experiment, nine degraded samples were obtained. Images of the samples have been obtained using scanning electron microscope (SEM). Raman spectroscopy has been used for analyse the chemical content of degraded areas of unmicrotomed samples and microtomed samples respectively.

6.1 Raman microprobe analysis on surface of voids of unmicrotomed samples

The Raman effect was discovered in the 1920s [99] yet which is with the invention and development of lasers and computation equipment, that it has been used as a spectroscopy technique. In its most basic terms, Raman spectroscopy involves using a monochromatic light source (such as a laser) to excite the molecules in a material into vibration. These vibrations are indicative of the molecule in question and a number of the light is reflected back elastically, however, a proportion of it is scattered inelastically. This change in frequency is indicative of the molecule. Therefore, it provides a 'fingerprint' of the molecular structure of the sample.

After observing images obtained from the microscope, the surface of voids have been degraded obviously compared with voids which do not experience PD. Though the images indicate voids have been degraded, it cannot identify this. Therefore, Raman spectroscopy is used to identify carbon content from surface of voids.

Samples were characterised at various positions on the surface of voids using a Lecia microscope coupled to a Renishaw Raman RM1000 system using a Renishaw NIR 780TF semiconductor diode laser (wavelength 780 nm) of power 50 mW. The spectrometer was set up in line with Renishaw's recommendations for confocal operation of the spectrometer. All spectra were obtained using an extended scan between 3500 cm^{-1} and 100 cm^{-1} and were built up of 25 accumulative scans of 10 s and were processed using SigmaPlot 10. The spectra to the surface of voids are described in Figure 6.1.

Figure (6.1(1)) shows six spectra, D1 to D6 that were measured for Sample 1 at six random different positions on the surface of the void. There are signs of silicone and some fluorescence, however, no evidence of graphitic carbon appear in this graph. Figure (6.1(2)) also shows six spectra, D1 to D6 that were measured for Sample 2 at six random different positions on the surface of the void. There are signs of silicone and some fluorescence, and no presence of graphitic carbon on the surface of the void as well. Figure (6.1(3)) also shows six spectra, D1 to D6 that were measured for Sample 3 at six random different positions on the surface of the void. However, Figure (6.1(3)) indicates the D and G bands of graphitic carbon (arrowed) between 1310 and 1590 cm^{-1} [100]. Figure (6.1(4)) shows six spectra, D1 to D6 that were measured for Sample 4 at six random different positions on the surface of the void. Figure (6.1(4)) indicates that for all spectra are similar with organic matrix. Figure (6.1(2)) shows six spectra, D1 to D6 that were measured for Sample 5 at six random different positions on the surface of the void. Figure (6.1(5)) shows signs of silicone and some fluorescence, however, also no evidence of graphitic carbon is present.

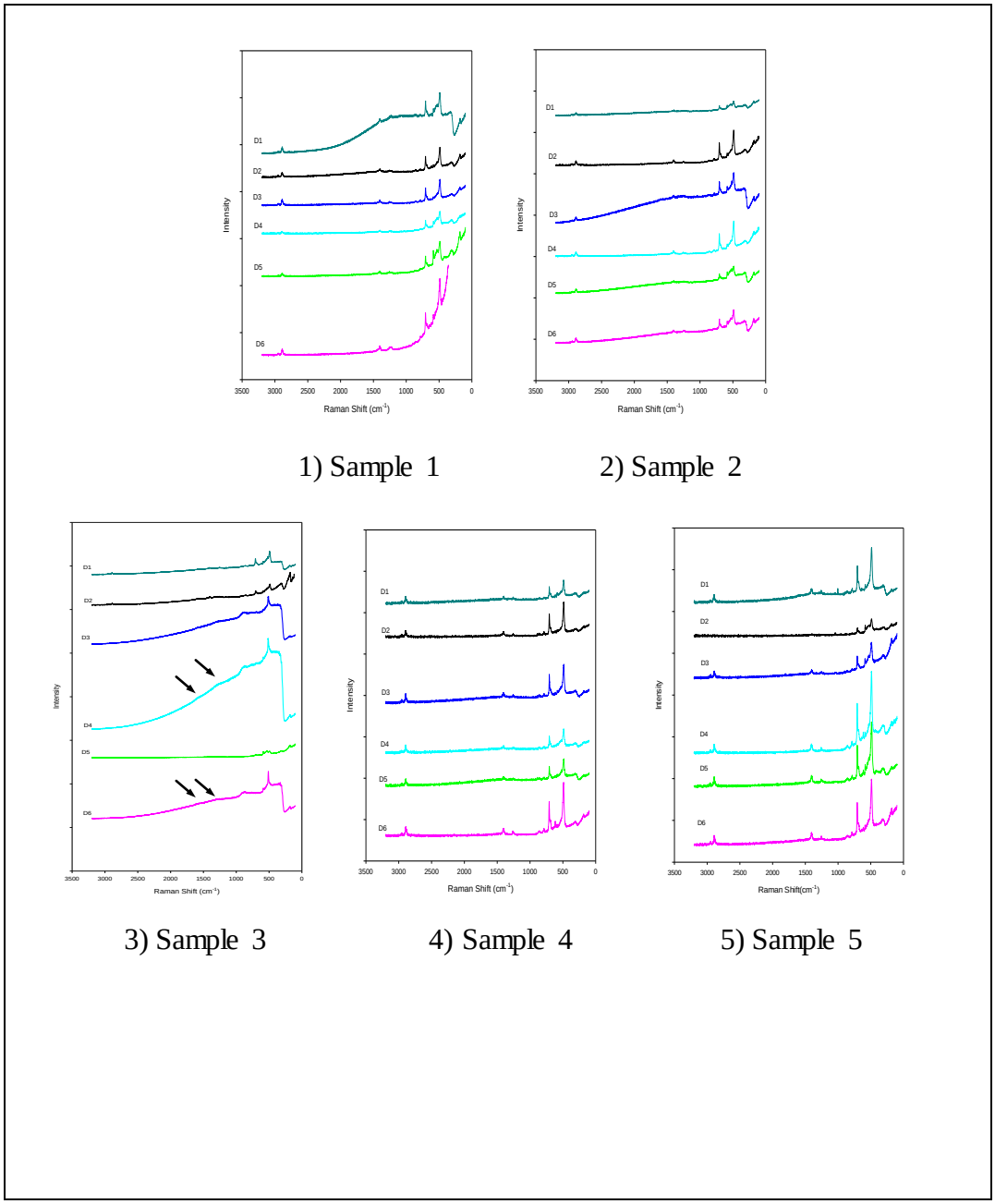

Figure 6.1 Raman spectra of positions for degraded unmicrotomed samples (D1-D6 are six random different points on degradation areas for each sample)

The presence of carbon in a void/silicone rubber interface indicates that degradation processes of the void involves the degradation of the bonds between the polymer backbone, which consist of silicone and oxygen, and the side groups of the polymer chain that contain carbon. Thus, it indicates the pits may be formed but no evidence of electrical bow-tie trees has been found. The presence of carbon found in aged PE samples in previous work [100] indicates chain

scission of the polymer backbone itself, this was also the case with silicone rubber.

Additionally, in all the spectra the typical peaks relating to silicone rubber can be seen between 200 and 900 cm^{-1} and these peaks of most of spectra are superimposed on varying degrees of fluorescence. Fluorescence is a substance which commonly appears in Raman spectroscopy especially in the case of contaminated or degraded samples [100]. The reason why there appears to be little or no fluorescence in Figure (6.1(4)), (6.1(5)) is unclear but as the associated degradation is a localised phenomenon, the lack of fluorescence could be due to the lack of degradation area below the surface at the points of analysis, as there was with the PE samples tested by Vaughan et al [100]. Therefore, the results cannot completely identify whether pits grow from voids or not. Further identification experiments should be conducted to confirm this.

6.2 SEM microscopy on microtomed samples

SEM can be used to obtain images of samples on a scale of microscope through the application of a high energy electron beam. Electrons are thermionically created from an electron gun which is with a tungsten filament cathode (though Lanthanum Hexaboride (LaB6) and field emission methods are be more widely used) and are focused on the sample. This beam interacts with the atoms in the sample surface and creates different emissions. Different categories of signal can be created by emissions which includes secondary electrons, back scattered emission, X-rays and light. Secondary electrons are created as ionization products of the electron beam (which has much more energy than the ionization potential) exciting the atoms in the sample and secondary electrons are most widely applied in SEM, though a machine maybe have used multiple detectors to obtain more than one signal. The electron beam makes a movement across the sample by a ‘raster’ pattern. The secondary electrons are detected and the signal is shown as an image of variation of

brightness related to the intensification of the signal emitted from each point. This results in images with a large depth of field where surfaces away from the detector are darker and the surfaces closer to the detector are brighter due to a larger number of secondary electrons measured [101].

SEM imaging is a suitable method to analyze electrically aged polymeric insulators as it supports high magnification images of the areas of electrical degradation which are interesting on the sample. The magnification can change from x10 to x500, 000 [102] and the resolution between less than 1 and 20 nm relying on the specification of the SEM instrumentation. One restriction to SEM imaging is that it is surface restricted and cannot be used to detect areas that are below the surface of a transparent sample. The only method to detect areas that are below the surface of a transparent sample by SEM is to reveal the surface of the features using methods such as microtomy.

Another problem to SEM is that the surface of the sample can be charged due to the incident electrons, which are increasingly becoming problem on non-conducting samples, which results in distorting images. The different categories of charging are general (through the whole surface), edge (high features), area (from different areas across the sample), line by line (leading to bright streaks across the image) and residual charging (due to the previous scan). These impacts can be decreased and the better images can be obtained by balancing the incoming beam electrons to the outgoing sample electrons, by choosing the parameters such as increasing voltage and spot size and finally by carrying out the imaging in a vacuum include samples which can be coated in a conductive layer.

Samples are sputter coated with gold (though other metals can be used relied on the category of sample) [103] in order to make the surface of the sample electrically conductive and earthed in order that electrostatic charge cannot accumulate. A

best application of SEM is field emission gun SEM (FEG-SEM) [104] which uses an electron gun that creates a sufficient potential gradient to result in field electron emission. The electron beam by this method is smaller in diameter than traditional methods mentioned earlier, which leads to a better signal to noise ration and spatial resolution. Another application of SEM is environmental SEM (ESEM), which images can use to be obtained from 'wet' or uncoated samples due to a gaseous environment within the sample chamber to make dispersion on the charge [105]. This is especially useful for biological specimens which are probably damaged by the sputter coating behavior. Many other applications to SEM imaging are used before and it is often used to be related to other analytical methods such as x-ray microanalysis [103, 106]. It should be noted the imaging has been applied in this study and a description of other methods has not been shown here.

SEM images were obtained using a FEG-SEM instrument on a number of samples through the study. After the samples were prepared and fixed onto SEM stubs and sputter coated with gold, they were inserted into the imaging chamber and placed under a vacuum of 2×10^{-5} mbar. An accelerating voltage of 15 kV and a spot size of 5.0 nm were used to obtain the images in this study. These parameters were selected in order that better images can be obtained efficiently and also it can avoid over charging the sample. The SEM images which are related to the surface of microtomed voids are shown in Figure 6.2.

Figures 6.2 show a selection of SEM images for the split voids. Figure 6.2.1 is an image of the untested void, Figure 6.2.2 is a detail of failed void and Figure 6.2.3 to 6.2.7 are images of the degraded voids. As can be seen from Figure 6.2.1, the surface of void is very smooth and no cracks and protrusions. However, the reason why there is a few debris in the centre of void is the fragments of silicone rubber fall to the inner surface of the void when microtoming the samples. As can be seen

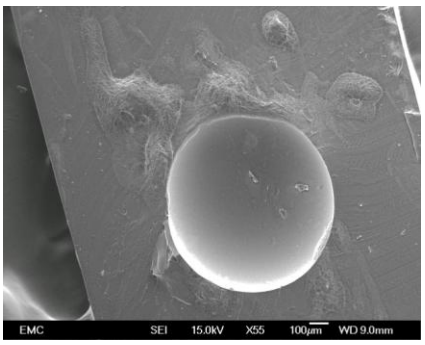

1) Sample 11 before PD experiment

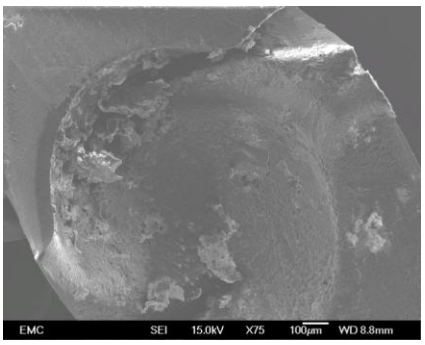

2) breakdown Sample 10

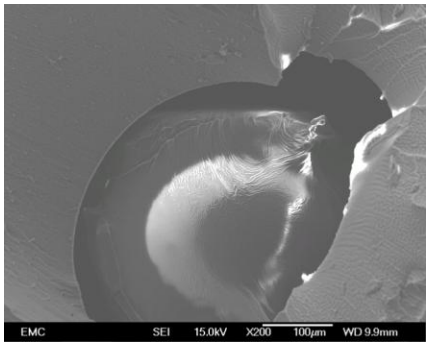

3)Sample 5

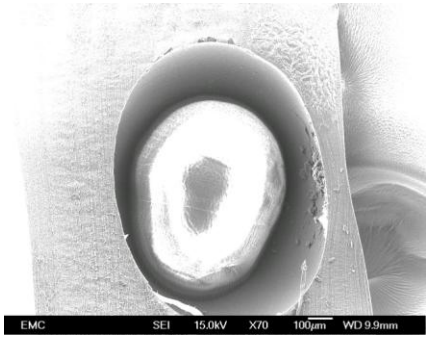

4) Sample 6

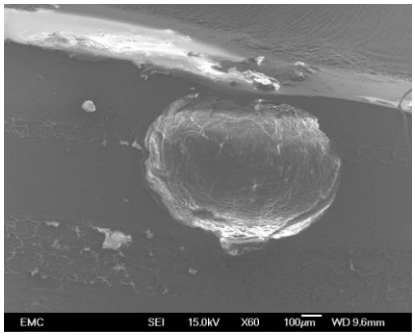

5) Sample 7

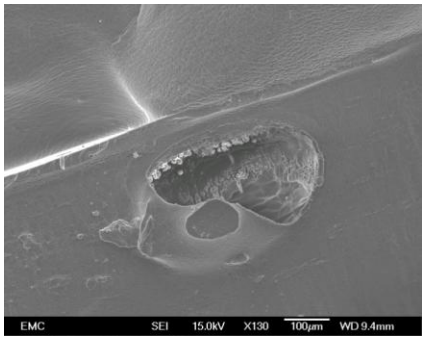

6) Sample 8

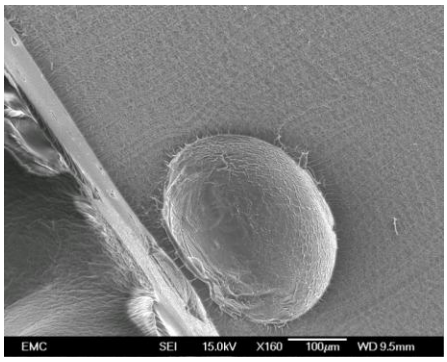

7) Sample 9

Figure 6.2: SEM images of (1) untested void, (2) failed void and (3-7) degraded voids

in figure 6.2.2, large protrusions have formed around the edges of the void. These protrusions are fairly large in comparison to the other samples and are nodular in appearance However, figure 6.2.3 shows there are no cracks and protrusions around the edges of the void because the void probably has not been cut open and a thin layer of silicone rubber is on the top of the degraded void. Figure 6.2.4 shows in the image of the whole void, it can be seen that it has an uneven surface with some protrusions around the edges of void. As can be seen in figure 6.2.6, large protrusions have formed around the edges of the void. These protrusions are fairly large in comparison to the other degraded samples and are nodular in appearance. Figure 6.2.5 and figure 6.2.7 shows the void surfaces are again not uniform and have large cracks and some protrusions across the surface. These cracks are possibly a response to the gas pressure during aging. However, the interface between voids and silicone rubber is smooth and no crack or protrusions. The reason is the surface of channels at the interface are not revealed as open because the size of channels is too small to see where the surface of the channels has been microtomed

6.3 Raman microprobe analysis on surface of voids of microtomed samples

Samples were then characterised at various positions around degradation area using a Lecia microscope coupled to a Renishaw Raman RM1000 system using a Renishaw NIR 780TF semiconductor diode laser (wavelength 780 nm) of power 10 mW. The detailed setup is similar with that described in section 6.1. The spectra (A1-A3; B1, B2; C1, C3) of five samples on degradation areas, area close to degradation area and area far away from degradation area and the spectra. The spectra (A1-A3) of four samples on degradation areas are described in Figure 6.3 and Figure 6.4. The five graphs in Figure 6.3(1) to Figure 6.3(5) all show seven spectra (A1-A3; B1, B2; C1, C2) which separately describe degradation areas, area

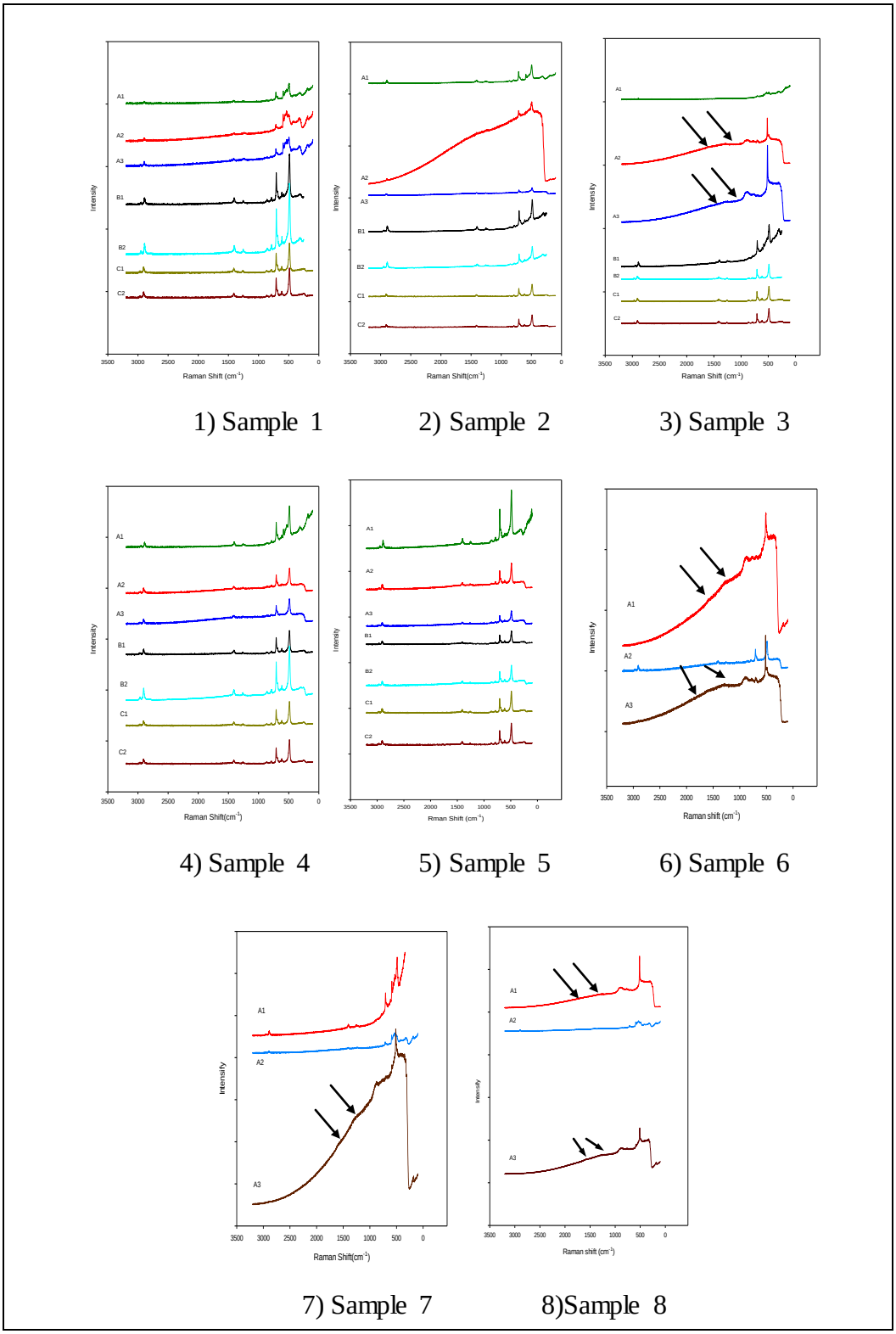

Figure 6.3 Raman spectra of positions for degraded microtomed samples (A1, A2, A3 indicate points in degradation area; B1, B2 indicate points in area close to degradation area; C1, C2 indicate points in area far away degradation area)

close to degradation area and area far away from degradation area. Specifically, the spectra A1, A2 and A3 describe degradation areas in Figure (6.3(1)) shows signs of silicone and some fluorescence, however, no evidence of graphitic carbon appear in the degradation area. The spectra B1, B2 (areas close to degradation area) and spectra C1, C2 (area far away from degradation area) in Figure (6.3(1)) are all similar to the organic matrix.

The spectra A2 describing degradation areas in Figure (6.3(2)) shows large amount of fluorescence, the spectra A1, A3 shows the sign of silicone which is similar as spectra B1,B2 (areas close to degradation area) and spectra C1,C2 (area far away from degradation area). However, these spectra all show no presence of graphitic carbon.

The spectra A2, C1 indicating degradation areas in Figure (6.3(3)) indicate the D and G bands of graphitic carbon (arrowed) between 1310 and 1590 cm^{-1} [100], but the spectra A1 (degradation area) only shows the sign of silicone which is similar as spectra A3, B1 (describing areas close to degradation area) and spectra B2, C2 (area far away from degradation area).

The spectra A2 and A3 (degradation area) in Figure (6.3(4)) indicates signs of silicone and a little amount of fluorescence, but the spectra A1 (degradation area) only shows signs of silicone. However, these three spectra all show no presence of graphitic carbon. The spectra B1 (areas close to degradation area) and spectra carbon appears in the degradation area. The spectra B1 (areas close to degradation area) and spectra C1, C2 (area far away from degradation area) in Figure (6.3(5)) are all similar with organic matrix, but the spectra B2 (areas close to degradation area) shows some fluorescence.

The spectra in Figure (6.3(6)), (6.3(7)), (6.3(8)) all indicate the D and G bands of

graphitic carbon (arrowed) between 1310 and 1590 cm^{-1} [102], which has been scanned on the degradation areas.

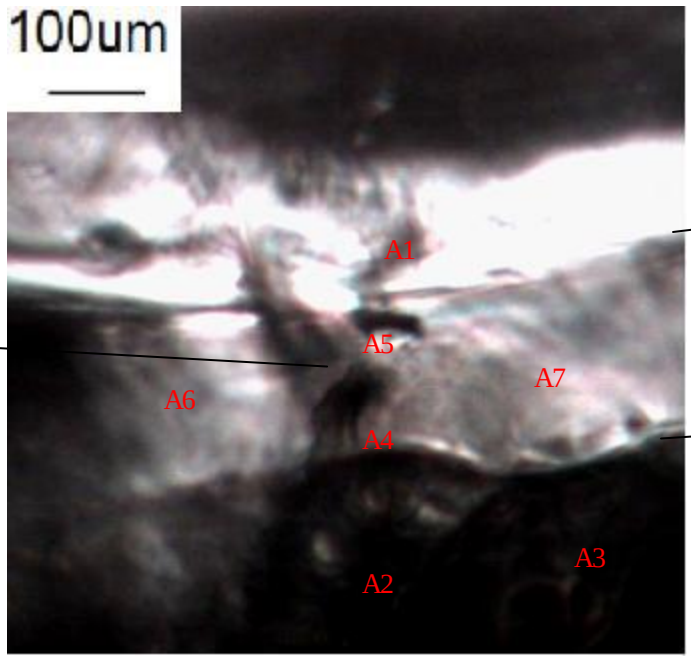

1)

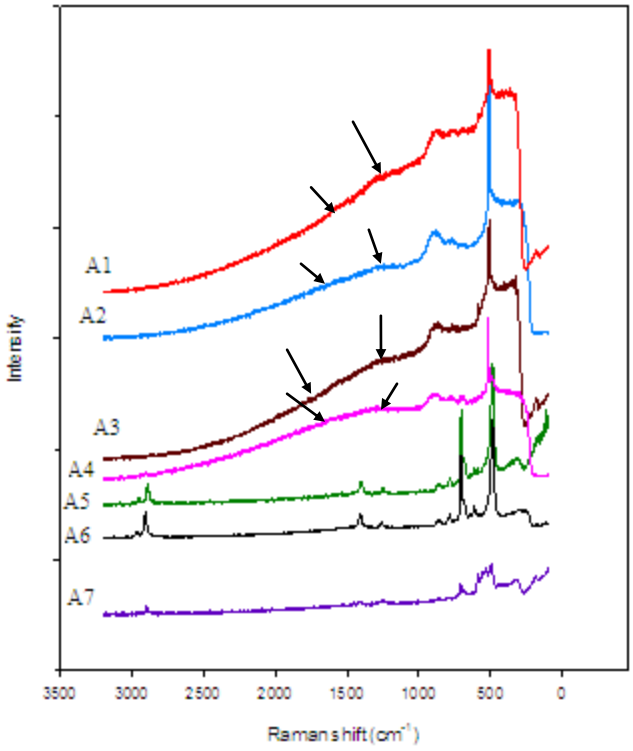

2)

Figure 6.4 1) Image of the microtomed sample 9 2) Raman spectra of positions for the microtomed sample 9

In addition, the spectra A1, A2, A3 and A4 in Figure (6.4(2)) indicate the D and G bands of graphitic carbon (arrowed) between 1310 and 1590 cm^{-1} [100]. The spectra A5, A7 only show signs of silicone and a little amount of fluorescence. The spectra A6 is similar to the organic matrix.

The presence of carbon in the degradation area of a microtomed void indicates that a degradation process of the void involves the degradation of the bonds between the polymer backbone, which consist of silicone and oxygen, and the side groups of the polymer chain that contain carbon. Thus, it further identifies the pits have grown from a void. The presence of carbon has been found in aged PE samples in previous work [100].

In addition, in all the spectra the typical peaks relating to silicone rubber can be seen between 200 and 900 cm^{-1} and these peaks of the spectra describing degradation area and areas close to degradation area are superimposed on varying degrees of fluorescence. Fluorescence is a substance which commonly appears in Raman spectroscopy especially in the case of contaminated or degraded samples [100]. Fluorescence appearing on these spectra shows that degradation behaviour has taken place on the interface between voids and silicone rubber. Moreover, it indicates that the areas close to degradation area have been impacted by degradation processes. The reason why there appears to be little or no fluorescence on some spectra of degradation areas is unclear but as the associated degradation is a localised phenomenon, the lack of fluorescence could be due to the lack of degradation area below the surface at the points of analysis as there was with the PE samples tested by Vaughan et al [100].

6.4 Raman microprobe analysis for breakdown in epoxy resin

The method for Raman microprobe analysis is the same as section 6.1. The five spectra representing random positions in the breakdown areas of three samples are shown in Figure 6.5.

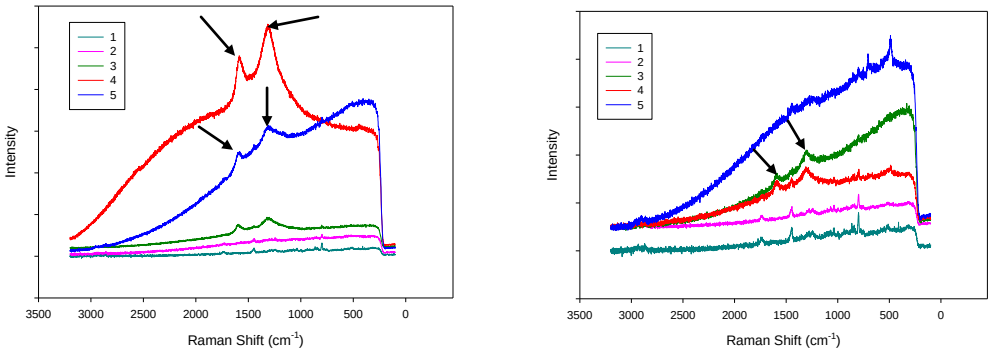

1) Epoxy Sample 1

2) Epoxy Sample 2

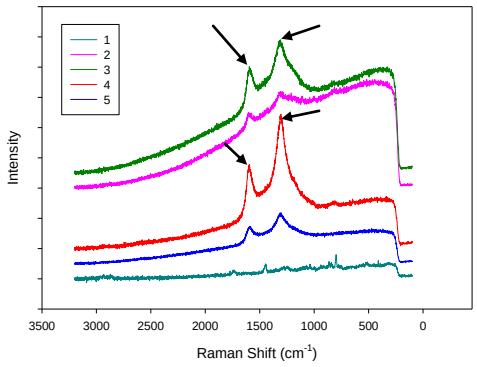

3) Epoxy Sample 3

Figure 6.5 Raman spectra of positions for failed samples (Random points 1 to 5 on breakdown areas for each sample)

In Figure (6.5(1)), the spectra 1 only shows signs of epoxy resin. The spectra 2 shows signs of epoxy resin and a little amount of fluorescence. The spectra 3,4,5 all indicate the D and G bands (arrowed) of graphitic carbon between 1310 and 1590 cm^{-1} [105]. In Figure (6.5(2)), the spectra 1, 2 only shows signs of epoxy resin. The

spectra 3,4 all indicate the D and G bands (arrowed) of graphitic carbon between 1310 and 1590 cm^{-1} [100]. The spectra 5 shows a large amount of fluorescence. In Figure(6.5(3)), expect for spectra 1, the other spectra all indicate the D and G bands (arrowed) of graphitic carbon between 1310 and 1590 cm^{-1} [100].

The presence of carbon in the breakdown areas of breakdown samples indicates that a degradation process of the void involves the degradation of the bonds between the polymer backbone and the side groups of the polymer chain that contain carbon. In addition, in some spectra the typical peaks relating to epoxy resin can be seen between 200 and 1300 cm^{-1}, which is different from that of silicone rubber and the peaks of all the spectra are superimposed on varying degrees of fluorescence. Fluorescence is a substance which commonly appears in Raman spectroscopy especially in the case of contaminated or degraded samples [100].

6.5 Summary

The SEM technique has been used to identify further the degradation processes. For the untested void, the SEM image shows that there are no cracks and protrusions on the surface of the void. For the failed void, it can be seen that large protrusions have formed around the edges of the void and these protrusions are fairly large in comparison to the other samples and are nodular in appearance. For the degraded voids, the large cracks and some protrusions appear on the surface of most of degraded voids, which indicates the voids have experienced degradation processes. Raman results show that different degree of fluorescence has been found on some degraded unmicrotomed samples. In addition, carbon content has been found on a degraded unmicrotomed sample. For microtomed samples, different amounts of fluorescence also appear on the degradation areas of microtomed samples. Small amounts of fluorescence appears on the areas close to degradation area. No

fluorescence can be found on areas far away from degradation areas. Carbon content has been also found on the degraded area of a microtomed sample. Fluorescence appears from spectra of unmicrotomed and microtomed samples shows that the scanned areas have been degraded. The presence of carbon content shows that the pits probably grow from the void. Additionally, the Raman spectroscopy for breakdown of epoxy resin containing voids has been performed. The spectra obtained from breakdown areas indicate D and G bands of graphitic carbon dominate the spectrum. The carbon and the fluorescence detected by Raman has confirmed the areas shown in images have been degraded and the degradation areas cause chain scission of insulation material and higher conductivity of surface of voids which is in agreement with the Raman results which show carbon content and the fluorescence appear. The higher conductivity of the surface of voids may lead to the distortion of local electric fields, which probably has an impact on degradation processes.

Chapter 7 Comparison between Measured and Simulated PD patterns

7.1 The revised Partial discharge model

The revised PD model developed in this work is based on the Finite Element Analysis (FEA) model described in [24]. The development of the model that consists of a spherical cavity within a solid dielectric material using FEA method to model PD activity during degradation processes is detailed in this chapter. Also, the equations associated with this model are introduced in the Appendix A, which is originally from Illias's PhD thesis [2]. The two-dimensional model geometry using the FEA method, equations associated with the model and the flowcharts of the MATLAB code are explained. The PD modelling section is separated into several sub sections; FEA model equations, development of the model, local field enhancement, discharge process model, discharge magnitude calculation, temperature variation in the void because of PD, surface charge decay via conducting processes along the wall of cavity after a PD takes place and the electron generation rate. For simplifying the simulation model, several assumptions have been applied in this model.

The model has been applied to simulate partial discharge (PD) behaviour during degradation processes. The obtained simulation results are then in comparison with measurement results to assure the critical parameters influencing PD activity and to confirm physical mechanisms having an impact on PD behaviour for different conditions. The critical parameters include the inception and extinction fields, effective charge decay time constant and the cavity surface conductivity.

The physical mechanisms which can be confirmed from this model which are related with PD behaviour are conduction of charge along the cavity wall, electron generation rate process, the electron generation rate and temperature variation in the void.

7.1.1 Finite Element Analysis model

The model is performed in two-dimensional (2D) axial symmetric COMSOL software and is interfaced with MATLAB programming code [107]. Partial Differential Equations (PDE) can solve the electric potential and temperature in the model.

PDE equations are provided into Ordinary Differential Equations (ODE) and ODEs are solved. By developing the model using 2D axial symmetric geometry, the simulation time can be decreased due to the request of less mesh elements. Two application modes are applied to solve the problem in the model, `Meridional Electric Current' and `Heat Transfer by Conduction'. In the `Model Navigator' window of COMSOL, the `2D Axial Symmetry' space dimension is applied and the `Quasi Statics, Electric' is chosen under the `AC/DC Module' to solve the electric field distribution and `Conduction' under `Heat Transfer Module' is added to the Multiphysics to deal with the temperature distribution in the model.

7.1.1 1 Field model equation

The distribution of electric potential in the dielectric is introduced by the field model. The fundamental governing equations of the field model are

$$\vec{\nabla} \cdot \vec{D} = \rho_f \tag{7.1}$$

$$\vec{\nabla} \cdot \vec{J}_f + \frac{\partial \rho_f}{\partial t} = 0 \tag{7.2}$$

where Equation 7.1 is the field model equation, Equation 7.2 is the current

continuity equation, $\vec{D}$ is the electric displacement field, ρ_f the free charge density or unpaired charge density and $\vec{J}_f$ is the free current density [108]. It is hypothesized that the dielectric model is a linear isotropic, non-dispersive material with an instantaneous polarization which is related to slowly variation field, Equation 7.3 can be written as

$$\vec{\nabla}\cdot\vec{D} = \vec{\nabla}\cdot(\varepsilon\vec{E}) = -\vec{\nabla}\cdot(\varepsilon\vec{\nabla}V) \tag{7.3}$$

According to equation 7.3, $\vec{E}$ is the electric field, V is the electric potential and ε is the permittivity of the material. Since $\vec{J}_f$ is equal to $-\sigma\vec{\nabla}V$ and ρ_f is equal to $-\vec{\nabla}\bullet(\varepsilon\vec{\nabla}V)$ where σ is the electric conductivity, Equation 7.4 can also be written as

$$-\vec{\nabla}\cdot(\sigma\vec{\nabla}V) - \vec{\nabla}\cdot\frac{\partial}{\partial t}(\varepsilon\vec{\nabla}V) = 0 \tag{7.4}$$

FEA is used to solve Equation 7.4 and assure the electric potential in the model.

7.1.1.2 Heat transfer equation

In order to study the temperature distribution in the cavity because of a PD, it is assumed that the heat energy is from electron ionization during a PD is transferred to the cavity by heat conduction, i.e. when the cavity changes its state from a non-conducting to a conducting state. Therefore, the temperature distribution can be calculated by using `Heat Transfer Module by conduction' in the FEA software. The governing PDE equation is

$$\rho C\left(\frac{\partial T}{\partial t}\right) - \vec{\nabla}\cdot(k\vec{\nabla}T) = Q \tag{7.5}$$

where ρ is the density, C is the specific heat capacity, T is the temperature, k is the thermal conductivity and Q is the heat source density.

7.1.2 Model geometry and mesh

Figure 7.1 to Figure 7.3 show details of the 2D axial-symmetric model geometry and the boundary line numbers of the test object which has been developed. The model consists of a homogenous dielectric material of 2.0 mm thickness and 50 mm diameter, a hemispherical cavity of around 1.1 mm diameter due to the centre axis of symmetry and the cavity surface of 0.05 mm thickness to simulate surface charge decay through conduction along the cavity wall. Also, at the top and bottom of center of the void, two tiny cavity surface degradation areas have been added. The diameter of the degradation areas is 0.005mm. The material of degradation areas is set to be within silicone rubber [109]. The maximum cross-sectional area of the cavity centre is applied to calculate dynamic current during PD for PD real charge magnitude calculation. The horizontal line in Figure 7.1 shows the centre of the cavity. A sinusoidal voltage is applied to the upper electrode and the lower electrode is always grounded. A 2D unstructured mesh with triangular elements is used. The meshes in the cavity and on the cavity surface are refined because higher accuracy is required in electric potential calculation within these methods. The meshing in the model is shown in Figure 7.3.

7.1.3 Boundary and subdomain settings

Tables 7.1 to Table 7.6 show the assigned constants, subdomain settings and boundary settings of the model that are used for the simulation.

After the boundaries and subdomains of the model have been set and chosen, the model is meshed and prepare for being solved. The `Transient, electric currents' analysis with `Time dependent' solver is selected under the `Solver Parameters'. The time stepping is set at 0:0.0025:0.005. Then, the model is solved by clicking the `Solve Problem' under the `Solve' tab. The solution can be completed no error is in the model. The electric field and temperature distributions in the model can be achieved by the selection to the options under the `Postprocessing' tab in the `Plot Parameter' window. The solved model is saved as .m file so that the model can be opened and edited in MATLAB.

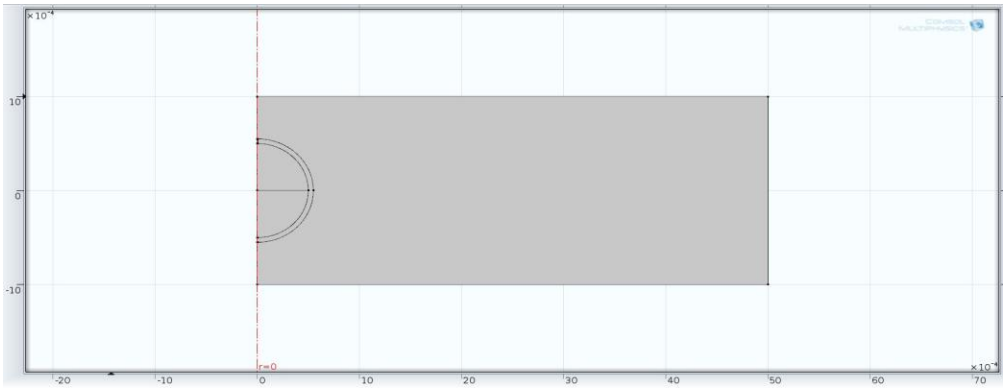

Figure 7.1 2D axial--symmetric model geometry in COMSOL software

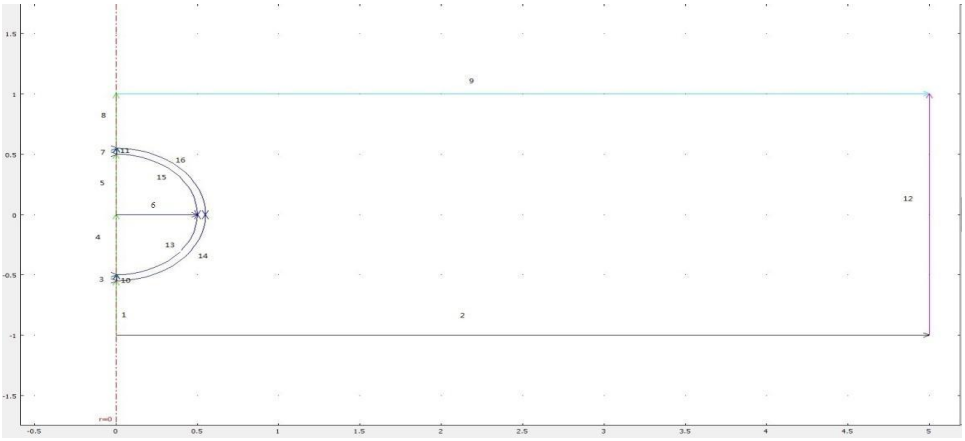

Figure 7.2 Model geometry with boundary line numbers.

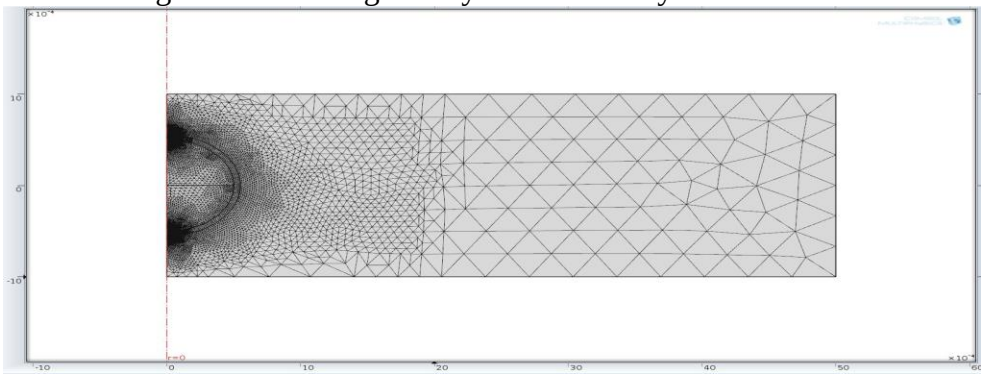

Figure 7.3 2D model geometry and mesh

Name	Expression	Description
Uapp	14 [kV]	Applied voltage amplitude
freq	50 [Hz]	Frequency of the applied voltage
Ermat	2.75	Relative permittivity of dielectric material
Ers0	2.75	Relative permittivity of cavity surface on no degradation area
Ercav	1	Relative permittivity of the cavity
Smat	1e-9 [S/m]	Conductivity of dielectric material
Ss0	1e-9 [S/m]	Initial conductivity of cavity surface on no degradation area
Ss1	1e-9 [S/m]	Initial conductivity of cavity surface on degradation area
Scav0	5e-3 [S/m]	Initial conductivity of cavity
Ers1	13	Relative permittivity of cavity surface on degradation area

Table 7.1 Defined constants for the Electric Currents application model

Subdomain	Relative permittivity	Electrical conductivity
Material	Ermat	Smat
Cavity Surface on no degradation area	Ers0	Ss0
Cavity	Ercav	Scav
Cavity Surface on degradation area	Ers1	Ss1

Table 7.2 subdomain settings for the Electric Currents application model

Boundary line	Boundary condition	Expression
9	Electric potential	$V = Uapp \cdot \sin(2 \cdot pi \cdot freq \cdot t)$
12	Electric insulation	$\vec{n} \bullet \vec{J} = 0$
1,3,4,5,7,8	Axial symmetry	r=0
2	Ground	V=0
All interior boundaries	Continuity	$\vec{n} \bullet (\vec{J}_1 - \vec{J}_2) = 0$

Table 7.3 Boundary settings for the Meridional Electric Currents application model

Subdomain	Thermal conductivity	Specific heat capacity	Density	Heat source density
Material	kmat	Cmat	rhmat	Qmat
Cavity surface	kmat	Cmat	rhmat	Qmat
Cavity	kcav	Ccav	rhcav	Qcav

Table 7.4: Subdomain settings for the Heat Transfer by Conduction application model

Boundary line	Boundary condition	Expression
1,3,4,5,7,8	Axial-symmetry	r=0
2,9,12	Thermal insulation	$\vec{n} \bullet (k \vec{\nabla} T) = 0$
All interior boundary	Continuity	$\vec{n} \bullet (k_1 \vec{\nabla} T_1 - k_2 \vec{\nabla} T_2) = 0$

Table 7.5: Boundary settings for the Heat Transfer by Conduction application Model

Name	Expression	Description
T0	273 [K]	Initial temperature
kcav	0.0257[W/m/K]	Thermal conductivity of the cavity
kmat	0.17[W/m/K]	Thermal conductivity of the material
Ccav	1005[J/(kgK)]	Specific heat capacity of the cavity
Cmat	1800[J/(kgK)]	Specific heat capacity of the material
rhcav	1.205[kg/m^3]	Density of the cavity
rhmat	1250[kg/m^3]	Density of the material
Qcav	0[W/m^3]	Heat source density of the cavity
Qmat	0[W/m^3]	Heat source density of the material
ks	110[W/m/K]	Thermal conductivity of the cavity surface on degradation area
Cs	0.71[J/(kgK)]	Specific heat capacity of the cavity surface on degradation area
Qs	2.09[kg/m^3]	Density of the cavity surface on degradation area

Table 7.6: Defined constants for the Heat Transfer by Conduction (at 20^{o}C, 100 kPa)

7.1.4 Parameters in the model for simulation

Table 7.7 details the parameters used for all simulations at ambient temperature. From Table 7.7, the time step during no PD, Δt_0, is set equal to 1/500f, where f is the frequency of the applied voltage. The simulation time is suitable and also high precision of phase of the applied voltage is kept using this value. If Δt_0 is too large, the field in the cavity will change too much in one time step, leading to a less precise display of the phase of PD occurrence. In addition, if Δt_0 is set too short, the simulation time will be increased for little benefit in obtained results.

The time interval during a PD event, Δt_1, is reduced to 1 ns because if Δt_1 is less than this value, the simulation time will be increased too much for no obvious benefit. The selected time step assures that the precision of PD charge magnitude is maximised. If Δt_1 is set larger than 1 ns, the simulation time will be decreased and the precision of the PD charge magnitude will also be reduced due to the rate of change of the field in the cavity during PD. The material conductivity, σ_{mat}, is set as 1×10^{-9} Sm^{-1} because the conductivity of silicone resin is found to be 1×10^{-9} Sm^{-1} [110]. As the material is a dielectric with a non-zero DC conductivity, a current is flowing through the material when a voltage is applied. The electric field distribution is not influenced if σ_{mat} is smaller than $1\times10^{-9}Sm^{-1}$ by the simulation using the FEA method. Therefore, setting σ_{mat} as $1\times10^{-9}Sm^{-1}$ is suitable. The cavity conductivity between PD events, σ_{cav0} is set equal to 0 Sm^{-1} because no current is flowing in the cavity during this time. The value for the maximum cavity conductivity during a PD event, σ_{cavmax} is set equal to $5\times10^{-3}Sm^{-1}$.

This value is in comparison with the value that is calculated using Equation A.1 and Equation A.2 with the measured maximum charge magnitude from the experiment. This value is suitable to remain the simulation time short and monitor to avoid the field in the cavity from dropping too fast during the PD. If σ_{cavmax} is set higher than $5\times10^{-3}Sm^{-1}$, the field in the cavity will drop too fast and will stop when field level is much lower than the extinction field, which leads to larger PD charge magnitudes. If σ_{cavmax} is set lower than $5\times10^{-3}Sm^{-1}$, the simulation time will be increased for little benefit. The σ_{cavmax} is lower than $5\times10^{-3}Sm^{-1}$ cannot

significantly influence the PD charge magnitude and the field when discharge stops, however, more than 100 time steps are obtained to deal with a PD event. Different values of σ_{cavmax} do not have an influence on the rate of temperature variation in the cavity during a discharge occurs.

It is assumed that the relative permittivity of silicone resin is 2.75 [110]. For the degradation areas, the cavity surface permittivity and the initial cavity surface conductivity are set to ε_{rs1} and σ_{s1} respectively. For areas that have no degradation areas, the cavity surface permittivity and the initial cavity surface conductivity are set to ε_{rs0} and σ_{s0} respectively. The relative permittivity of the cavity, ε_{rcav} is set equal to 1 because it is assumed that the gas in the cavity is air. The stress-dependent coefficient for surface conductivity, α is set equal to 10 mm·kV^{-1} in order to control the rate of change of σ_s. If α is set too small, σ_s will increase too slowly to tend to σ_{smax}, which leads to the decrement of E_s is not adequate, which results in larger simulated maximum PD magnitudes than those obtained from the measurement data.

However, if α is set too large, the increment of σ_s will become too fast, which leads to a decrement of E_s is too fast. It also can be applied on the thermal-dependent coefficient for surface conductivity, β, which is set as 1/293 K^{-1} for all simulations.

The effective charge decay time constant, τ_{dec}, is 2 ms for all simulations at room temperature. However, for degradation processes, the τ_{dec} should be set higher on the degradation areas than that on no degradation areas. This value was based on published literature which uses silicone rubber as a dielectric material, where the value for τ_{dec} used is between 1 to 4 ms at room temperature [111].

The cavity surface thickness, h_s is set to 0.05 mm. This value is reasonable as the difference in the electric field distribution on the cavity surface for different surface thicknesses is very small. However, if the thickness is too small, the simulation time is longer because of the use of more mesh elements in the model geometry. In addition, the thickness of degradation area of cavity surface is estimated 0.0005mm through the observation to the degraded samples under

microscope.

Definition	Symbol	Value	Unit
Time step during No PD	dt	0.001	s
Time step during PD	dt	1	ns
Material relative permittivity	ε_{rmat}	2.75	
Cavity surface of degradation areas relative permittivity	ε_{rs}	13	
Cavity relative permittivity	ε_{rcav}	1	
Material conductivity	σ_{mat}	1e-9	S/m
Initial cavity surface conductivity of no degradation areas	σ_{s0}	1e-9	S/m
Maximum cavity conductivity	σ_{cavmax}	5e-3	S/m
Initial cavity surface conductivity of degradation areas	σ_{s1}	1e-9	S/m
Cavity initial temperature	T_0	293	K
Specific heat capacity of the material	C_{mat}	1800	J/(kgK)
Specific heat capacity of air	C_{cav}	1005	J/(kgK)
Thermal conductivity of the material	k_{mat}	0.17	W/(mK)
Thermal conductivity of air	k_{cav}	0.0257	W/(mK)
Density of the material	ρ_{mat}	1250	Kg/m^3
Density of air	ρ_{cav}	1.205	Kg/m^3
Maximum cavity surface conductivity on no degradation areas	σ_{smax0}	1e-5	S/m
Specific heat capacity of degradation areas	C_s	0.71	J/(kgK)
Thermal conductivity of degradation areas	k_s	110	W/(mK)
Density of degradation areas	ρ_s	2.09	Kg/m^3

Table 7.7 Definition and symbol of parameter used for all simulations (at ambient temperature)

7.2 Comparison of PD patterns and pulse

A comparison of PD activity measurement and simulation results has been made in order to study PD behaviour during degradation processes. From the comparison, the critical parameters and physical mechanisms influences the sequence of PD events for degradation processes to be assessed by the variation in certain model parameters. Comparisons are normally preceded using the φ-q-n plots, number of PDs per cycle, maximum charge magnitude and minimum charge magnitude. Simulation of field as the function of the time of the applied field, PD charge magnitude and temperature in the cavity has been finished to analyse the sequence of PD events. The stage of degradation processes typically is separated into three types. Initially, the turtle-like pattern or the rabbit-ear pattern occurs at the beginning of the degradation processes. Then, the unidentified patterns occur after several hours towards the end of degradation processes. The results from sample 2 were obtained by stressing five samples simultaneously, however, as the difference between the size of degraded sample (sample 2) and the size of failed sample (sample f) is big, therefore the PD patterns from sample 2 can be identified clearly because the PD magnitude from the failed sample is larger than that from the degraded sample. In addition, all the simulated PD patterns and pulses were attempting to match the experimental PD patterns and pulses by adjusting the three types of parameters (EGR, effective charge decay time constant and maximum surface conductivity on degradation areas).

7.2.1 Turtle-like patterns

Figure 7.4-7.8 show φ-q-n plots of measurement and simulation results of PD activity as a function of amplitude of the applied 50 Hz ac sinusoidal voltage for 100 cycles for PD patterns and 10 cycles for pulses. The simulation results shown in Figure 7.4-7.8 are obtained from the model when the temperature change in the cavity due to PD events is considered. This is because the simulation results from the model when the temperature change in the cavity is neglected are nearly similar to that of the model when the temperature change is considered. At the beginning of the degradation processes, the turtle-like patterns

normally have been found. However, the turtle-like pattern in figure 7.8 will be described in specific because it occurs at the end of degradation processes. The figures shown in Figure 7.4-7.8 describe the model results for turtle–like patterns for the four different samples. Most of turtle-like patterns are very concentrated, but in figure 7.8, the turtle-like pattern is more dispersed than the other turtle-like patterns.

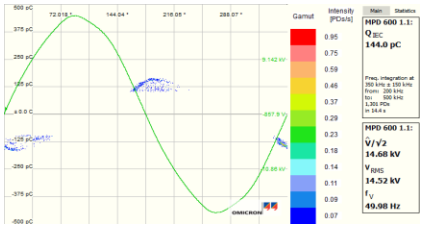

1) 14kV

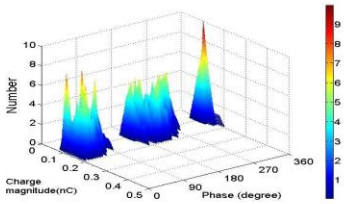

3) 14kV

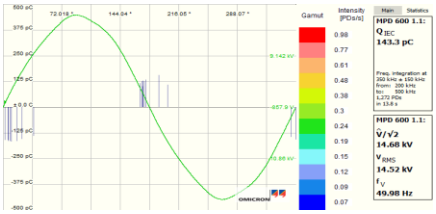

2)14kV

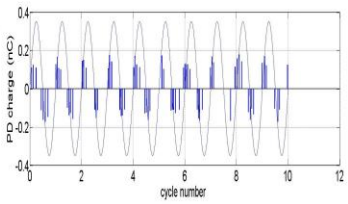

4) 14kV

Figure 7.4 PD patterns and pulses of the measurement (1-2) and simulation (3-4) for sample 2 after 20mins for degradation processeS

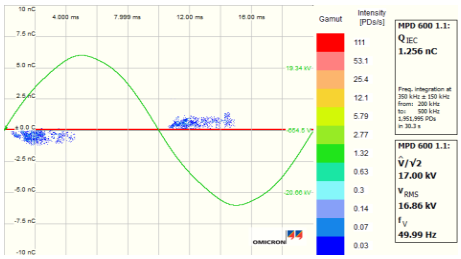

1) 17kV

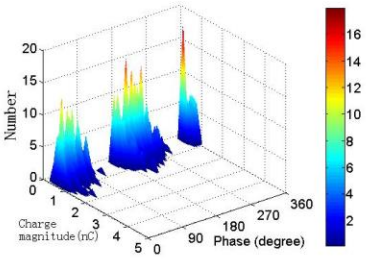

3)17kV

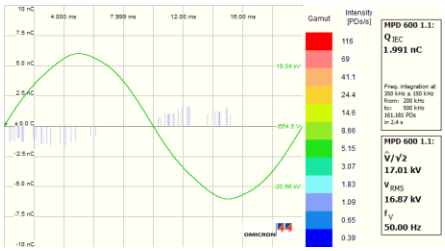

2) 17kV

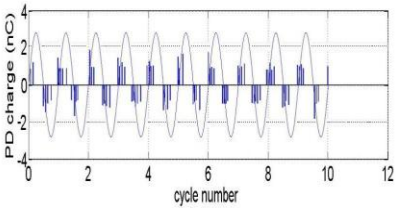

4)17kV

Figure 7.5 PD patterns and pulses of the measurement (1-2) and simulation (3-4) for sample 6 after 1hour for degradation processes

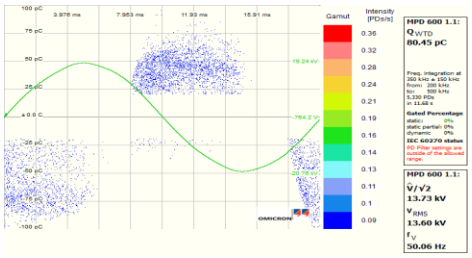

1) 14kV

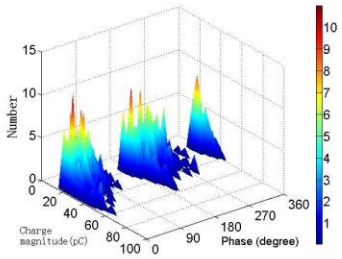

2) 14kV

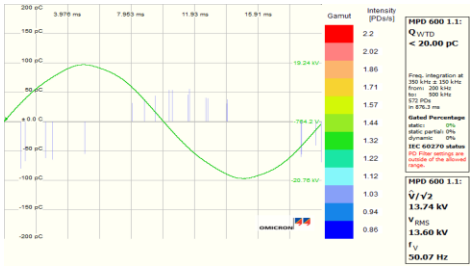

3) 14kV

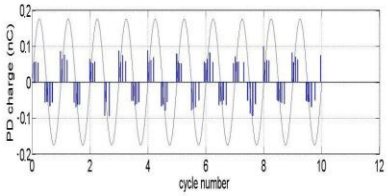

4) 14kV

Figure 7.6 PD patterns and pulses of the measurement (1-2) and simulation (3-4) for sample 8 after1hour for degradation processes

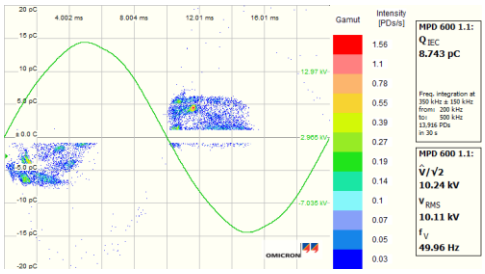

1) 10kV

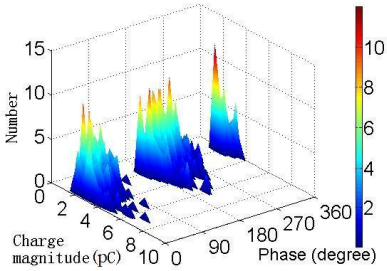

2) 10kV

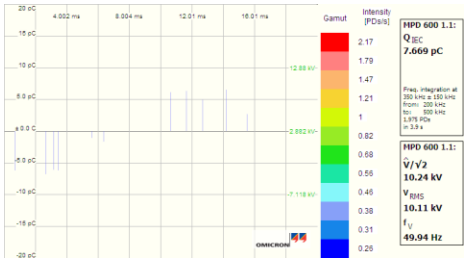

3)10kV

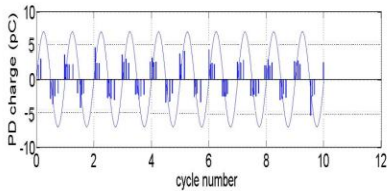

4)10kV

Figure 7.7 PD patterns and pulses of the measurement (1-2) and simulation (3-4) for sample 9 after 10hours for degradation processes

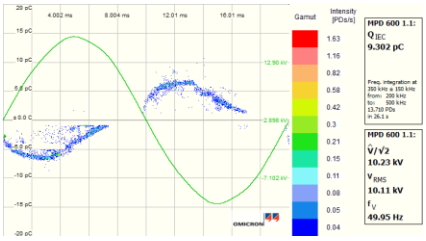

1)10kV

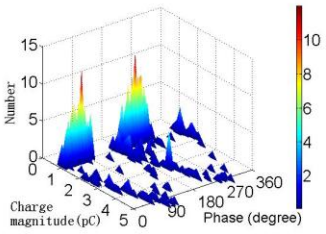

3)10kV

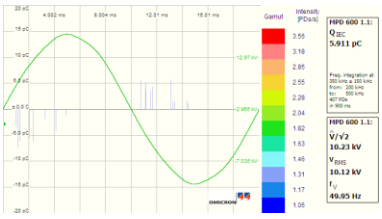

2)10kV

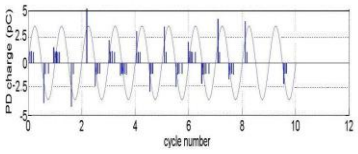

4) 10kV

Figure 7.8 PD patterns and pulses of the measurement (1-2) and simulation (3-4) for sample 9 after 20hours for degradation processes

Table 7.8 to Table 7.9 compares the measurement and simulation results. Comparison between measurement and simulation results clearly indicates that the simulation results are in reasonable agreement with the measurement results for all types of voids. The simulation of φ-q-n plots shown here are only for the model considering the temperature change in the cavity due to PD events because the simulation by ignoring the temperature change in the cavity also creates the similar patterns.

Sample numbers	Sample 2	Sample 6	Sample 8	Sample 9	
Numbers of PDs per cycle	8	9	8	10	10
Mean charge magnitude (pC)	140	1590	55	5.2	4.2
Maximum PD magnitude (pC)	152	2210	85	7	7.2
Minimum PD magnitude (pC)	110	530	20	1	1

Table 7.8: Measurement results for different samples

Sample numbers	Sample 2	Sample 6	Sample 8	Sample 9	
Numbers of PDs per cycle	8.2	9.1	8.3	9.1	9.2
Mean charge magnitude (pC)	149	1403	56	4.5	4.7
Maximum PD magnitude (pC)	180	2110	95	5.2	6.2
Minimum PD magnitude (pC)	101	520	25	1.1	1.1

Table 7.9: Simulation results for different samples (When the temperature change in the cavity is considered)

For the turtle-like patterns, the critical parameters have been shown in Table 7.10. From the Table 7.10, in a larger cavity, there may be more free charges accumulated on the cavity surface than charge trapping in surface state. This reduces the amount of charge detrapping from the cavity surface, which act as initial free electrons for the next PD. Therefore, this is the reason why lower initial electron generation rate due to surface charge is obtained in the simulation. However, the electron generation rate due to volume ionization, N_{ev} is higher for the larger cavity size because there may be more free electrons generated from background radiation in a larger cavity volume. The maximum surface conductivity, σ_{smax1} is found to be higher for the larger cavity size. Because the cavity surface conductivity is a field dependent parameter, larger σ_{smax1} is obtained for the larger cavity in order to match the measured and simulated maximum PD charge magnitude. Hence, free surface charge decay through conduction along the cavity wall is more significant for the larger cavity size. There may be high amount of charges accumulated on the cavity surface, which decays through surface conduction with time. The effective charge decay time constant, $\tau_{dec,}$ is independent of the applied voltage because it is assumed that charge decay of the trapped charges is only influenced by the thermal process. Furthermore, the measured mean, maximum and minimum charge magnitudes are higher in the larger cavity because the maximum avalanche propagation length parallel to the

applied field and the resulting avalanche head perpendicular to the applied field are larger. Finally, the reason why the turtle like curve of φ-q-n plot in figure 7.8 has a dispersed pattern, compared to the turtle-like curve for the other voids can be hypothesized. It is assumed that since the cavity surface conductivity is a field dependent parameter, larger σ_{smax1} is obtained for the turtle-like pattern in figure 7.8 in order to match the measured and simulated maximum PD charge magnitude. Thus, free surface charge decay through conduction along the cavity wall is more significant for this turtle-like pattern. There may be high amount of charges accumulated on the cavity surface, which decays through surface conduction with time. The reason why higher conductivity for this kind of turtle-like pattern has been hypothesized that the conducting channel leads to make the charge combination and neutralization in the conducting channel, which result in lower initial generation rate because a conducting channel has been observed to have formed within the sample 9 shown in Figure 5.12.

Definition	**Symbol**	**Different samples**					**Unit**
		Sample 2	**Sample 6**	**Sample 8**	**Sample 9**		
Initial EGR due to surface emission	N_{es0L}	1000	500	1500	2000	1500	1/s
Initial EGR due to surface emission	N_{es0H}	6000	5000	6500	7000	7000	1/s
EGR due to volume ionization	N_{ev}	60	100	50	10	10	1/s
Effective charge decay time constant	τ_{dec}	2e-3	2e-3	2e-3	2e-3	2e-3	s
Maximum surface conductivity on degradation areas	σ_{smax1}	1e-8	1e-7	1e-9	1e-9	1e-7	S/m
Size of voids	d	1.0	1.8	0.9	0.5		mm
The applied voltage	U_{app}	14	17	14	10		kV

Table 7.10 Definition of parameters used in the simulation for turtle-like patterns

7.2.2 Rabbit-ear patterns

Figure 7.9 shows φ-q-n plots of measurement and simulation results of PD activity as a function of amplitude of the applied 50 Hz ac sinusoidal voltage for 100 cycles for PD patterns and 10cycles for pulses. The simulation results shown in Figure 7.9 are obtained from the model when the temperature change in the cavity due to PD events is considered. This is because the simulation results from the model when the temperature change in the cavity is neglected are similar to that of the model when the temperature change is considered. At the beginning of the degradation processes, the rabbit-ear patterns also normally have been found. However, it should not be believed that rabbit-ear patterns must occur after the turtle-like patterns. The figures shown in Figure 7.9 describe the rabbit ear patterns for only one sample.

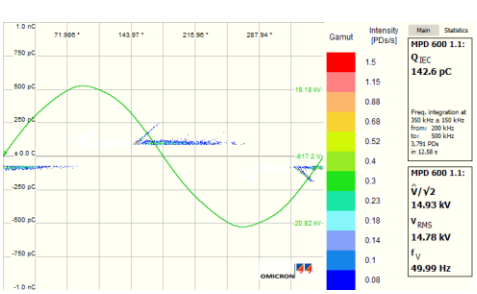

1) 14kV

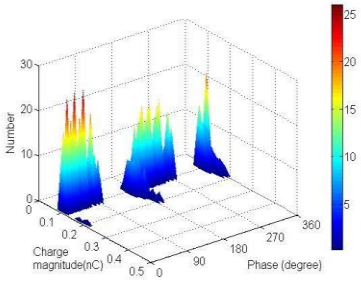

3) 14kV

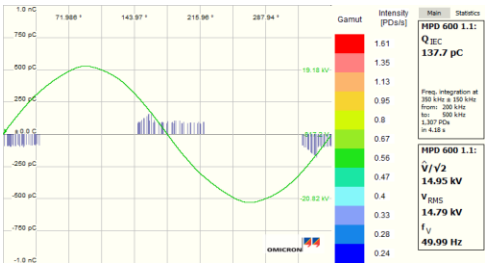

2) 14kV

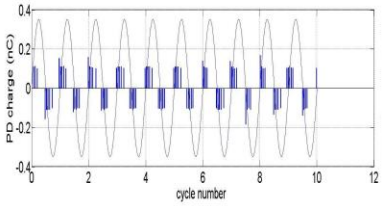

4) 14kV

Figure 7.9 PD patterns and pulses of the measurement (1-2) and simulation (3-4) for sample 2 after 35 mins for degradation processes

Table 7.11-7.12 compares the measurement and simulation results. Comparison between measurement and simulation results clearly indicates that the simulation results are in reasonable agreement with the measurement results for this type of void. The simulation of φ-q-n plots shown here are only for the model considering

the temperature change in the cavity due to PD events because the simulation by neglecting the temperature change in the cavity also produces the similar patterns. From the φ-q-n plots, referring to the charge magnitude-phase axes, the 'rabbit-ear' like curves appear when PDs occur with higher charge magnitude and broad 'straight-line' patterns appear when PDs occur with a lower charge magnitude are obviously displayed. However, the rabbit-ear like curve is shorter than the other kinds of rabbit-ear like curve.

Sample numbers	Sample 2
Numbers of PDs per cycle	19
Mean charge magnitude (pC)	146
Maximum PD magnitude (pC)	251
Minimum PD magnitude (pC)	100

Table 7.11: Measurement results for sample 2

Sample numbers	Sample 2
Numbers of PDs per cycle	15
Mean charge magnitude (pC)	152
Maximum PD magnitude (pC)	256
Minimum PD magnitude (pC)	102

Table 7.12: Simulation results for sample 2(When the temperature change in the cavity is considered)

For the rabbit-like patterns, the critical parameters have been shown in Table 7.13. The reason why the rabbit ear is shorter than the other rabbit ear patterns is the electron generation rate is higher because of degradation on surface of voids. Moreover, in comparison with the turtle-like patterns in Figure 7.4, the electron generation rate N_{esoH}, N_{esoL} is increased, maximum surface conductivity σ_{smax1} on degradation areas is also increased, and the effective charge decay time constant is also increased. It is assumed that the electron generation rate and charge decay time is higher than that of turtle-like as the surface of void has been slightly degraded, but not as seriously as the unknown shape. The degradation behaviour leads to increase the conductivity at the degradation areas. Furthermore, an increase of electronegative gases such as CO_2 obtained from degradation processes in the voids which may result in greatly increased electron attachment [8], which leads to increase the statistical time lag for PD events occurrence. Therefore, the rabbit –ear has a larger charge magnitude at the early phase. However, due to the degradation behavior, more electrons and positive ions emit from the surface of voids, which results in the increase of electron generation rate. Thus, the length of rabbit-ear is shorter than the typical rabbit-ear.

Definition	Symbol	Sample 2	Unit
Initial EGR due to surface emission	N_{es0L}	5000	1/s
Initial EGR due to surface emission	N_{es0H}	18000	1/s
EGR due to volume ionization	N_{ev}	60	1/s
Effective charge decay time constant	τ_{dec}	3e-3	s
Maximum surface conductivity on degradation areas	σ_{smax1}	1e-6	S/m
Size of void	d	1.0	mm
The applied voltage	U_{app}	14	kV

Table 7.13 Definition of parameters used in the simulation for rabbit-ear patterns

7.2.3 The unidentified patterns

Figure 7.10-7.13 show φ-q-n plots of measurement and simulation results of PD activity as a function of amplitude of the applied 50 Hz ac sinusoidal voltage for 100 cycles PD patterns and 10cycles for pulses. The simulation results shown in Figure 7.10-7.13 are obtained from the model when the temperature change in the cavity due to PD events is considered. This is because the simulation results from the model when the temperature change in the cavity is neglected are similar to that of the model when the temperature change is considered. In the end of the degradation processes, the unidentified patterns normally have been found. The figures shown in Figure 7.10-7.13 describe the model results for the unidentified patterns for the four different samples. The charge magnitude for the all unidentified patterns is very low and the curve seems like "bar-like".

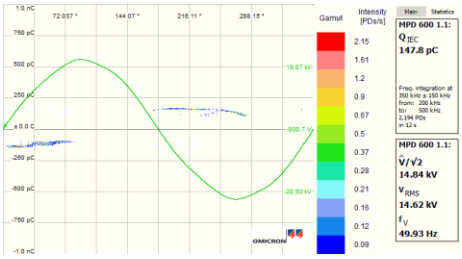

1) 14kV

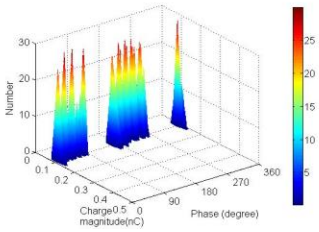

3) 14kV

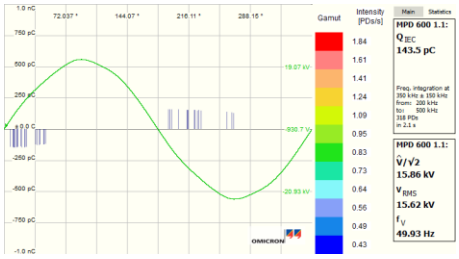

2)14kV

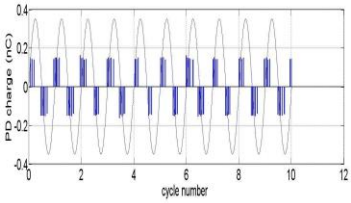

4) 14kV

Figure 7.10 PD patterns and pulses of the measurement (1-2) and simulation (3-4) for sample 2 after 6hours for degradation processes

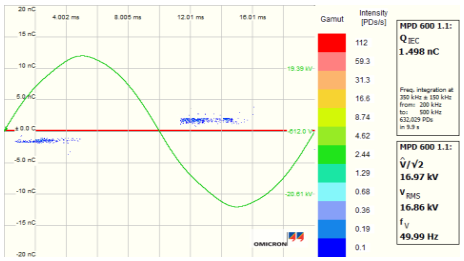

1) 17kV

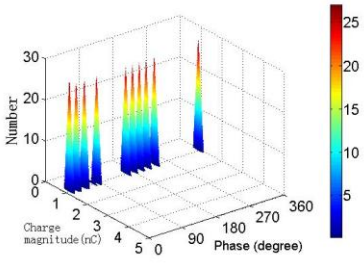

2)17kV

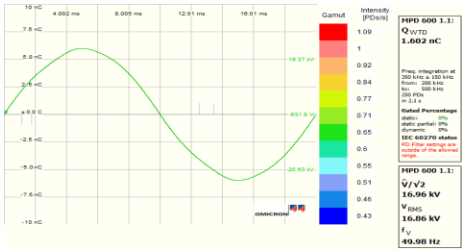

3) 17kV

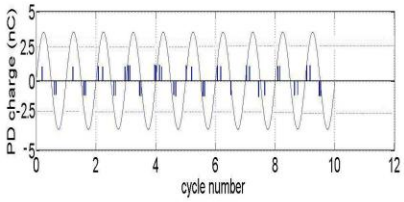

4) 17kV

Figure 7.11 PD patterns and pulses of the measurement (1-2) and simulation (3-4) for sample 6 after 4hours for degradation processes

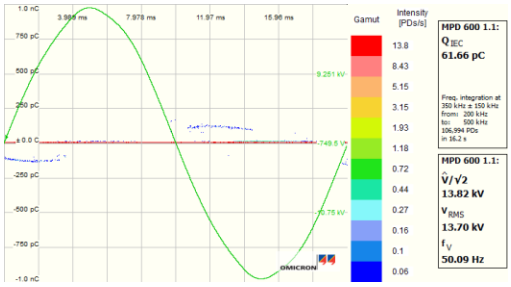

1)14kV

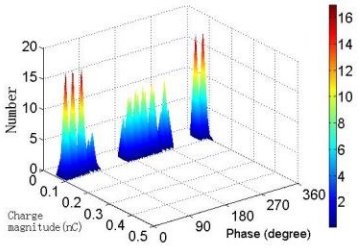

2) 14kV

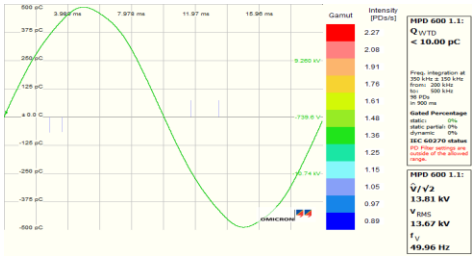

3)14kV

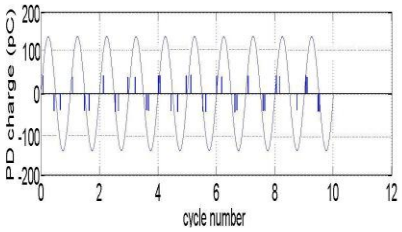

4)14kV

Figure 7.12 PD patterns and pulses of the measurement (1-2) and simulation (3-4) for sample 8 after 5hours for degradation processes

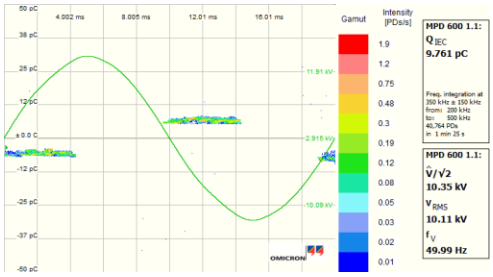

1) 10kV

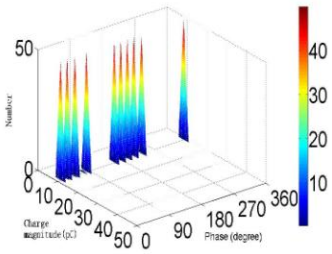

2) 10kV

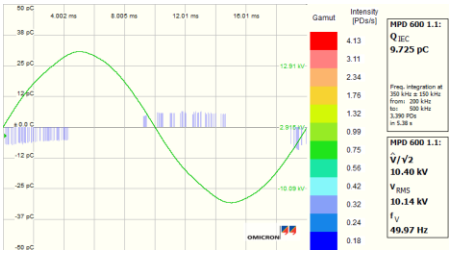

2)10kV

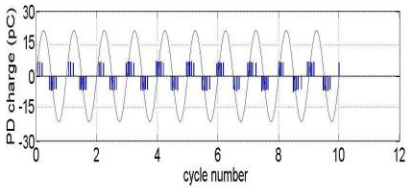

4) 10kV

Figure 7.13 PD patterns and pulses of the measurement (1-2) and simulation (3-4) for sample 9 after 3hours for degradation processes

Table 7.14 compares the measurement and simulation results. Comparison between measurement and simulation results clearly indicates that the simulation results are in reasonable agreement with the measurement results for all types of voids. The simulation of φ-q-n plots shown here are only for the model considering the temperature change in the cavity due to PD events because the simulation by neglecting the temperature change in the cavity also produces the similar patterns.

Sample numbers	Sample 2	Sample 6	Sample 8	Sample 9
Numbers of PDs per cycle	14	4	4	19
Mean charge magnitude (pC)	152	1003	65	4.5
Maximum PD magnitude (pC)	181	1510	80	10
Minimum PD magnitude (pC)	125	1000	60	4

Table 7.14: Measurement results for different samples

Sample numbers	Sample 2	Sample 6	Sample 8	Sample 9
Numbers of PDs per cycle	14.2	4.5	4.3	18.1
Mean charge magnitude (pC)	154	1004	62.5	4.3
Maximum PD magnitude (pC)	192	1520	75	10.2
Minimum PD magnitude (pC)	101	1001	50	4

Table 7.15: Simulation results for different samples (When the temperature change in the cavity is considered)

For the unidentified patterns, the critical parameters have been shown in Table 7.16. In comparison with the other patterns on same samples under the same applied voltage, the parameters that related to electron generation rate such as Nes_{0H}, Nes_{0L} and τ_{dec} for unknown shape PD patterns are much higher. It is because the surface of conductivity is increased by degradation processes, which leads to electron generation rate increasing by surface emission. Therefore, the effective charge decay time constant is also increased because bond breaking of the material caused by bombardment of electrons, which result in more electrons detrapping from surface of voids. Moreover, according to [8], another explanation can be combined with previous explanations. An increase of electronegative gases such as CO_2 obtained from degradation processes in the voids which may result in greatly increased electron attachment [8]. Therefore, the behavior may lead to increase the statistical time lag for PD events to occur. However, because much more electrons detrap from the surface of voids due to degradation processes, the electronegative gas cannot

strongly affect the increase of the electron generation rate. In addition, for the sample 9, in the end of the degradation processes, the turtle-like pattern in Figure 7.8 has been observed, not the unidentified patterns. It is hypothesized that the conducting channel leads to make the charge combination and neutralization in the conducting channel, which result in lower initial generation rate because a conducting channel has been observed to have formed within the sample 9 shown in Figure 5.12. In addition, from the table 7.16, the PD numbers per cycle is lower for sample 6 and sample 8. It might be because that the maximum surface conductivity is higher which leads to the decrease of probability of the PD occurrence.

Definition	**Symbol**	**Different samples**				**Unit**
		Sample 2	**Sample 6**	**Sample 8**	**Sample 9**	
Initial EGR due to surface emission	N_{es0L}	5500	5000	6500	7000	1/s
Initial EGR due to surface emission	N_{es0H}	19500	18000	19000	20000	1/s
EGR due to volume ionization	N_{ev}	60	100	50	10	1/s
Effective charge decay time constant	τ_{dec}	4e-3	4e-3	4e-3	4e-3	s
Maximum surface conductivity on degradation areas	σ_{smax1}	1e-3	1e-2	1e-2	1e-3	S/m
Size of voids	d	1.0	1.8	0.9	0.5	mm
The applied voltage	U_{app}	14	17	10	10	kV

Table 7.16 Definition of parameters used in the simulation for turtle-like patterns

7.2.4 MSE analysis

The mean square error (MSE) between the simulation and measurement results is calculated. The MSE plot for different patterns is shown in figure 7.17. The MSE

of all combinations that fall within this range is evaluated in figure 7.10, where the least MSE or global minimum is identified. Table 7.17 shows the processes to calculate the MSE in detail.

Combination number	N_{ev}	N_{es0L}	N_{es0H}
1	10	0	0
2	10	0	Increases by 1000
3	.	.	.
.	.	.	.
.	.	.	.
.	.	.	.
.	.	10	Until 20000
.	.	Increases by 1000	For each N_{es0L}, increases N_{es0H} by 1000 Until 20000
.	.	.	
.	.	.	
.	.	8000	
.	10		
.	Increases by 10	For each N_{ev}, Increases N_{es0L} by 1000 Until 8000	For each N_{ev} and N_{es0L}, increases N_{es0H} by 1000 Until 20000
.	.		
.	.		
1920	Until 100		

Table 7.17 Numbers of combination values of N_{es0H}, N_{es0L} and N_{ev}

It was found that the global minimum of MSE for rabbit ear PD patterns was found in the combination range between 1850 and 1860. The global minimum of MSE for turtle like PD patterns was found in the combination range between 1750 and 1760. The global minimum of MSE for unknown PD patterns was found in the combination range between 1890 and 1920. As seen from the Table 7.18, the least mse values are small, which indicates the error between measurement results and simulation results is small.

Least MSE values					
	Sample numbers				
PD patterns	Sample 2	Sample 6	Sample 8	Sample 9	
Turtle-like patterns	8.021	8.312	9.908	10.782	14.891
Rabbit-ear patterns	12.578				
Unidentified patterns	9.787	9.667	8.086	9.078	

Table 7.18: Least MSE for PD charge magnitude distribution between measurement and simulation results for different samples

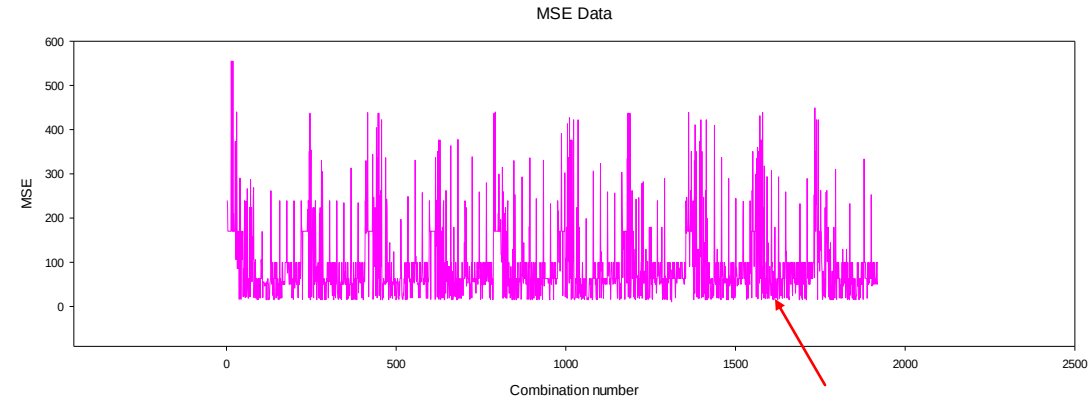

a)

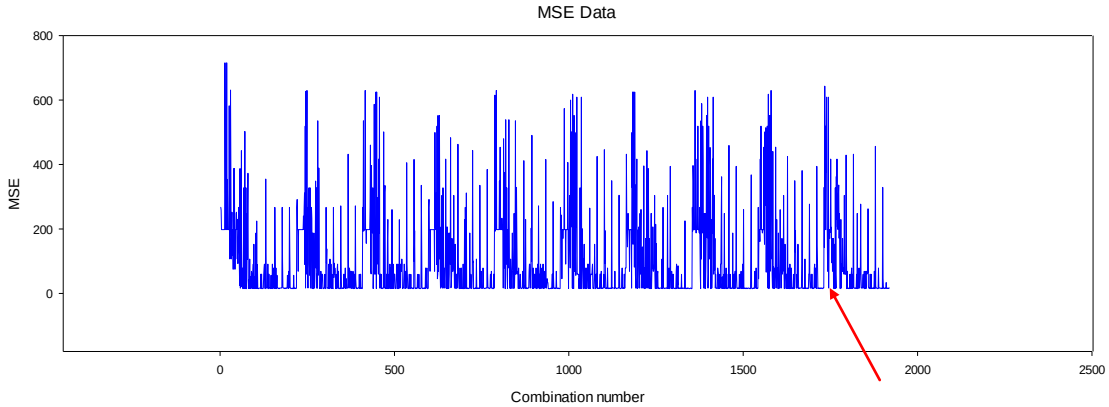

b)

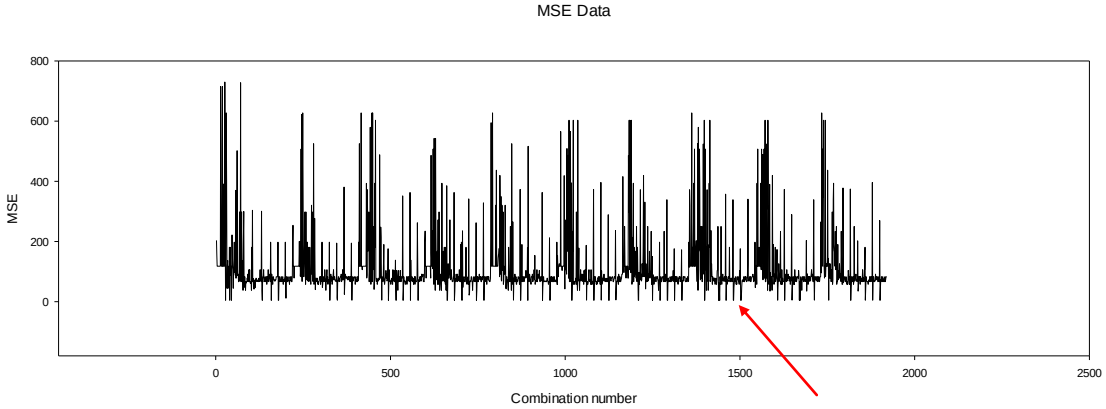

c)

Figure 7.14. Results from the sensitivity analysis performed to select the best values for N_{es0H} , N_{es0L} and N_{ev} a) short- rabbit ear b) bar-like c) turtle-like

In addition, as can be seen from 7.14, the least values are basically similar when the N_{ev} is changing every time. Therefore, from the analysis, it can be seen the N_{esoH} and N_{esoL} mainly control and adjust the charge magnitude of the PD patterns in the simulation.

7.3 Summary

A model for degradation processes on surface of void has been adapted to simulate the degradation behaviour observed in the experiments. The simulation data are in good agreement compared with the measurement results for the three categories of PD patterns. At the beginning of degradation processes, the PD pattern is turtle like pattern. However, over time, the rabbit ear pattern appears. An increase of electronegative gases such as CO_2 obtained from degradation processes in the voids which may result in greatly increased electron attachment [8], which leads to increase the statistical time lag for PD events occurrence. Therefore, the rabbit –ear has a larger charge magnitude at the early phase. However, due to the degradation behavior, more electrons and positive ions emit from the surface of voids, which results in the increase of electron generation rate. Thus, the length of rabbit-ear is shorter than the typical rabbit-ear. Furthermore, according to the simulation, the unknown PD pattern is caused by a too high surface generation rate and higher conductivity on the degradation area, which may be caused by bond-breaking of the material. Moreover, the reason why the patterns are turtle-like pattern when the sample in Figure 5.12 has been degraded can be assumed that a conducting channel has been observed to have formed within the sample in Figure 5.12. Thus, the conducting channel leads to make the charge combination and neutralization in the conducting channel, which results in lower initial generation rate. MSE analysis has been used to aid the selection of simulation parameters.

Chapter 8 Conclusions and Future Work

The images of degraded samples which have experienced long stressing periods have been obtained. The surface of the voids has been degraded compared with voids which do not experience PD behaviour in voids. In order to identify whether the degradation processes are the pre-cursor to development of bow-tie electrical trees, nine samples containing degradation areas were then cut open in order to provide a surface containing open segments of degradation area or pits. From images taken by microscope, blunt pits have occurred in the voids/silicone rubber interface. However, authors in [4, 5] describe that sharp pits may occur from surface of voids before bow-tie electrical trees grow from voids. Therefore, the pits shown in the Figure 5.11.3 may be due to the start of a thermal degradation processes. Also, from Figure 5.10.1 to Figure 5.10.3, the three samples were experienced different PD levels (1nC, 200pC, 50pC) respectively. From the figures, all degraded areas were thermally damaged with a large amount of heat. From Figure 5.12, the structure of the degradation area seems like electrical channels. After 30 hours, the sample has experienced very low PD with around 10pC, which may be reasonable to get rid of thermal damage to formation of electrical trees as the electrical trees normally are caused by the bond-break through impinging of PD. It can be seen that the channels has been displayed in the Figure 5.12. Electrical trees normally grow from a sharp pit at first. However, from the figure, the sharp pits cannot be found. In addition, the repeatable experiment for confirm the electrical channels caused by PD bombardment cannot obtain the repeated results. Therefore, whether the electrical channels were caused by the PD in the void cannot be assured.

The SEM technique has been used to identify the degradation processes further. For the untested void, the SEM image shows that there are no cracks and protrusions on the surface of the void. For the failed void, it can be seen that large

protrusions have formed around the edges of the void and these protrusions are fairly large in comparison to the other samples are nodular in appearance. For the degraded voids, the large cracks and some protrusions appear on the surface of most of degraded voids, which indicates the voids have experienced degradation processes.

Raman spectroscopy has been used to analyse the chemical content of the degradation area on unmicrotomed samples. The presence of carbon in a void/silicone rubber interface indicates that a degradation process of the void involves the degradation of the bonds between the polymer backbone, which consist of silicone and oxygen, and the side groups of the polymer chain that contain carbon. Thus, it indicates the pits probably grow from the void. Additionally, in all the spectra the typical peaks relating to silicone rubber can be seen between 200 and 900 cm^{-1} and these peaks of most of spectra are superimposed on varying degrees of fluorescence. The reason why there appears to be little or no fluorescence in some spectra is unclear. However, as the associated degradation is a localised phenomenon, the lack of fluorescence could be due to the lack of the degradation area below the surface at the points of analysis.

Raman spectroscopy has been used to analyse the chemical content of degradation area on microtomed samples as well. Degradation areas, areas close to degradation area and areas far from degradation area have been scanned. The Raman results of microtomed surface of samples indicates that fluorescence appearing on the spectra of degradation areas and areas close to degradation area shows that degradation behaviour have taken place on the interface between voids and silicone rubber. Moreover, it indicates that the areas close to degradation area have been impacted by degradation processes. As same as the unmicrotomed samples, some spectra of degradation area do not indicate fluorescence. The reason for this is as the same as that for unmicrotomed samples. Additionally, the presence of carbon has been found in one sample. It further identifies that pits have grown from the void.

The Raman spectroscopy for breakdown epoxy resin containing voids has been performed. The spectra obtained from breakdown areas indicate D and G bands of

graphitic carbon dominate the spectrum. The presence of carbon in the breakdown areas of breakdown samples indicates that a degradation process of the void involves the degradation of the bonds between the polymer backbone and the side groups of the polymer chain that contain carbon. In addition, in some spectra the typical peaks relating to epoxy resin can be seen between 200 and 1300 cm^{-1}, which is different from that of silicone rubber and the peaks of all the spectra are superimposed on varying degrees of fluorescence.

At early stage of degradation processes, PD patterns can be identified as void discharge patterns. At final stage of degradation processes before breakdown, PD patterns cannot be assured because different PD patterns have been found. Moreover, at final stage of degradation processes, electrical discharge patterns have not been found. According to [32], it shows that partial discharge patterns from a void is regarded as the rabbit-like or turtle-like pattern and electrical tree discharge patterns is regarded as the wing-like pattern. According to observation of PD patterns shown in Figure 5.3, these PD patterns of five degraded samples are different from electrical tree discharge patterns. Also, they are different from typical void discharge patterns called turtle-like or rabbit-like pattern. Therefore, the change of PD pattern is probably caused by the change of surface conductivity of wall due to chemical modification to surface of voids [10] or increase of electronegative gases such as CO_2 obtained from degradation processes in the voids which results in capability of electron attachment is strong [8]. The identification of PD patterns transition during degradation processes for a single sample has been performed. As seen from Figure 5.6, it displays high magnitude PD (1nC) during degradation processes. However, the degradation area includes the thermal damage channel caused by high magnitude PD. High magnitude PD may interrupt the formation of electrical trees. From Figure 5.7, it displays lower magnitude PD (above 50 pC) during degradation processes. However, as seen from the the degraded samples, the degradation behaviour also seems like to be caused by thermal damage. The transition of PD patterns for the two samples is similar, which is from turtle-like PD patterns to unknown PD patterns. Therefore, it can be assumed that the PD transition is similar and PD pattern before breakdown is same to the samples which experienced the thermal degradation. In addition, the transition of PD patterns is not consistent for the low magnitude of

PD in the end of degradation processes. From Figure 5.7, the transition of PD patterns is from rabbit ear to turtle like, and to unknown PD patterns. However, the transition of PD patterns in Figure 5.8 is from unknown PD patterns to two different kinds of turtle-like patterns. The simulation has been used to validate the reason of transition of PD patterns obtained from measurement.

A model for degradation processes on surface of void has been adapted to simulate the degradation behaviour observed in the experiments. The simulation data are in good agreement compared with the measurement results for the three categories of PD patterns. At the beginning of degradation processes, the PD pattern is the turtle like pattern. However, over time, the rabbit ear pattern appears. An increase of electronegative gases such as CO_2 obtained from degradation processes in the voids which may result in greatly increased electron attachment [8], which leads to increase the statistical time lag for PD events occurrence. Therefore, the rabbit –ear has a larger charge magnitude at the early phase. However, due to the degradation behavior, more electrons and positive ions emit from the surface of voids, which results in the increase of electron generation rate. Thus, the length of rrabbit-ear is shorter than the typical rabbit-ear. Furthermore, according to the simulation, the unknown PD pattern is caused by a too high surface generation rate and higher conductivity on the degradation area, which caused by bond-breaking of the material. Moreover, the reason why the patterns are turtle-like pattern when the sample has been degraded is that there may be a conducting channel as has been seen in microscopy studies. The conducting channel leads to make the charge combination and neutralization in the conducting channel, which results in a lower initial generation rate. MSE analysis has been used to aid the selection of simulation parameters.

In the future, a Finite Element Analysis (FEA) model representing material thermal degradation due to PD within a cavity in silicone rubber will be developed to increase understanding of insulation breakdown due to PD in void cavities. The temperature, electric field, electric current of degradation areas changing with time will be presented. Simulation results can be validated through comparison with measurement results presented in this thesis.

Appendix A The Existing Model

A.1 Discharge model and charge magnitude calculation

The existing model was produced in Illias's PhD thesis [2]. The description to the existing model has been detailed in the appendix A. PD is caused by the local electric field enhancement in the cavity, which is due to the applied electric field and surface charges on the cavity surface. In this model in which simulation is dynamic, the electric field distribution in the cavity is calculated numerically at each time step using FEA method which solves the PDE in Equation 7.4 for the time dependent electric field. From the FEA model, in the absence of any PD and surface charge, the field distribution in a spherical cavity has been found to be uniform. However, for a spherical cavity which is large in diameter compared to the thickness of the material, as in Figure 7.1, the field distribution in the whole cavity is no longer uniform. The electric field on the cavity surface nearest to the electrode is slightly lower than the field at the cavity centre due to the influence of the electrode. However, the electric field in the cavity is symmetrical along the r and z-axes [110]. Because of this, FEA model is used continuously throughout the simulation to calculate the field distribution in the cavity. Symmetry of both the electric field and charge distribution in the cavity along the r and z axes is assumed before and after the occurrence of a PD. This is obtained in FEA modelling by assuming that during a PD event, the whole cavity is influenced.

There are some suggestions made to simplify the model. The discharge model does not include details of PD mechanisms which includes the movement of free electrons and ions during the electron avalanche propagation in the cavity. These parameters influence the characteristics of the cavity surface after each PD but it is difficult to assure physical parameters related to the surface. For this simulation, it has been assumed that a simplified PD model is representative of the phenomena

and this has been identified using related experimental measurements.

It is assumed that the PD in the cavity will have the characteristics of a steamer discharge. Published research has simulated streamer propagation in air by charge carriers experiencing drift and diffusion in the electric field [111]. The development of partial discharge has been modelled by [112, 113] as well. However, a detailed mechanism of streamer propagation is not modelled in this work because the parameters are only related to PD phase and charge magnitude only. Discharge is assumed to influence the whole spherical cavity and is assumed to occur only along the cavity symmetry axis. Thus, only the field in the cavity centre at an instantaneous time, t, $E_{cav}(t)$ is extracted from the FEA model and it is a function of time only.

A.1.1 Cavity conductivity

When partial discharge is modelled dynamically, the discharge event can be indicated by changing the state of the cavity from that of non-conducting to conducting. This can be simulated by increasing the cavity conductivity from its initial conductivity when there is no discharge, σ_{cav0} to maximum cavity conductivity, σ_{cavmax} during the discharge event. σ_{cavmax} is the cavity conductivity which leads to the field in the cavity centre, $E_{cav}(t)$ to decrease until it becomes less than the extinction field, E_{ext} during the discharge process. The value for the maximum cavity conductivity during PD, σ_{cavmax}, can be estimated using the electron conductivity in the plasma because the conductivity due to ions is assumed to be negligible. The electron conductivity in the plasma, σ_e is calculated using [13]

$$\sigma_e = \frac{\alpha_e^{\,2} N_e \lambda_e}{m_e c_e} \tag{A.1}$$

where α_e is the coefficient related to electron energy distribution and mean free path (~0.85), e is the electric charge of the electron, m_e is the electron mass, λ_e is

the electron mean free path (~4 um), c_e is the electron thermal velocity ($\sim 3\times10^{8} ms^{-1}$) and N_e is the electron density, which is defined as

$$N_e = \frac{q/e}{4/3\pi r^3} \tag{A.2}$$

where q/e is the number of electrons in the streamer channel, q is the total charge in the streamer channel and r is the cavity radius. For estimation of σ_{cavmax}, q in Equation A.2 is taken as the maximum charge magnitude determined from analysis of the measurement results, q_{max}. During discharge, the current through the cavity, $I_{cav}(t)$ increases from zero until a certain maximum value but $E_{cav}(t)$ starts to decrease. After that, $I_{cav}(t)$ starts to decrease whilst $E_{cav}(t)$ keeps decreasing. Discharge stops when the field in the cavity, $E_{cav}(t)$ drops to less than the extinction field, E_{ext}. After PD is over, the conductivity is reset to its initial values and current in the cavity becomes zero.

A.1.2 PD charge magnitude

In this model, because the discharge process is modelled dynamically, the charge magnitude can be calculated numerically. The real and apparent charge magnitudes, q_{PD} are calculated by time integration of current, I(t) flowing through the cavity (boundary 6 in Figure 7.3) and through the ground electrode (boundary 2 in Figure 7.3) during the PD time interval, where

$$q_{PD} = \int I(t)dt \tag{A.3}$$

The current, I, through the ground electrode is calculated by integration of current density, J over the ground electrode surface area, where J depends on the electric field distribution. Because the electric field distribution on the ground electrode is not uniform due to the presence of the cavity, the field distribution in the whole cavity and material is calculated using the FEA method to determine the PD

apparent charge magnitude.

A.2 Modelling of temporal temperature and pressure change

After a PD event, the temperature in the cavity will have increased due to the electron ionization process. However, in other previous PD models, the influence of temperature change in the cavity on PD activity has not been considered [114].

A.2.1 Cavity temperature dependent using FEA model

After a PD event, the temperature in the cavity have increased due to the electron ionization process. The hot gas due to the discharge is assumed to form a spherical shape in order to simplify the model. From the FEA model, the temperature in the whole cavity immediately after the first PD is uniform as the PD affects the whole cavity. However, a certain time after a PD has occurred, the temperature distribution in the cavity becomes non-uniform but is symmetrical along the cavity symmetry axis. The distribution is obtained from the FEA model. The temperature at the cavity centre is the highest and is the lowest at the region near the cavity surface as the heat dissipation near the cavity surface is greater through the surrounding material. Thus, the temperature in the cavity immediately after the next PD occurs is no longer uniform but symmetrical along the symmetry axis because the temperature distribution is influenced by the previous PD event. It can be assumed that the highest temperature is influencing the occurrence of a PD, only the temperature in the cavity centre is assumed to affect the inception field in the cavity, which is denoted as $T_{cav}(t, 0, 0)$, where (0,0) is the location of the cavity centre in the model.

In this model, all energy released from discharge is assumed to be in the form of heat energy. Thus, during a PD event, the heat source density in the whole cavity, Q_{cav} from Equation A.4 is increased from zero while the heat source density in the

material, Q_{mat} is always set to zero. The increase in Q_{cav} causes $T_{cav}(t, 0, 0)$ to increase. Discharge is modelled by changing the state of the cavity from that of non-conducting to conducting, which causes current to flow in the cavity. Because the electric field along the r-axes is very near to uniform, discharge channels can be assumed to be in the form of a cylindrical channels. Thus, $Q_{cav}(t)$ can be calculated using [115]

$$Q_{cav}(t) = J_{cav}(t)E_{cav}(t) \tag{A.4}$$

where $J_{cav}(t)$ is the current density in the middle of the cavity during discharge and $E_{cav}(t)$ is the field in the cavity centre. $J_{cav}(t)$ and $E_{cav}(t)$ are calculated from Equation 7.4. Equation A.4 indicates the specific heat power of heat released due to the electric current in the discharge channel. After a PD event, $Q_{cav}(t)$ is reset to zero. Thus, the coupled equations allow the electric potentials and temperature to be determined for a set of given boundary conditions at each time step instant.

A.2.2 Temperature dependence of inception and extinction fields

During a discharge event, $T_{cav}(t_n, r, z)$ increases from its previous value, $T_{cav}(t_{n-1}, r, z)$, where n is the nth time step and r and z are the locations in the cavity. The rise of $T_{cav}(t_n, r, z)$ may cause the pressure in the cavity, $p(t_n, r, z)$ to increase from its previous value, $p(t_{n-1}, r, z)$. It can be assumed that the cavity volume is constant, the changes of the number of gas molecules in the cavity after each PD is negligible and the gas in the cavity is assumed as an ideal gas, the new pressure in the cavity at the current time step t, $p(t_n, r, z)$ is calculated using

$$p(t_n, r, z) = \left[\frac{p(t_{n-1}, r, z)}{T_{cav}(t_{n-1}, r, z)}\right] T_{cav}(t_n, r, z) \tag{A.5}$$

The inception field, E_{inc} is defined as the minimum electric field in the cavity that a discharge can occur, which relies on the cavity pressure and cavity diameter. It is assumed that the inception field is dependent on the temperature in the cavity

centre, $T_{cav}(t, 0, 0)$ and the initial temperature in the cavity is the same as the material temperature. Using the obtained measurement data of E_{inc} as a function of temperature in the cavity, T_{cav} in the experiment, the best fit function that can be used to represent this relationship as a function of time, t is

$$E_{inc}(t) = \kappa + \chi T_{cav}(t,0,0) \tag{A.6}$$

where κ and χ are constants in kV mm respectively, determined from the experiment. Thus, $E_{inc}(t)$ changes from the initial cavity inception field, E_{inc0} when the temperature in the cavity changes with time. E_{inc0} is equal to the field in the cavity when the inception voltage from the measurement is reached. In the model, E_{inc0} depends on the cavity diameter, d because it has been assumed that discharge only take places along the symmetry axis of the cavity, where the distance over the cavity symmetry axis is the cavity diameter. The pressure in the cavity may also determine the extinction field, E_{ext} because it controls the streamer propagation field, where discharge is restricted at a higher field in the cavity at higher pressure [114]. It can be assumed that E_{ext} is approximately proportional to the cavity pressure, if E_{ext0} is the extinction field in the cavity centre at the initial cavity pressure, p_0, $E_{ext}(t)$ at an instantaneous time t is estimated as

$$E_{ext}(t) \approx E_{ext0} p(t,0,0) / p_0 \tag{A.7}$$

The temperature in the cavity will decay towards the initial temperature after a PD occurs. As the temperature is calculated numerically using the FEA method, there is no need to set any temperature decay time constant because the temperature decreases when the heat source density, $Q_{cav}(t)$ is reset to zero following a PD event. Therefore, this method can be considered as an alternative approach to a previous model which uses a lower probability of PD occurrence as the temperature on the cavity surface is higher than the initial temperature [116].

A.2.3 Thermal properties of the cavity and material

The thermal properties of the cavity can also be set as temperature and pressure dependent. It can be assumed the gas content in the cavity is air, the thermal

properties of the cavity can be assumed to have air thermal properties. The temperature in the cavity relies on the cavity density, ρ_{cav}, specific heat capacity, C_{cav}, thermal conductivity, k_{cav} and heat source density, Q, where these parameters depends on the pressure and temperature in the cavity. Using curve fitting technique on the given data sets of air temperature, pressure, specific heat capacity, thermal conductivity and density from [117, 118], the simplest functions that can be used to indicate the cavity thermal properties, as a function of time, temperature and pressure are where $T_{cav}(t, r, z)$ and $p(t, r, z)$ are the temperature and pressure in the cavity at an instantaneous time, t. The mass density, specific heat capacity and thermal conductivity of the dielectric material are regarded as independent of the temperature because the temperature range used in the experiment is only 20° C. Therefore, variation in the silicone rubber thermal properties can be assumed to be minimal and can be neglected in the model. From analysis using the FEA model, the temperature distribution in the cavity is not influenced by a small variation in these silicone rubber thermal properties. As there is a wide variation of the thermal properties values for silicone rubber because of variation of silicone components, their thermal properties are assigned using values found in [110], where those values are for the pressure and temperature of the material at 100 kPa and 20° C. Therefore;

$$\begin{aligned} C_{cav}(t,r,z) &= 1033 - 0.279T_{cav}(t,r,z) + 1.096\times10^{-4}\,p(t,r,z) \\ &\quad + 7.429\times10^{-4}[T_{cav}(t,r,z)]^2 - 5.003\times10^{-7}T_{cav}(t,r,z)\,p(t,r,z) \\ &\quad + 1.891\times10^{-12}[p(t,r,z)]^2 - 4.19\times10^{-7}[T_{cav}(t,r,z)]^3 \\ &\quad + 6.184\times10^{-10}[T_{cav}(t,r,z)]^2\,p(t,r,z) \\ &\quad - 4.881\times10^{-15}T_{cav}(t,r,z)[p(t,r,z)]^2 - 7.753\times10^{-20}[p(t,r,z)]^3 \end{aligned} \tag{A.8}$$

$$\begin{aligned} k_{cav}(t,r,z) &= 1\times10^{-5}\{57.88 + 9.43T_{cav}(t,r,z) + 1.049\times10^{-4}\,p(t,r,z) \\ &\quad - 2.915\times10^{-3}[T_{cav}(t,r,z)]^2 - 1.726\times10^{-7}T_{cav}(t,r,z)\,p(t,r,z) \\ &\quad + 3.115\times10^{-10}[p(t,r,z)]^2 \end{aligned}$$

$$\begin{aligned} p_{cav}(t,r,z) &= 3.562 - 0.03445T_{cav}(t,r,z) + 3.464\times10^{-5}\,p(t,r,z) \\ &\quad + 1.094\times10^{-4}[T_{cav}(t,r,z)]^2 - 1.13\times10^{-7}T_{cav}(t,r,z)\,p(t,r,z) \\ &\quad + 3.494\times10^{-13}[p(t,r,z)]^2 - 1.142\times10^{-7}[T_{cav}(t,r,z)]^3 \\ &\quad + 1.211\times10^{-10}[T_{cav}(t,r,z)]^2\,p(t,r,z) \\ &\quad - 9.868\times10^{-16}T_{cav}(t,r,z)[p(t,r,z)]^2 \end{aligned}$$

A.3 Charge decay through surface conduction

The assumption of charge decay through conduction along the cavity wall is reasonable as the amount of charge trapped in the cavity is time dependent. During the discharge process, when the first layer of charge arrives on the cavity surface before being trapped, it expels oncoming charge, and increases their landing time. Therefore, it can be assumed that repelled charges might remain on the cavity surface for a certain period of time or may move along the cavity wall before being trapped in a surface state. The influence will be significant if the cavity surface time constant is less than the period of the applied voltage [119]. After a PD, any charges that still remain free on the cavity surface will decay through conduction along the cavity wall before the next PD event occurs, leading to charge recombination. This surface charge decay can be simulated using a field-dependent cavity surface conductivity, which relies on free charge movement along the cavity wall through surface conduction. The movement of these charges is assumed to be dependent on the magnitude and direction of the electric field in the cavity center, $E_{cav}(t)$ and the electric field due to the cavity surface charge, $E_s(t)$.

Since the charge movement along the cavity wall is modelled associated with the direction of field in the cavity centre, $E_{cav}(t)$ and field due to surface charge, $E_s(t)$, $E_s(t)$ needs to be calculated in the model. $E_s(t)$ is calculated using

$$E_s(t) = E_{cav}(t) - E_{cav0}(t) \tag{A.9}$$

Some PD charges will be trapped in surface states and some may remain on the cavity surface. In this model, field due to surface charge immediately after a previous PD occurrence, $E_{sPD}(t_{PD})$ is assumed as sum of field due to trapped charge, $E_{strapPD}(t_{PD})$ and field due to free surface charge, $E_{sfreePD}(t_{PD})$, where t_{PD} is the time of the previous PD occurrence. It is assumed that free surface charge which remains on the cavity wall do not become trapped in surface states to simplify the model. The amount of free surface charge after a PD, $q_{sfreePD}(t_{PD})$ can be calculated

from the FEA model by integration of field displacement, D over the upper cavity surface area, such that

$$q_{sfreePD}(t_{PD}) = \int [D_{z(up)}(t_{PD}) - D_{z(down)}(t_{PD})] dS \tag{A.10}$$

where $D_{z(up)}$ and $D_{z(down)}$ are the upper and lower side of the upper cavity surface. Thus, the field due to free surface charge immediately after a PD event, $E_{sfreePD}(t_{PD})$ can be calculated using where $q_{totalPD}(t_{PD})$ is the total PD real charge up to time (t_{PD}) and its equivalent field is $E_{sPD}(t_{PD})$. It is calculated using

$$E_{sfreePD}(t_{PD}) = \left| \frac{q_{sfreePD}(t_{PD})}{q_{PDtotal}(t_{PD})} \right| E_s(t_{PD}) \tag{A.11}$$

where m is the number of PD events and $q(_{PD})_i$ is PD real charge magnitude of i-th PD event. Therefore, the field due to trapped charge immediately after a PD takes place is

$$q_{PDtotal}(t_{PD}) = \sum_{i=1}^{m} (qPD)_i \tag{A.12}$$

When $E_s(t)$ reaches $E_{strapPD}(t_{PD})$ during surface charge decay, no more surface charge can decay through conduction along the cavity wall.

$$E_{strapPD}(t_{PD}) = E_{sPD}(t_{PD}) - E_{sfreePD}(t_{PD}) \tag{A.13}$$

The surface charge decay rate through conduction along the cavity wall depends on the field on the cavity surface, $E_{ons}(t)$ and the temperature on the cavity surface, $T_{ons}(t)$ because σ_s is strongly dependent on the cavity environment and the material [120]. When $E_{ons}(t)$ and $T_{ons}(t)$ are larger, kinetic energy for surface charge is higher; the charge movement along the cavity wall faster, leading to increased charge decay rate through charge recombination.

Therefore, when the directions of $E_{cav}(t)$ and $E_s(t)$ are the same at an instantaneous time t and Es(t) is larger than $E_{strapPD(tPD)}$), the surface conductivity, σ_s is increased from initial surface conductivity value, σ_{s0} to model the charge movement through conduction along the cavity wall [121]. In the simplest case it might represent the surface conductivity, $\sigma_s(t)$ at each time step using [122]

$$\sigma_s(t) = \sigma_{s0} \exp[\alpha |E_{ons}(t)| + \beta T_{ons}(t)] \tag{A.14}$$

where α is the stress coefficient and β is the thermal coefficient for the cavity surface conductivity. From Equation A.14, $\sigma_s(t)$ may increase to a very high value due to the increasing $E_{ons}(t)$. For avoiding numerical convergence problems in the simulation, $\sigma_s(t)$ is limited by a maximum cavity surface conductivity, σ_{smax}, which is defined as the maximum conductivity that can be reached by the cavity surface. However, when the direction of $E_{cav}(t)$ is opposite of $E_s(t)$, $\sigma_s(t)$ is set to initial surface conductivity, σ_{s0} because there is no charge movement along the cavity wall.

A.4 Initial electron generation

For initiating a PD in a cavity after the inception field has been exceeded, an initial free electron is required for electron avalanche generation. The supply of free electrons determines the characteristics of PD activity which includes phase and charge magnitude of PD occurrences, the numbers of PD per cycle and the total charge magnitude per cycle. The sources of initial electron generation rate are volume ionization and surface emission [121-124].

A.4.1 Total electron generation rate

A simple term is used in the model to describe the electron generation rate equation in order to reduce the use of physical parameters of the material properties. When the field in the cavity centre, $E_{cav}(t)$ exceeds the inception field,

$E_{inc}(t)$ at an instantaneous time, t, PD may occur in the cavity if there is a free electron in the cavity to start an avalanche. The amount of free electrons available in the cavity to start a PD is simulated using the total electron generation rate (EGR), $N_{et}(t)$ which is defined as the number of free electrons created in the cavity per unit time. It is assumed as the sum of EGR due to surface emission, $N_{es}(t)$ and EGR due to volume ionization, N_{ev}, where

$$N_{et}(t) = N_{es}(t) + N_{ev} \tag{A.15}$$

As discharge has been assumed to occur only along the cavity symmetry axis, $N_{et}(t)$ becomes a function of time only.

A.4.2 Electron generation rate due to surface emission

It is assumed that electron generation rate due to surface emission, $N_{es}(t)$ is dominated by charge detrapping from the cavity surface, which is from the charge that has been trapped in the cavity surface from previous PD event. The amount of charge that can be detrapped for a PD probably to occur is dependent on the charge magnitude of the previous PD. Therefore, initially, $N_{et}(t)$ only depends on N_{ev}, which is a constant. After the first PD takes place, $N_{et}(t)$ depends on both $N_{es}(t)$ and N_{ev}.

Using a simple model to describe a PD behaviour, $N_{es}(t)$ is defined as the number of free electrons created in the cavity per unit time through surface emission. If N_{es0} is the number of free electrons created in the cavity per unit time at the initial inception field, E_{inc0}, then, the number of free electrons generated in the cavity per unit time for a PD is probably to occur due to the previous PD occurrence can be defined as

$$N_{PD} = N_{es0}\left|E_{cav}(t_{PD}) / E_{inc}\right| \tag{A.16}$$

where $E_{cav(tPD)}$ is the field in the cavity of the previous PD occurrence at a time t_{PD}. However, the amount of charge, N_{PD} that can be detrapped through surface emission for a PD is possible to occur after a time interval after the previous PD occurred, decays with time. The charge is assumed to decay into deeper traps exponentially with time and the decay rate is controlled by the effective charge decay time constant, τ_{dec}. Charges that have decayed no longer is useful to the initial electron generation because charges in deeper traps are harder to detrap [26]. Although surface charge decays, the potential due to surface charge is assumed constant because charge near to the cavity surface still contributes to the potential of the surface charge.

The electron generation rate due to surface emission has been expressed as a function which increases with increasing electric field and temperature of the material [125]. Thus, for avoiding the use of parameters that are difficult to be determined, it is assumed that the EGR due to surface emission, $N_{es}(t)$ increases exponentially with the field in the cavity, $E_{cav}(t)$ and material temperature, T_{mat}. This is based on the assumption that surface emission is affected by the electric field and material temperature. Therefore, the complete equation of $N_{es}(t)$ for a PD is probably to occur, through considering the charge decay effect since the previous PD occurrence and the field and temperature dependent terms, can be defined as

$$N_{es}(t) = N_{PD} \exp\left[-\frac{(t - t_{PD})}{\tau_{dec}}\right] \exp\left[\frac{E_{cav}(t)}{E_{inc0}} \cdot \frac{T_{mat}}{T_{amb}}\right] \qquad \text{(A.17)}$$

where τ_{dec} is the effective charge decay time constant and T_{amb} is the ambient temperature. $E_{cav}(t)/E_{inc0}$ and T_{mat}/T_{amb} indicates a simplified field and temperature dependency. For the purpose of simulation, T_{amb} is assumed to be 293 K as a reference for simulation at different material temperatures, T_{mat} and this temperature has been used to the measurement of PD activity.

The value for N_{es0} is subdivided into N_{es0L} which is used when the polarity of $E_{cav}(t)$ changes after previous PD event and N_{es0H} when there is no polarity change between consecutive discharges. This is based on the assumption that when the

polarity of the field in the cavity, $E_{cav}(t)$ changes between PD events, the cavity surface work function is higher when detrapping electrons from a negative cavity surface charge than from a positive cavity surface charge [117]. N_{es0} can be defined as

$$N_{es0} = \begin{cases} N_{es0L} & \text{when} \quad E_{PD2}/E_{PD1} < 0 \\ N_{es0H} & \text{when} \quad E_{PD2}/E_{PD1} > 0 \end{cases} \tag{A.18}$$

where E_{PD1} and E_{PD2} are field in the cavity of previous and current PD event. The exponential charge decay term in Equation A.18 is similar to the term used in equation for surface charge decay through volume conduction in the material. If the solid dielectric is assumed to be a non-dispersive, homogenous, isotropic material, has an instantaneous polarization, a constant permittivity ε_{rmat} and a constant conductivity σ_{mat}, a simple surface charge decay model can be obtained by neglecting the space charge effects [126]. Thus, from Equation A.19, the solution obtained is

$$V(t) = V_0(t)\exp(-t/\tau_{mat}) \tag{A.19}$$

where $V_0(t)$ is the potential at time zero and τ_{mat} is equal to $\varepsilon_{mat}/\sigma_{mat}$ is the material time constant. τ_{mat} determines the surface charge decay rate through volume conduction in the material.

A.4.3 Electron generation rate due to volume ionization

When there is no initial free electrons from the cavity surface to initiate a PD, free electrons may also come from volume ionization, which is assumed to be always available in the cavity. The EGR due to volume ionization, N_{ev} has been defined as dependent on pressure in the cavity, cavity volume and applied voltage amplitude [114]. There are many physical parameters related to volume ionization, such as the radiative cosmic, radioactive quantum flux density and pressure reduced gas density. For simplifying the term for N_{ev}, N_{ev} is modeled as a constant number, which indicates the number of free electrons created in the cavity per unit time

through volume ionization. Its value may vary associated with the applied stress and cavity conditions.

A.4.4 Probability of a PD occurrence

For considering the statistical time lag effect on PD to reproduce the PD repetition rate and phase and charge magnitude distributions of the measurement results, a probability is used to determine the likelihood of a PD occurring. The probability of a PD occurrence, P(t) is set as proportional as the total electron generation rate, $N_{et}(t)$ and the time stepping interval during no PD event, Δt,

$$P(t) = N_{et}(t)\Delta t \tag{A.20}$$

When the field in the cavity exceeds the inception field level, P(t) is calculated and compared with a random number, R that is between 0 and 1. As long as P is greater than R, a discharge will occur. When P will larger than 1, PD is always occur.

A.5 Design simulation program in MATLAB

A.5.1 Value assignment for electron generation rate parameters

Referring to Table A.1, parameters related to electron generation rate, i.e. N_{es0H}, N_{es0L} and N_{ev} do not represent the real value of physical properties of the dielectric material. Their values are representive of the initial electron generation rate that changes with applied stress and cavity condition.

The values of N_{es0H}, N_{es0L} and N_{ev} are dependent on each other. Unsuitable choice of values will lead to significant error between measurement and simulation results. For example, if the electron generation rate is set too high, the PD patterns of the simulation will not be comparable to the measured patterns and the simulated number of PDs per cycle will be too large. However, if the electron generation rate

is set too low, it will lead to no PD occurring at all for many voltage cycles, consequently leading to a very low simulated number of PDs per cycle. Therefore, a sensitivity analysis was performed to select the optimum values of N_{es0H}, N_{es0L} and N_{ev}.

The sensitivity analysis for the selection of N_{es0H}, N_{es0L} and N_{ev} values was performed using an optimization method once other parameter values in Table A.1 had been determined. Figure A.1 details the algorithm used for the sensitivity analysis to choose the best fit value for these parameters. For each different combination of N_{es0H}, N_{es0L} and N_{ev}, the total mean square error (MSE) between simulation and measurement of $H_n(\varphi)$ and total charge vs. phase distribution, $H_{qs}(\varphi)$ was calculated. Initially, Nes0H, Nes0L and Nev were defined with small values.

The optimization uses the initial values and N_{es0H} is increased until the global minimum from the MSE vs. N_{es0H} curve is identified. After that, the value for N_{es0L} is increased and the simulation is running again with initial value of N_{es0H}. N_{es0H} is increased until the global minimum from the MSE vs. N_{es0H} curve is identified. The value for N_{es0L} and N_{es0H} is reinitialized.

The simulation is run until the global minimum from the MSE vs. N_{es0L} curve is identified. Once it has been identified, the value for N_{ev} is increased and the values for N_{es0L} and N_{es0H} are reinitialized. The whole process above is repeated and only stops once the global minimum from the MSE vs. Nev curve is identified. The values for N_{es0H}, N_{es0L} and N_{ev} at that point give the best simulation results when compared to measurement data.

A.5.2 Flowcharts of the test program

The FEA model is used in parallel with MATLAB programming code, which is divided into several parts; loops over time, a discharge event, calculation of initial free electron generation to start an electron avalanche, surface charge decay model,

determination of temperature in the cavity, graphical user interfaces (GUI) and post-processing of simulation results.

Definition	Symbol	Unit
Temperature of the material	T_{mat}	K
Cavity diameter	d	mm
Dielectric material thickness	h_{mat}	mm
Applied frequency	f	Hz
Applied voltage amplitude	U_{app}	kV
Initial pressure in the cavity	P_0	kPa
Maximum cavity surface conductivity	σ_{smax}	Sm^{-1}
Measured inception voltage	U_{incapp}	kV
Initial cavity inception field	E_{inc0}	$kV.mm^{-1}$
Initial cavity extinction field	E_{ext0}	$kV.mm^{-1}$
Higher initial EGR due to surface emission	N_{es0H}	s^{-1}
Lower initial EGR due to surface emission	N_{es0L}	s^{-1}
Electron generation rate due to volume ionization	N_{ev}	s^{-1}

Table A.1 Stress and cavity condition -dependent parameters

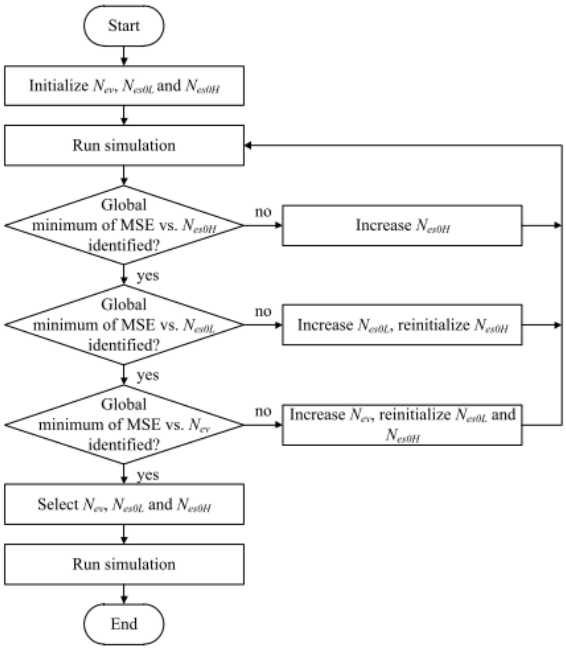

Figure A.1 Flowchart of sensitive analysis for parameter values determination

Figure A.2 to Figure A.4 show flowcharts of the main code and functions used in the main code. Firstly, the workspace in MATLAB is cleared. Then, all constants, variables and parameters that are used in the simulation are defined and initialized. For creating friendly simulation environment, some GUIs are introduced before the simulation. The first GUI allows user to key in the dimensions of the cavity. The next GUI allows user to key in all input data for simulation, such as the applied frequency, applied voltage amplitude and numbers of cycles to simulate. $N_{ext,}$ the model geometry is meshed and initialized. Boundary and subdomain settings are assured with parameters that have been chosen. The model is then solved using initial condition values.

After that, the main loop commences. At each time step, the code interacts with the FEA model. Boundary and subdomains are updated and the model is solved for electric potential and temperature using the FEA method. The temperature in the cavity, T_{cav} is extracted from the model to update the pressure in the cavity, which is used to update the inception field, E_{inc}. The field in the cavity, E_{cav} obtained from the model is compared with the field due to surface charge, Es. If the polarity of E_{cav} is the same with Es, the cavity surface conductivity, σ_s, is increased to model

the charge decay through surface conduction. Moreover, σ_s is maintained at its initial value, σ_{s0} and σ_{s1}. The cavity surface temperature is also extracted to update the value of σ_s. However, if the polarity of E_{cav} is opposite to Es, the surface conductivity is set to its initial value. Then, E_{cav} is compared with E_{inc}. If E_{cav} is higher than E_{inc}, the total electron generation rate, N_{et} is calculated. Then a probability, P of a PD occurrence is calculated using Equation A.20 and compared with a random number, R which is within 0 to 1. If P is greater than R, discharge is set to occur. Otherwise, the status is set to a no discharge condition and the programme goes to the next time step.

Once discharge is set to take place in the cavity, the electric equipotential line, electric field and temperature distributions in the model immediately before the first PD are stored. Then, the cavity conductivity is increased. The parameter values for boundary and subdomains are updated and the electric field and the current are extracted from the model. At the same time, the heat source density in the cavity is increased to allow the temperature to increase. Discharge stops when E_{cav} drops below the extinction field, $E_{ext.}$ In addition, the program keeps extracting the electric field and the current at each time step during the PD. When discharge stops, the cavity conductivity and the heat source density in the cavity are reset to their initial values and the program proceeds to next time step. The phase of PD occurrence and charge magnitude are saved in the workspace. The electric equipotential line, electric field and temperature distributions in the model immediately after the first PD are also stored.

The cycle repeats until a specified number of cycles are reached. The code then calculates the number of PDs per cycle, the mean, minimum and maximum charge magnitudes. PD phase and charge magnitude distributions, 2D PRPD pattern and 3D φ-q-n plot are obtained.

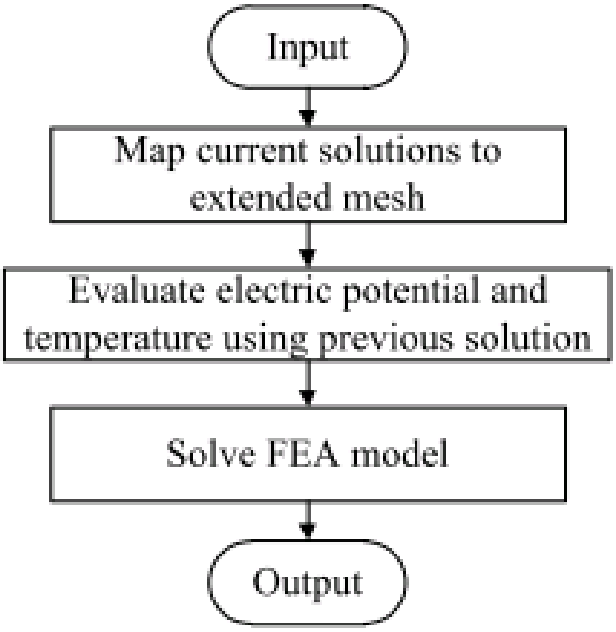

Figure A.2: Flowchart of the 'Process' function[2]

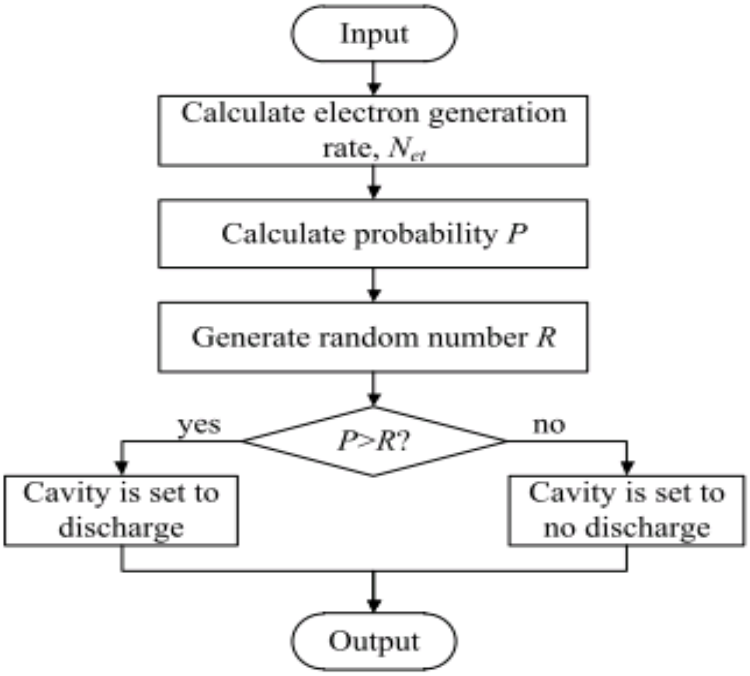

Figure A.3: Flowchart of the 'CheckPD' function [2].

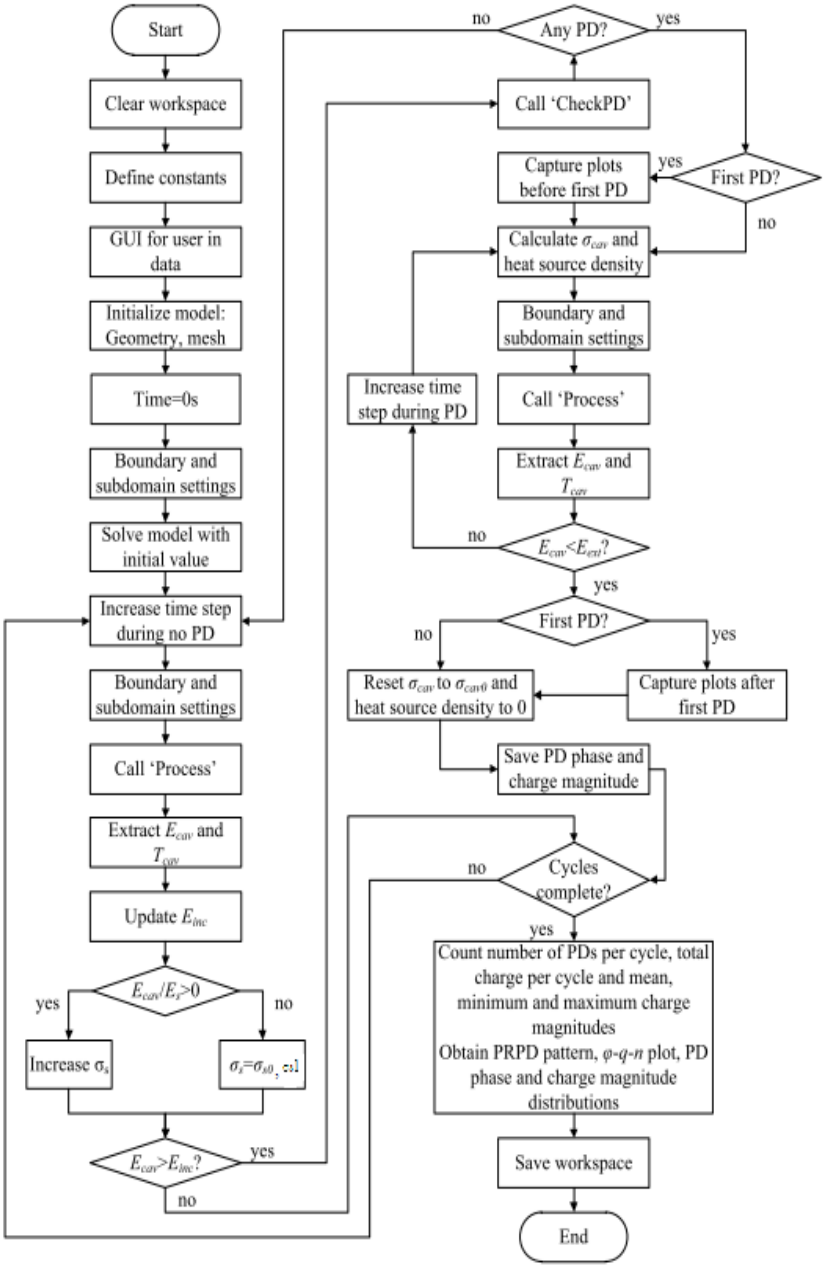

Figure A.4: Flowchart of the main code in MATLAB[2].

References

[1] La Wang, Andrea Cavallini and Gian Carlo Montanari, "Patterns of Partial Discharge Activity in XLPE: from inception to breakdown", 2010 International Conference on Solid Dielectric, Potsdam, Germany, July 4-9, 2010

[2] Hazlee Azil Illias, " Measurement and Simulation of Partial Discharges within a Spherical Cavity in a Solid Dielectric Material" , PhD Thesis, University of Southampton, 2011

[3] LA Dissado, John C. Fothergill., "Electrical Degradation and breakdown in Polymers", ed. S.GC. 1992, London: Peter Perigrins.

[4]R.M.Eichhorn, "Treeing in solid extruded electrical insulation" IEEE Transactions on electrical insulation, VOL. EI-12, NO. 1, February, 1976

[5] J. H. Mason, "The Deterioration and Breakdown of Dielectrics Resulting from Internal Discharge". Proceedings of the IEE - Part I: General, Vol 98, pp.44-59, January 1951

[6] Hozumi.N, Okamoto.T, and Fukugawa,H. "Simultaneous Measurement of Microscopic Image and Discharge Pulses at the Moment of Electrical Tree Initiation" Jap.J.Appl.Phys.,1988,pp.572-576

[7] H. Ichikawa, F. Komori, M. Hikita, Y. Swuoki, T. Mizutani, "Partial Discharge Pattems and Degradation Diagnosis of Insulating Polymers ",8th International Symposium on High Voltage Engineering(Yokohama, 1993), paper 60.02

[8] Choong-Sik Kim, Takeshi Kondo and Teruyoshi Mizutani, " Change in PD Pattern with Aging" , IEEE Transactions on Dielectrics and Electrical Insulation Vol. 11, No. 1; February 2004

[9] Peter Morshuis "Assessment of Dielectric Degradation by Ultrawide-band PD

Detection" IEEE Transactions on Dielectrics and Electrical Insulation Vol.2 No.5, October 1995

[10] P.H.F. Morshuis, "Partial Discharge Mechanisms", Ph.D. Thesis, Delft University of Technology, 1993

[11] S. L. Reynolds, " On the Behavior of Natural and Artifcial Voids in Insulation Under Internal Discharge" AIEE Trans. Power App. Sys., Vol. 77, Pt. 111, pp. 1604-1608, 1959

[12] E. Kuffel, W.S.Zaengl, J. Kuffel, “High Voltage Engineering: Fundamentals”, 2nd ed. Newnes, 2000

[13] L. Niemeyer, "A generalized approach to partial discharge modeling", IEEE Transactions on Dielectrics and Electrical Insulation, vol. 2, pp. 510-528, 1995

[14] R. Schifani, R. Candela, and P. Romano, "On PD mechanisms at high temperature in voids included in an epoxy resin", IEEE Transactions on Dielectrics and Electrical Insulation, vol. 8, pp. 589-597, 2001

[15] G. C. Crichton, P. W. Karlsson, and A. Pedersen, 'Partial discharges in ellipsoidal and spheroidal voids”, IEEE Transactions on Electrical Insulation, vol. 24, pp. 335-342,1989

[16] Hazlee A. Illias, George Chen, Paul L. Lewin "Modelling of Cycle to Cycle Behaviour for Partial Discharge Events within a Spherical Cavity in a Solid Dielectric Material by Using Finite Element Analysis" 2010 international Conference on Solid Dielectric,Potsdam, Germany, July 4-9, 2010.

[17] I. W. McAllister, "Decay of charge deposited on the wall of gaseous void," IEEE Transactions on Electrical Insulation, vol. 27, pp. 1202-1207, 1992.

[18] F. Gutfleisch and L. Niemeyer, "Measurement and simulation of PD in epoxy voids," IEEE Transactions on Dielectrics and Electrical Insulation, vol. 2,

pp. 729-743, 1995.

[19] W. Kai, T. Okamoto, and Y. Suzuoki, "Effects of discharge area and surface conductivity on partial discharge behavior in voids under square voltages," IEEE Transactions on Dielectrics and Electrical Insulation, vol. 14, pp. 461-470, 2007.

[20] K. Temmen, "Evaluation of surface changes in flat cavities due to ageing by means of phase-angle resolved partial discharge measurement," Journal Physics. D: Applied Physics, vol. 33, pp. 603-608, 2000.

[21] C. Hudon, R. Bartnikas, and M. R. Wertheimer, "Surface conductivity of epoxy specimens subjected to partial discharges," IEEE International Symposium on Electrical Insulation, pp. 153-155, 1990

[22] H. A. Illias, G. Chen, and P. L. Lewin, "Modelling of surface charge decay in a spherical cavity within a solid dielectric material using Finite Element Analysis", International Symposium on High Voltage Engineering, 2009.

[23] George Chen and Fauzan Baharudin, "Partial Discharge Modelling Based on a Cylindrical Model in Solid Dielectrics", 2008 International Conference on Condition Monitoring and Diagnosis, 2008

[24] Hazlee Azil Illias, George Chen and Paul L Lewin " The influence of spherical cavity surface charge distribution on the sequence of partial discharge events", Jounal of Physics D: Applied Physics 44 (2011) 245202 (15pp)

[25] Devins,J.C. ' The 1984 J. B. Whitehead Memorial Lecture: the Physics of Partial Discharges in Solid Dielectrics' IEEE Trans.Elec.Insul.,1984,EI-19,pp. 475-495

[26] H. A. Illias, G. Chen, and P. L. Lewin, "Partial discharge modelling in a spherical cavity within a dielectric insulation material as a function of frequency," IEEE Electrical Insulation Conference, pp. 55-59, 2009

[27] H. A. Illias, G. Chen, and P. L. Lewin, "Partial Discharge Measurements for Spherical Cavities within Solid Dielectric Materials under Different Stress and Cavity Conditions," Conference on Electrical Insulation and Dielectric Phenomena, 2009

[28] H. A. Illias, G. Chen, and P. L. Lewin, "Modelling of Partial Discharge Activity in Different Spherical Cavity Sizes and Locations within a Dielectric Insulation Material", 9th International Conference on Properties and Applications of Dielectric Materials, 2009

[29] Bloor, T.B.a.D, Electrical Properties of Polymers (2nd Ed). 2005:Cambridge University Press.

[30] Hozumi.N, Okamoto.T, and Fukugawa.H. "The influence of morphology on electrical tree initiation in polyethylene under AC and impulse voltages" Ann.Rep. Conf. Elec. Insul.&Diel.Phenom, 1987, pp. 531-535

[31] http://www.duniway.com/images/pdf/pg/Paschen-Curve.pdf [cited 26/07/13]

[32] Junhao Li, Wenrong Si, Xiu Yao and Yanming Li, "Measurement and simulation of partial discharge in oil impregnated pressboard with an electrical aging process" Meas. Sci. Technol. 20 (2009) 105701 (7pp)

[33] M. G. Danikas, "The Definitions Used for Partial Discharge Phenomena", IEEE Trans. Elec. Insul., Vol. 28, pp. 1075-1081,1993

[34] N. Shimizu and C. Laurent, "Electrical Tree Initiation", IEEE Trans. Dielectr. Electr. Insul., Vol. 5, pp. 651-659, 1998

[35] Peter H.F. Morshuis, " Degradation of Solid Dielectrics due to Internal Partial Discharge: Some thoughts on progress made and where to go now", IEEE Transactions on Dielectrics and Electrical Insulation Vol. 12, No. 5; October 2005

[36] K. D. Wolter, J. Tanaka and J. F. Johnson, "A Study of the Gaseous Degradation Products of Corona-exposed Polyethylene", IEEE Transactions on EI, Vol.17, pp. 248-252, 1982

[37] K. D. Wolter, J. F. Johnson, and J. Tanaka, "Polymer Degradation and its Measurement Techniques", ed. R. Bartnikas, STP926, ASTM press, Philadelphia 1987

[38] P. Dejean, N. Foulon, M. Goldman and H. Dejean, "Chemical Aspects of the Aging of Solid Insulating Materials Submitted to Partial Discharges", 4th Int.Conf.on Conduction and Breakdown in Solid Dielectrics, Sestri Levante, pp. 181-185, 1992

[39] M. Goldman, A. Goldman and J. Gatellet, "Physical and Chemical Aspects of Partial Discharges and their Effects on Materials", IEE Proceedings Science, Measurement and Technology, Vol. 142, no.1, pp. 11-16, 1995

[40] M. Gamez-Garcia, R. Bartnikas and M. R. Wertheimer, "Synthesis Reactions Involving XLPE Subjected to Partial Discharges", IEEE Transactions on EI, Vol. 22, pp. 199-205, 1987

[41] R. S. Sigmond, T. Sigmond, A. Goldman and M. Goldman, "In Situ Spectrometric Analysis of the Deterioration of Polymer Surfaces by Low Pressure ac Discharges", 3rd International Conference on Conduction and Breakdown in Solid Dielectrics, Trondheim, pp. 451-455, 1989

[42] J.T. Holbøll, The Resistance of Composite Materials Against Electrical Discharges, Ph.D. thesis, Technical University of Denmark, 1992.

[43] T. Tanaka " Internal Partial Discharge and Material Degradation" IEEE Transactions on Electrical Insulation Vol. EI-21 No.6, December 1986

[44] Takahiro Ishida, Yukio Mizuno, Masayuld Nagao and Masamitsu Kosaki "Development and Application of Partial Discharge Analysing System for Swarming Pulsive Microdischarges" Proceedings of the 3rd International Conference on Properties and Applications of Dielectric Materials, July 8-12, 1991, Tokyo, Japan

[45] M. G. Danikas, "The Definitions Used for Partial Discharge Phenomena",

IEEE Trans. Elec. Insul., Vol. 28, pp. 1075-1081,1993

[46] Bamji,S, Bulinski, A.T and Densley, R.J "Etching and the Morphology of Cross-Linked Polyethylene Cable Insulation" 1984, IEEE int symp elec insul pp.37-40

[47] Nakanishi,K, Hirabayashi,S, Inuishi,Y "Phenomena and Mechanisms of Tree Inception in Epoxy Resins" IEEE Trans elec insul 1979 EI-14 pp. 306-314

[48] Laurent, C, Noel, S, Mayoux, C, "An Investigation of Ac Electrical Aging Phenomena in Polyethylene by Thermally Stimulated Discharge Current Measurement" IEEE Int. symp.elec. insul 1984, pp 76-79

[49] Bamji,S, Bulinski,A, Densley,R.J and Himizu,N. "Light Emission from PE subjected to High Divergent Field" Ann.Rep. Conf. Elec. Insul.&Diel.Phenom, 1982, pp. 592-597

[50] Kosaki,M, Shimizu,N, Horii,K "Treeing of Polyethylene at 77K" IEEE Trans elec insul 1977 EI-12 pp 40-45

[51] Bamji,S.S, Bulinski,A.T, Densley, R.J "Light emission and subsequent tree inception due to polarity reversal of the local field in polymeric insulation" Ann. Rep. Conf. elec insul& Diel. Phenom, 1988, pp 173-179

[52] C. Laurent , C. Mayous and S. Noel "Dielectric Breakdown of Polyethylene in Divergent Field: Role of Dissolved Gases and Electroluminescence", J. Appl. Phys., vol. 54, pp.1532 -1539 1983

[53] Bamji,S.S, Bulinski,A.T, Densley,R.J "The Role of Polymer Interface During Tree Initiation in LDPE" IEEE Trans elec insul 1986, EI-21 pp. 639-644

[54] Ieda, M "Dielectric Breakdown Process of Polymers" IEEE Trans elec insul 1980 EI-15 PP 206-224

[55] B. Fruth, Th. Baumann, F. Stucki, "Space Charge Injection and Partial Discharge Inception at the Metal Polymer Interface", Proc. 3rd Int. Conf. on

Conduction and Breakdown in Solid Dielectrics, Trondheim, 1989, pp. 35-39

[56] Nath, R and Perlman, M.M 'Steady-state bulk trap-modulated hopping conduction in doped linear low-density polyethylene' IEEE Trans. Elec. Insul, 1989, EI-24, pp. 409-412

[57] Reich, L and Stivala, S A, "Elements of polymer degradation" (McGraw-Hills, New York, 1971)

[58] Noel.S, Das-Gupta,D.K, Laurent,C, Mayoux,C "Study of Space Charges and Oxygen Ions in Polyethylene" Conf.Diel. Mats. Meas. & Applics, 1984, IEE Conf . Pub. 239, pp 61-63

[59] Shimizu, N , Horiii,K "The Effect of Absorbed Oxygen on Electrical Treeing in Polymers " IEEE Trans elec insul, 1985, EI-20 pp 561-566

[60]Okamoto,T, and Tanaka,T, "Novel Partial Discharge Measurement Computer-Aided Measurement Systems " IEEE Trans. Elec.Insul.,1985,EI-20,pp. 643-645

[61] Struik, L.C.E, " Physical aging in amorphous polymers and other materials" (Elsevier Press, Amsterdam, 1978)

[62] Ashcraft,A.C, Proc, world Electrochem. Congress (Moscow), 1977, section 3A, paper 13, pp 21-25

[63] Wu,C.Y , Wertheimer,M.R, Yelon,A, Boggs,S.A, Densley,R.J " Free Radical Formation in Electrical Trees in Polyethylene" Ann. Rep. Conf. elec insul& Diel. Phenom, 1976, pp 354-362

[64] Mitsui,H, Yoshimitsu,T, Mitzutani,Y, Umemoto "Electrical Failure Properties of Cast Epoxy Resins " IEEE Trans elec insul, 1981, EI-20 pp 533-542

[65] Cocks, A.C.F. and Ashby, M.F. “On Creep Fracture by Void Growth” , Proc. Mat. Sci , 1982, 27 pp 189-244

[66] Kagawa,T, Yamazaki,S “Acoustic Emission Associated with Tree Growth in Polymeric Materials” IEEE Trans elec insul, 1982, EI-17 pp.314-318

[67] H. R. Zeller , T. Hibma and P. Pfluger "Electrofracture Mechanics of Dielectric Aging", Annual Report Conf. Electr. Insul. and Dielectric Phenom., pp.85 -88 1984

[68] Hozumi,N, and Okamoto.,T, "The initiation and growth of ac tree in polyethylene" Proc.3rd Int.Conf.Cond.Break-down in Solid Dielectrics (Trondheim), 1989,pp, 543-547

[69]Hozumi.N, Okamoto,T, and Fukugawa,H. "TEM Observation of Tree Paths and Microstructures in Polyethylene" Jap.J.Appl.Phys.,1988,27,pp. 1230-1233

[70] Bammert,U,and Beyer,M. "Partial Discharges Measured with an Automated System in Epoxy Resin and Polyethylene" IEEE Trans. Elec.Insul.,1988,EI-23,pp. 215-225

[71] Tanaka,T, Reed,C.W, Devins,J.C, and Greenwood,A 'Effects of Gas Phase on Tree Initiation in Polyethylene' Ann.Rep. Conf. Elec. Insul.&Diel.Phenom, 1978, pp. 333-341

[72] Esaich,J.J, Laurent,C., and Mayoux,C. 'A Study of Electrical Discharges Growing in Short Confined Gaps' Ann.Rep. Conf. Elec. Insul.&Diel.Phenom, 1983, pp. 279-285.

[73] Auckland,D.W, Borishade,A.B, and Cooper,R,' The Electric Strength of a Narrow Column of Air. Bounded by a Dielectric Wall' Conf. Diel. Mats., Meas.& Applics, 1975, IEE Conf. Pub.129,pp.15-18

[74] Borishade, Auckland,D.W and Cooper.R, " Breakdown characteristics of air-filled Tubules in solid insulation" IEEE Trans. Elec. Insul, 1977, EI-12, pp.

348-354

[75] Klein,N, "Impact ionization in silicon dioxide at fields in the breakdown range" Adv.Phys.,1972,21,pp.605-645

[76] Okamoto,T, and Tanaka,T, "Partial Discharge Characteristics in phase Domain for Various Cylindrical Voids" Ann.Rep. Conf. Elec. Insul.&Diel.Phenom, 1985, pp. 498-503

[77] Tanaka,T. "Similarity between Treeing Lifetime and PD Resistance in Aging Mechanisms for Epoxy Nanocomposites" IEEE Trans. Elec.Insul., 1986,EI-21,pp. 899-905

[78] Okamoto,T,and Tanaka,T " Prediction of Treeing Breakdown from Pulse of Partial Discharge on Voltage-Phase Angle" Jap.J Appl.Phys.,1985,24,pp. 156-160

[79] Kai Wu, Yasuo Suzuoki, Teruyoshi Mizutani and Hengkun Xie, "Model for partial discharges associated with treeing breakdown: II. tree growth affected by PDs" J. Phys. D: Appl. Phys. 33 (2000) 1202–1208.

[80] Fujita,H, Nakanishi,T, and Yamaguchi,K, "Acoustic Emission Distributions and Types of Electrical Trees in Polyester Resin" IEEE Trans. Elec.Insul.,1983,EI-18, pp.520-527

[81] Laurent,C and Mayoux,C, " Analysis of the propagation of electrical treeing using optical and electrical methods" Elec.Insul.,1980,EI-15,pp.33-42

[82] Bamji,S, Bulinski,A, Densley,R.J and Shimizu,N. "Light Emission from PE subjected to High Divergent Field' Ann.Rep. Conf. Elec. Insul.&Diel.Phenom, 1982, pp. 592-597

[83] Fujita,H 'An Analysis of Mechanical Stress in Solid Dielectrics Caused by Discharges in Voids' IEEE Trans. Elec.Insul.,1987,EI-22,pp.277-285

[84]Mayoux,C.J, "Partial-Discharge Phenomena and the Effect of Their

Constituents on Polyethylene" IEEE Trans. Elec.Insul.,1976,EI-11,pp.139-148

[85] Mayoux,C.J ,'Corona Discharge and Ageing Process of an Insulation' IEEE Trans. Elec.Insul.,1977,EI-12,pp.153-158

[86]Cooper,D.E, Farber,M and Harris,S.P. "Mass spectrometric determination of S2F10 resulting from high-voltage arcing of SF6" Ann.Rep. Conf. Elec. Insul.&Diel.Phenom, 1984, pp. 32-37.

[87] Bahder,G, Garrity,T, Sosnowsi,M, Eaton,R, and Katz,C. "Electrical Breakdown Characteristics and Testing of High Voltage XLPE and EPR Insulated Cables" IEEE Trans. Power Appar.&Syst.,1982,PAS-101,PP.1379-1390

[88] Katz, C., Bernstein,B. S., " Electrical and Electrochemical Treeing Effect in Polyethylene and Cross-Linked Polyethylene Cables" 1973 Annual Report Conference Electrical Insulation and Dielectric Phenomena, Nat. Acad. Sci., Washington, D.C., 1974, p. 307

[89] Okawa, K., Ono, M., "Contaminants in Crosslinked Polyethylene Insulated PowerCable", Fujikura Report, June 1974

[90] http://en.wikipedia.org/wiki/Silicone_rubber [cited 23/07/2013]

[91] George G. Karady , Minesh Shah, R. L. Brown, " Flashover Mechnisams of Silicone rubber insulators used for outdoor insulator- I" IEEE Transactions on Power Delivery, Vol. 10. No. 4, October 1995

[92] R.G. Houlgate et al., "Field Experience and Laboratory Research on Composite Insulators for Overhead Lines", CIGRE Paper 15-12,1986.

[93] A.E. Vlastos and E.M. Sherif, "Experience from Insulators with Silicone Rubber Sheds and Shed Coatings", IEEE Trans. on Power Delivery, Vol. 5.No.4, pp. 2030 - 2038, Oct. 1990

[94] H.M. Schneider, W.W. Guidi, J.T.Burnham, R.S. Gorur, J.F. Hall, "Accelerated aging and flashover tests on 138 kV Nonceramic line post insulators" , 92WM 264-2 PWRD.

[95] R.S. Gorur, G.G. Karady, A. Jagota, M. Shah and A.M. Yates, "Aging in silicone rubber used for outdoor insulation", IEEE Trans. on Power Delivery Vol. 7, N0.2, pp 525-538, April 1992

[96] H.M. Schneider and A.E. Lux, "Mechanism of HVDC Wall Bushing Flashover", IEEE Trans. on Power Delivery, Vol. 6, No. 1, pp. 448-455, Jan. 1991

[97] H.M. Schneider, J.F. Hall and G.Karady, "Non-Ceramic Insulators for Transmission Lines," IEEE Transactions on Power Delivery, Vol.4, No.4, April 1992, pp. 2214-2221.

[98] Y. Shibuya, S. Zoledziowski, and J. H. Calderwood, "Void Formation and Electrical Breakdown in Epoxy Resin". IEEE Trans. on Power Apparatus and Systems, Vol. PAS-96, No. 1, pp. 198-207, Jan/Feb 1977.

[99] Laserna,J."An Introduction to Raman Spectroscopy"

http://www.spectroscopynow.com/coi/cda/detail.cda?page=2&id=1882&type=EducationFeature&chld=6 [cited 26/07/13]

[100] A. S. Vaughan, I. L. Hosier, S. J. Dodd, S. J. Sutton, "On the structure and chemistry of electrical trees in polyethylene", J. Phys D: Appl. Phys., Vol. 39, pp. 962-977, 2006

[101] J.L.Goldstein," Scanning Electron Microscopy and X-Ray Microanalysis". 3rd ed.New York: Springer. 2003.

[102] L. Dolgov, O. Yaroshchuk, and L.Qiu, "SEM investigations of the polymer morphology in the liquid crystal-polymer composites with different polymer contents". Molecular Crystals and Liquid Crystals, 2007. 468: p. 687-696.

[103]E.Suzuki, "High-resolution scanning electron microscopy of immunogold-labelled cells by the use of thin plasma coating of osmium". Journal of Microscopy-Oxford, 2002. 208: p. 153-157.

[104]. N. Erdman, N. Kikuchi, A. Laudate, V. Robertson, "Multispectral imaging in an FEG-SEM". Advanced Materials & Processes, 2009. 167(9).

[105]. J. E. McGregor, and A. M. Donald, "The application of ESEM to biological samples", Electron Microscopy and Analysis Group Conference. 2009.

[106]. D. Bassi, F. Cappa, and P. S. Cocconcelli, " A combination of a SEM technique and X-ray microanalysis for studying the spore germination process of Clostridium tyrobutyricum". Research in Microbiology, 2009. 160(5): p. 322-329.

[107] H. A. Illias, G. Chen, and P. L. Lewin, "Partial discharge behavior within a spherical cavity in a solid dielectric material as a function of frequency and amplitude of the applied voltage", IEEE Transactions on Dielectric and Electrical Insulation, vol. 18, no. 2, pp. 432–443, 2011.

[108] I. W. McAllister, "Surface current density k: an introduction", IEEE Transactions on Electrical Insulation, vol. 26, no. 3, pp. 416–417, 1991.

[109] Bai, T. and Lewin, P.L. "Degradation behaviour of voids in silicone rubber under applied AC electric fields". 2012 IEEE Conference on Electrical Insulation and Dielectric Phenomena, Montreal, Canada, 14 Oct 2012. 4pp, 589-592.

[110] G. Kaye, Tables of physical and chemical constants, 16th ed. Harlow : Longman, 1995

[111] Y. V. Serdyuk and S. M. Gubanski, "Computer modeling of interaction of gas discharge plasma with solid dielectric barriers", IEEE Transactions on Dielectrics and Electrical Insulation, vol. 12, no. 4, pp. 725–735, 2005.

[112]A. Bojovschi, W. S. T. Rowe, and K. L. Wong, "Dynamics of partial discharge in dielectrics: a computational approach", International Symposium on High Voltage Engineering, 2009.

[113] A. A. Ganjovi, N. Gupta, and G. R. G. Raju, "A kinetic model of a PD pulse within voids of sub-millimeter dimensions", IEEE Transactions on Dielectrics and Electrical Insulation, vol. 16, no. 6, pp. 1743–1754, 2009.

[114] S. Matsumura and S. Chen, "Effect of plasma resistance on electron temperature measurement by means of an electrostatic probe", Journal of Applied Physics, vol. 43, no. 8, pp. 3357–3361, 1972.

[115] B. M. Smirnov, "Modeling of gas discharge plasma", Physics-Uspekhi, vol. 52, no. 6, p. 559, 2009.

[116] P. Das and S. Chakravorti, "Studies on partial discharge simulation based on a stochastic model considering the variation of discharge area and temperature of the void surface", International Journal for Computational Methods in Engineering

Science and Mechanics, vol. 10, no. 5, pp. 393 – 405, 2009.

[117] J. Hilsenrath, Tables of thermal properties of gases. U.S. Govt. Print. Off, 1955

[118] A. A. Vasserman, Thermophysical properties of air and air components. Academy of Sciences of the USSR, 1971.

[119] H.A. Illias, G. Chen, and P.L.Lewin, "Modeling of partial discharges from a spherical cavity within a dielectric material under variable frequency electric fields", Conference on Electrical Insulation and Dielectric Phenomena, pp. 447–450, 2008.

[120] J. Kindersberger and C. Lederle, "Surface charge decay on insulators in air and sulfurhexafluoride part i: Simulation", IEEE Transactions on Dielectrics and Electrical Insulation, vol. 15, no. 4, pp. 941–948, 2008.

[121] A. K. Jonscher and E. F. Owede, "Time and frequency-resolved surface currents on insulators", IEEE Transactions on Electrical Insulation, vol. 25, no. 6, pp. 1077–1084, 1990.

[122] B. M. Weedy, D. Chu, and A. E. Davies, "Electric stresses in an hvdc cable through joint", IEEE Transactions on Power Apparatus and Systems, vol. PAS-103, no. 2, pp. 383–388, 1984.

[123] R. Bodega, A. Cavallini, P. H. F. Morshuis, and F. J. Wester, "The effect of voltage frequency on partial discharge activity", Conference on Electrical Insulation and Dielectric Phenomena, pp. 685–689, 2002.

[124] G. C. Montanari, A. Cavallini, L. Testa, S. Serra, and L. A. Dissado "Model of ageing inception and growth from microvoids in polyethylene-based materials under ac voltage", Conference on Electrical Insulation and Dielectric Phenomena, pp. 29–32, 2008.

[125] P. Morshuis, A. Cavallini, G. C. Montanari, F. Puletti, and A. Contin, "The behavior of physical and stochastic parameters from partial discharges in spherical voids", Proceedings of the 6th International Conference on Properties and Applications of Dielectric Materials, vol. 1, pp. 304–309, 2000.

[126] P. Molinie, "Measuring and modeling transient insulator response to

charging: the contribution of surface potential studies", IEEE Transactions on Dielectrics and Electrical Insulation, vol. 12, pp. 939–950, 2005.

.